FAILURE MODE MAPS AND MINIMUM WEIGHT DESIGN FOR STRUCTURAL SANDWICH BEAMS WITH RIGID FOAM CORES

by

Thanasis C. Triantafillou
Diploma in Civ. Eng., University of Patras, Greece
(1985)

SUBMITTED IN PARTIAL FULFILLMENT
OF THE REQUIREMENTS OF THE
DEGREE OF

MASTER OF SCIENCE
IN CIVIL ENGINEERING

at the

MASSACHUSETTS INSTITUTE OF TECHNOLOGY
January 1987

Signature of Author ___

Department of Civil Engineering
January 12, 1987

Certified by _____

Lorna J. Gibson
Thesis Supervisor

Accepted by _____

Ole S. Madsen
Chairman, Department Committee on Graduate Studies

FAILURE MODE MAPS AND MINIMUM WEIGHT DESIGN FOR STRUCTURAL SANDWICH BEAMS WITH RIGID FOAM CORES

by

THANASIS C. TRIANTAFILLOU

Submitted to the Department of Civil Engineering
on January 12, 1987 in partial fulfillment of the
requirements for the Degree of Master of Science in
Civil Engineering

ABSTRACT

Structural sandwich panels can fail in several ways. The faces and core can yield plastically or fracture depending on the nature of the materials from which they are made; the compressive face can buckle locally, or "wrinkle"; and the bond between faces and core can fracture causing delamination. The critical failure mode, which occurs at the lowest load, depends on the properties of the face and core materials and on the design of the beam. Here, we develop equations describing the load at which failure occurs for each possible failure mode for a rectangular sandwich beam with face and core materials that yield plastically. We then develop a failure mode map, with axes of core relative density and the ratio of face thickness to span length, which, for a given loading configuration and set of face and unfoamed solid core materials, shows the dominant failure mode for every possible beam design. Tests on sandwich beams with aluminium faces and rigid polyurethane foam cores show that the equations and map describe failure well. The map can then be used to design the minimum weight sandwich beam for a given strength requirement.

Thesis Supervisor: Lorna J. Gibson

Title: Assistant Professor of Civil Engineering

ACKNOWLEDGEMENTS

I would like to express my appreciation and gratitude to my advisor, Professor Lorna J. Gibson, for the help and guidance she provided in carrying out this study. Her constant encouragement and inexhaustible patience are greatly appreciated.

I am also very thankful to Laura Demsetz for her valuable technical advice.

For his technical assistance, I am thankful to Arthur Rudolph.

For her assistance in typing part of this thesis, I am very thankful to Claire Benoit.

And last but certainly not least, I would like to thank my parents for their love and encouragement in all of my academic endeavors.

TABLE OF CONTENTS

TABLE OF CONTENTS (continued)

LIST OF FIGURES

LIST OF FIGURES (continued)

LIST OF FIGURES (continued)

LIST OF FIGURES (continued)

LIST OF TABLES

LIST OF SYMBOLS

I. ENGLISH CHARACTERS

A = Area [in^2] or
= Constant in the compressive modulus equation [-]

B = Constant in the core shear strength equation [-] or
= Width [in]

B_1 = Constant in the face wrinkling equation [-]

b = Width [-]

C = Constant in the core tensile strength equation [-]

c = Core depth [-]

c_1 = Constant depending on the loading-support conditions [-]

c_2 = Constant depending on the loading-support conditions [-]

c_3 = Constant in the core compressive modulus equation [-]

c_4 = Constant in the core shear strength equation [-]

c_5 = Constant in the core tensile strength equation [-]

c_6 = Constant in the core compressive strength equation [-]

c_{opt} = Optimum core depth [-]

D = Constant in the core compressive strength equation [-] or
= Flexural rigidity [$lbin^2$]

d = Distance between centroids of opposite faces [in]

E = Young's modulus [psi]

E_c = Core Young's modulus [psi]

E_{c_1} = Core Young's modulus parallel to the rise [psi]

E_{c_2} = Core Young's modulus in one direction perpendicular to the rise [psi]

E_{c_3} = Core Young's modulus normal to E_{c_1} and E_{c_2} [psi]

$E_{c_{\parallel}}$ = Core Young's modulus parallel to the rise [psi]

$E_{c_{\perp}}$ = Core Young's modulus perpendicular to the rise [psi]

E_f = Young's modulus of face material [psi]

E_s = Young's modulus of cell-wall material [psi]

F = Axial force [lb]

G_c = Core shear modulus [psi]

h = Depth [in] or
= Thickness [in]

I = Second moment of inertia [in^4]

LIST OF SYMBOLS (continued)

K_{ICadh} = Adhesive critical stress intensity factor [Ksiin$^{1/2}$]
l = Span [in] or
= Half-wave length [in]
M = Bending moment [lbin]
P = Load [lb]
P_{cs} = Failure load by core shear [lb]
P_d = Failure load by debonding [lb]
P_f = Failure load [lb]
P_{fy} = Failure load by face yielding [lb]
P_{fw} = Failure load by face wrinkling [lb]
P_{ult} = Ultimate load [lb]
P_{yf} = Face yield load [lb]
Q = Shear force [lb]
R = Radius of curvature [in]
S = First moment of area [in^3]
T = Load [lb]
t = Face thickness [in]
t_{opt} = Optimum face thickness [in]
W = Weight [lb]
w = Displacement [in]
w_m = Displacement amplitude [in]
x - Denotes direction x
y - Denotes direction y
z - Denotes direction z or
= Parameter in the core optimum thickness equation [psi]
z_1 = Distance from neutral axis [in]

II. GREEK CHARACTERS

α = Initial flaw size [in]
α_o = Parameter in the adhesive toughness formula [in]
Δ = Deflection [in]
ν_c = Poisson's ratio of foam core [-]
π = 3.14...
ρ_c = Core density [lb/in^3]

LIST OF SYMBOLS (continued)

$\rho_{c_{opt}}$ = Optimum core density [lb/in^3]
ρ_f = Face material density [lb/in^3]
ρ_s = Solid foam material density [lb/in^3]
σ = Normal stress [psi] or
= Compressive critical stress [psi]
σ_{adh} = Normal stress in the adhesive [psi]
σ_c = Normal stress in the core [psi]
σ_{c_1} = Principal stress [psi]
$\sigma^*_{c,c}$ = Core compressive strength [psi]
σ^*_{c,c_1} = Core compressive strength parallel to the rise [psi]
σ^*_{c,c_2} = Core compressive strength in one direction perpendicular to the rise [psi]
σ^*_{c,c_3} = Core compressive strength normal to $_{c,c_1}$ and $_{c,c_2}$ [psi]
$\sigma^*_{c,c_{\parallel}}$ = Core compressive strength parallel to the rise [psi]
$\sigma^*_{c,c_{\perp}}$ = Core compressive strength perpendicular to the rise [psi]
σ_{cr} = Critical stress [psi]
$\sigma_{c,t}$ = Tensile stress in the core [psi]
$\sigma^*_{c,t}$ = Core tensile strength [psi]
σ^*_{el} = Elastic collapse stress [psi]
σ_f = Normal stress in the face [psi]
σ^*_{pl} = Plastic collapse stress [psi]
σ_{yf} = Yield stress of face [psi]
σ_{ys} = Yield stress of cell-wall material [psi]
σ_y = Normal stress in y direction [psi]
σ_z = Normal stress in z direction [psi]
τ = Shear stress [psi]
τ_{adh} = Shear stress in the adhesive [psi]
τ^*_{adh} = Shear strength of the adhesive [psi]
τ_c = Shear stress in the core [psi]
τ^*_c = Core shear strength [psi]
$\tau_{c_{max}}$ = Maximum shear stress in the core [psi]

CHAPTER 1

INTRODUCTION

1.1 GENERAL

Composite structural members made of two thin, stiff faces separated by a weak, light-weight core are known as sandwich panels. Separation of the stiff faces by the core increases the moment of inertia of a sandwich beam or plate with little increase in weight, giving an efficient member for resisting bending and buckling. Sandwich construction is frequently found in nature, where mechanical design is often optimized. For example, in the human skull, two thin, outer layers of dense, compact bone are separated by a light-weight core of sponge-like cancellous bone; and in the iris leaf, the almost fully dense and relatively stiff, fibre-composite-like ribs on the outer skin of the leaf are separated by weak, low density cells in the core. In both instances, the sandwich structure results in a lower weight member.

In man-made sandwich structures aluminium, wood and fibre-reinforced plastics, are commonly used as face or skin materials while balsa, honeycombs and polymeric foams are often used in the core. Honeycomb cores are used in applications where the weight of the panel is the only critical factor as, for example, in structural components of aircraft. Foam cores are usually preferred in applications where low thermal conductivity is required in addition to low weight, as in portable buildings, mobile homes and refrigerated shipping containers. In this study we analyze the failure of foam-core sandwich beams made up of materials which yield plastically and describe how the weight of such a sandwich beam can be minimized for a given strength. Sandwich beams with rigid foamed polyurethane cores and aluminium faces were used in the experimental portion of the project. These are typical materials; the analysis is applicable to any combination of isotropic face and foamed core materials which fail by yielding.

1.2 APPLICATIONS

To date, panels for use in the building industry have been of a

mainly semi-structural character, carrying relatively small loads over fairly long spans. In the non-residential building market sandwich panel roofing is gaining increasing popularity because of its low weight. Other construction applications include: portable buildings and fold-up bridges (of potential use to the Army); energy efficient housing using prefabricated steel panels with urethane insulation between them for use in Arctic areas (which minimizes the use of electricity and heating fuel); and construction in remote areas (a recent application of this is in the replacement of remote lighthouses with new units of balsa-cored sandwich structures which are flown in by helicopter). Some of the above construction applications are illustrated in Fig. 1.1.

Sandwich construction has been widely applied in the aircraft industry for flooring, helicopter rotor blades, and tail and wing components. Panels for aircraft structures almost invariably employ fibre composite faces with metal or paper-resin honeycomb or corrugated cores. The automobile industry is beginning to use the concepts developed by the aircraft industry for sandwich construction in the cars of the future. Sandwich panels are also used in modern sports equipment: the decks and hulls of racing yachts, and water and snow skis are often made using sandwich construction.

The use of structural sandwich members has already gained wide acceptance in several applications, especially those in which the weight of the member is critical.

1.3 MINIMUM WEIGHT DESIGN OF SANDWICH PANELS

Sandwich construction is most beneficial for building a light, cheap structure. Consider a simple example: let us assume that we want to construct a simply supported beam (l = span = 96 in (2438.4 mm); b = width = 6.3 in (160 mm)) subject to three-point bending load, with a given stiffness requirement, i.e. load/mid-span deflection, of, say, 3654.5 $lbin^{-1}$ (640 Nmm^{-1}). If we decide to make a rectangular beam of aluminium alone, the required weight is 126.42 lb (57.34 Kgf). Based on a recent optimization analysis [16] for sandwich beams with rigid polyurethane cores we can estimate the weights of the aluminium and the foam material, if we decide to construct the beam using these materials, as 9.247 lb (4.194 Kgf) and 37.19 lb (16.87 Kgf), respectively. The

total weight of the resulting member is 46.437 lb (21.064 Kgf) (see also Fig. 1.2). This simple example reveals that for the same structural requirement (bending stiffness in this case), sandwich construction leads to a weight reduction of about 63%! It can be argued that this is an unrealistically high figure for the weight reduction as a solid aluminium I beam would have a lower weight than a rectangular one. Perhaps of more significance is the fact that similar weight reductions can be obtained in sandwich plates; in this case there is no equivalent of the I beam for a solid aluminium plate. The large weight reduction possible with sandwich panels is advantageous in reducing transit and labor costs for portable structures or structures in remote areas.

A cost comparison of the two different approaches of constructing the beam of the previous example reveals that sandwich construction in this case will result in an approximately 25% cheaper member.

In conclusion, the need for the optimum use of the materials in the design of lightweight sandwich panels is imperative. Optimization analyses of sandwich members aim to develop a method of designing the lightest possible member for some specified structural requirement. The requirement may be that the panel must have some given stiffness, or strength, or combination of stiffness and strength. There may be dimensional constraints also: the face and the core may have to be within certain size limitations determined by the availability of materials, or the depth of the panel may have to be less than some maximum allowable dimension. Previous optimization studies have usually focused on determining the core and face thickness which minimize the weight of a panel assuming that the core and face materials are completely specified, and that their densities, elastic moduli and strengths are known. Work on relating core properties (such as the elastic and shear moduli) to core density allows core density to be optimized. Previous analyses based on linear relationships between core properties and density do not provide reliable solutions to the optimization problem, because these relationships are not valid for foams. Recent analyses for non-linear relationships between foam properties and density have also been done and are considered in the present research work. So far, this work has successfully been applied to minimizing the weight of sandwich beams and plates for a given

stiffness requirement. Closed form solutions for the core density and the core and face thicknesses which minimize the weight of foam core sandwich beams and plates subject to a stiffness constraint have been developed.

Here we are interested in minimizing the weight of a sandwich beam for a strength constraint, or a combination of stiffness and strength constraints. The first step in analyzing the strength constraint problem is to identify the possible modes of failure in a sandwich beam and to develop equations which describe the failure loads for each mode. Given the failure mode equations we can plot them on a failure mode map, a diagram with the horizontal axis corresponding to the ratio of the thickness of the face, t, over the span-length, l, and the vertical axis corresponding to the ratio of the density of the core material, ρ_c, over the density of the unfoamed solid material, ρ_s. The plot is divided into several regions, each one reflecting a failure mode. A typical failure mode map is illustrated in Fig. 1.3. It should be noticed that different maps must be constructed for different loading configurations.

The main goal of this work is to develop failure equations and failure mode maps for sandwich beams and to use the failure maps to suggest a method for designing the minimum weight sandwich beam for a given strength. With a map describing the way in which a sandwich beam can fail, the equations giving the failure load and the optimization analysis, the designer will be able to select his materials properties and dimensions appropriately.

1.4 OUTLINE OF THE THESIS

The present work is organized in seven chapters, with the main emphasis given in chapters 3, 4, 5, and 6 in which both the analytical and experimental work are described and the optimization analysis is presented.

Chapter 2 is devoted to a brief literature review. This review describes the literature on: a) the observed failure modes in sandwich beams; b) the optimization of sandwich panel design; c) property-density relationships for foamed core materials.

The analytical work for this research is presented in Chapter 3. After identifying stresses in structural sandwich beams and analyzing each possible failure mode, an equation is obtained, describing the failure load for the mode given the properties of the face material and the solid from which the core is foamed, and the loading configuration.

Chapter 4 presents the experimental procedure and all of the experimental results. Material properties of the aluminium used in the face and of the foamed polyurethane used in the core are reported. The constants of proportionality for core properties are calculated from test data. Using the correct constants of proportionality, a failure mode map for a sandwich beam loaded in three-point bending is plotted using reasonable ranges of the design variables with a FORTRAN program, given in the Appendix. A set of sandwich beams which should have the various failure modes shown in the failure mode map can then be designed and tested to failure. Results of the tests are given, noting the way in which failure occurs. These results are finally plotted on the failure mode map.

A discussion of the results is given in Chapter 5. The agreement of the experimental results with the analytical work is discussed and a description of any anomalies in the experimental procedure is also presented. Suggestions for simplification of the analysis are also given.

The optimization analysis is presented in Chapter 6. The failure mode maps developed in Chapters 3 and 4 are used in the minimum weight analysis of a sandwich beam for a given strength requirement. By noting that the face and core of a sandwich beam should fail simultaneously (otherwise, the unfailed componenent is overdesigned), the minimum weight design of a beam is found for a given strength, in a closed form solution.

Chapter 7 summarizes the main findings that have come out of the research work. The validity of both the analytical and the experimental work is discussed, as well as new ideas to have come out of the project. Finally, a description of additional work suggested by the project, and new research directions is presented.

CHAPTER 2

LITERATURE REVIEW

2.1 GENERAL

The literature from three relevant areas is reviewed in this chapter. First, the failure modes observed in sandwich beams are identified and described; the load required to cause failure in each case is given in Chapter 3. Next, previous minimum weight design studies are reviewed and the ways in which this study differs from them are indicated. And finally, the non-linear property-density relationships for the foam core, used in developing the failure mode maps and in the optimization analysis, are summarized.

2.2 FAILURE MODES IN SANDWICH BEAMS

Several failure modes have been observed in sandwich composites (Fig. 2.1). Which mode occurs depends on the loading configuration, the properties of the face and the core materials and the member dimensions. The main modes of failure of sandwich composites made of face and core materials which yield plastically are summarized in this section. A more detailed presentation, including the failure equations for each mode, is given in Chapter 3.

Under axial loading, failure may occur in two ways: by overall buckling or by face dimpling. Overall buckling can be described by the Euler load for a column, using the equivalent flexural rigidity for the sandwich [2,11,24]. Face dimpling occurs with a wavelength equal to the cell size of the core [2,11,22,28]; it is usually only significant for honeycomb cores with a large cell size (eg. 1/4"-1/2"). Because sandwich panels are typically used to resist flexural loads rather than axial ones, the axial failure modes are not considered in any more detail in this thesis (Fig. 2.1 a, b).

In flexure, several modes of failure exist. The face may either yield or wrinkle; delamination of the bond between the face and the core may occur; and the core may fail in tension, compression, shear, or by

local crushing.

A common failure mode of composite sandwich members is the yielding of the face material due to high normal stresses generated by bending [2,26]. When these normal stresses exceed the yield stress of the face material, it yields and eventually ruptures (Fig. 2.1c).

The compression faces of sandwich members are sometimes subject to a particular kind of local instability described as wrinkling, in which the wavelength of the buckled form is of the same order as the thickness of the core (Fig. 2.1d). A special theory is needed to predict this behavior; the analysis [2] is presented in Chapter 3.

A failure mode of considerable importance is the so-called bond decohesion or simply debonding or delamination (Fig 2.1e). A current search in the literature shows that there is not a unique theory for the problem of delamination. Basically, two entirely different approaches exist. A summary is given here [8,10,21]. The fracture mechanics approach explains the debonding of the face and core materials based on the critical stress intensity factor of the adhesive. A second approach compares the shear stress between the face and the core, caused by the externally applied loads, with the shear strength of the adhesive. A more complete description for both cases is given in the next Chapter.

We should also mention that, theoretically it is also possible for the core to yield in shear, tension or compression, depending on how the corresponding strengths compare to the stresses caused by the loads [2,28]. These last three modes of failure are shown in Fig. 2.1f), g) and h) and a more detailed treatment is given in the subsequent Chapter.

As may be expected, when high lateral loads are applied on a small area of the member, high local stresses may arise leading to local crushing of the core material, as is shown in Fig. 2.1i) [2,11]. The use of bearing plates at the loading points avoids this type of failure.

2.3 OPTIMIZATION OF SANDWICH PANEL DESIGN

Optimization analyses in sandwich members minimize the weight subject to a given stiffness or strength or some combination of both. Most of the work done to date has aimed at finding the values of the face and core thicknesses which minimize weight; in these studies it has

been assumed that the face and core materials are completely specified and that their moduli, strengths and densities are known. Allen [2] shows how this can be done for sandwich beams subject to a stiffness constraint. Huang and Alspaugh [20] and Ueng and Liu [27] have done the optimization analysis of the core and face thicknesses for highly constrained members. Huang and Alspaugh minimized the weight for the strength requirements of maximum allowable bending stress and shear stress, as well as for a deflection requirement. Ueng and Liu did analogous work for a specific type of corrugated core. Due to the complexity of the constraints in both these problems, the solutions were obtained by numerical techniques; no closed form solution was possible.

Little attention has been paid to the optimum design of sandwich members not only with respect to the core and face thicknesses but also with respect to the core density. Wittrick [29] and Ackers [1], working on sandwich columns with foamed calcium alginate cores, both recognized that there is an optimum core density which minimizes the weight. Their optimization analyses were based on the given strength requirement. They considered the Euler buckling, face wrinkling and face yielding failure modes. Tests on foamed calcium alginate showed that its Young's modulus varied linearly with density. From this, Wittrick assumed that the shear modulus also varied linearly with density. By substituting these expressions into the failure equations and considering Euler failure and face wrinkling to occur simultaneously, Wittrick developed expressions for core and face thicknesses as well as for core density which minimized the weight for a given strength requirement. A similar analysis has been made by Kuenzi [23], who worked on the use of the wood cores in sandwich construction. He optimized sandwich design for the cases of a given equivalent flexural rigidity requirement, a given bending moment capacity (strength) requirement and a given buckling resistance. In the last two cases he used linear relationships between moduli and density, valid for wood cores.

A recent extensive study of the mechanical behavior of cellular solids has shown that these linear moduli-density relationships are not generally valid for foams [13,14,15]. Using non-linear relationships between moduli and densities, Gibson and Demsetz [12,16] minimized the weight of sandwich beams and plates with rigid foam cores with respect

to core density as well as with respect to the core and face thicknesses for a given stiffness requirement. That was very important because realistic core property-density relationships for foams were used for the first time in weight minimization analyses. The present work adds something new: the use of non-linear core property-density relationships in minimum weight design of structural sandwich beams for a given strength requirement.

2.4 FOAM CORE PROPERTY-DENSITY RELATIONSHIPS

Relating core properties such as the moduli and collapse strengths to core density allows core density to be included as a variable in the optimization analysis for sandwich beams. Early optimization studies used a linear relationship between the core moduli and density [1,23,29]. A recent extensive study into the mechanics of cellular solids such as foams and woods has shown that these linear moduli-density relationships are not generally valid [13,14,15]. Instead, it was found that, for foams, Young's modulus and the shear modulus are theoretically proportional to the density squared:

$$E_c/E_s = (\rho_c/\rho_s)^2 \quad , \tag{2.1}$$

$$G_c/E_s = 0.4(\rho_c/\rho_s)^2 \quad , \tag{2.2}$$

where E_c, G_c and ρ_c are the core Young's modulus, shear modulus and density, respectively. E_s and ρ_s correspond to the cell-wall material's Young's modulus and density. Similar expressions were derived for the elastic and plastic strengths of a foam core. Elastic collapse occurs when the core cells buckle elastically causing the foam to collapse elastically. Cellular materials may also collapse by a second mechanism. If the cell-wall material has a plastic yield point, then the foam as a whole may show plastic behavior. The following two formulas have been derived for the strength of the core [14]:

$$\sigma^*_{el}/E_s = 0.05(\rho_c/\rho_s)^2 \quad , \tag{2.3}$$

$$\sigma^*_{pl}/\sigma_{ys} = 0.30(\rho_c/\rho_s)^{3/2} \quad . \tag{2.4}$$

σ^*_{el} and σ^*_{pl} are the stresses at failure for elastic (buckling) or plastic behavior respectively and σ_{ys} is the yield stress of the cell-wall material. The last two formulas are valid for $\rho_c/\rho_s < 0.30$ and $\rho_c/\rho_s < 0.63$ respectively. It must be noted that the agreement of the above expressions with experimental results is very good (Fig. 2.2-2.5).

In this study we are concerned with the failure of sandwich beams made up of materials which yield plastically; in this case equation (2.4) gives the relevant strength for a core.

The next Chapter is devoted to the formulation of equations describing the failure modes of sandwich beams subject to bending.

CHAPTER 3

ANALYTICAL FORMULATION OF FAILURE MODE EQUATIONS

3.1 GENERAL

As we have already mentioned in Chapter 3, six different failure modes are possible for rectangular sandwich beams made from materials which yield plastically and are subjected to bending. They are: face yielding, face wrinkling, bond decohesion, core shear, core tension and core compression. In this Chapter we first describe the stresses acting in a sandwich beam and then derive an equation describing the failure load for each mode given the loading conditions, the member dimensions and the properties of the faces, the foam core and the adhesive used to construct the beam. The procedure followed is general without considering for example, specific values for materials properties or support conditions. This Chapter concludes by introducing the construction of a failure mode map using the failure equations.

3.2 STRESSES IN SANDWICH BEAMS

Allen [2] presents a good review of the application of ordinary beam theory to sandwich beams; the following summary is based on his review. A typical sandwich beam is illustrated in Fig. 3.1. The faces are each of thickness t and the low density core is of thickness c. The overall depth is h and the width b. The face and core materials are assumed to be isotropic. Use of the ordinary beam theory leads to the well-known relationship between bending moment (M) and curvature (1/R):

$$\frac{M}{EI} = -\frac{1}{R} \tag{3.1}$$

where EI is the flexural rigidity, which, for convenience, is denoted by the single symbol D. The flexural rigidity of a sandwich beam is given (from the parallel axis theorem) by:

$$D = E_f \frac{bt^3}{6} + E_f \frac{btd^2}{2} + E_c \frac{bc^3}{12} \tag{3.2}$$

where E_f and E_c are the Young's moduli of the faces and core respectively and d is the distance between the centroids of the two faces:

$$d = \frac{h+c}{2} \quad . \tag{3.3}$$

The beam is assumed to be narrow, so that stresses in the y direction can be taken as zero. The first and third terms in equation (3.2) are the bending stiffnesses of the faces about their own centroidal axis and that of the core about its centroidal axis. The second term is the bending stiffness of the faces about the beam's centroidal axis and in practical sandwiches is invariably dominant. The first amounts to less than 2% of the second when

$$3\left(\frac{d}{t}\right)^2 > 50 \quad . \tag{3.4}$$

The error introduced by neglecting the first term is therefore negligible provided $d/t > 4.08$. The third term amounts to less than 2% of the second when

$$6\,\frac{E_f}{E_c}\,\frac{t}{c}\left(\frac{d}{c}\right)^2 > 50 \quad . \tag{3.5}$$

We can conclude that if the "thin face and compliant core approximation" holds (first and third terms in equation (3.2) can be neglected) the flexural rigidity of the sandwich beam is given by:

$$D = E_f \frac{btd^2}{2} \quad . \tag{3.6}$$

Use of ordinary bending theory leads to the following equations for the normal stresses in the faces and the core, respectively:

$$\sigma_f = \frac{Mz}{D} E_f \qquad \left(\frac{c}{2} < z < \frac{h}{2} \; ; \; -\frac{h}{2} < z < -\frac{c}{2}\right) , \tag{3.7a}$$

$$\sigma_c = \frac{Mz}{D} E_c \qquad \left(-\frac{c}{2} < z < \frac{c}{2}\right) \quad . \tag{3.7b}$$

Now, consider a section of a homogeneous beam with second moment of

inertia I and width b, at a level z_1. The shear stress, τ, at a depth z, below the centroid of the cross-section is given by

$$\tau = \frac{QS}{Ib} \quad . \tag{3.8}$$

In the above formula S is the first moment of area of the part of the section for which $z > z_1$ and Q is the shear force at that section. Equation (3.8) is not directly applicable to a sandwich beam because the modulus of elasticity is not the same for all elements of the cross-section. To account for this, the expression for the shear stress can be written as

$$\tau = \frac{Q\sum(SE)}{Db} \quad , \tag{3.9}$$

where $\sum(SE)$ represents the sum of the products of S and E of all parts of the section for which $z > z_1$. Based on this formulation we can express the shear stress at a level z in the core of a sandwich beam as:

$$\tau = \frac{Q}{D}\left[E_f \frac{dt}{2} + \frac{E_c}{2}\left(\frac{c^2}{4} - z^2\right)\right] \quad . \tag{3.10}$$

A similar expression can be obtained for the shear stress in the faces. The complete distribution of shear stresses across the depth of the cross-section of the sandwich beam is illustrated in Fig. 3.2a. Using equation (3.10) we can derive that the ratio of the maximum core shear stress to the minimum core shear stress is

$$\frac{\tau_{c_{max}}}{\tau_{c_{min}}} = \left(\frac{E_c}{E_f}\frac{1}{4}\frac{c^2}{td} + 1\right) \quad .$$

This expression is within 2% of unity if

$$4\,\frac{E_f}{E_c}\,\frac{t}{c}\,\frac{d}{c} > 50 \quad . \tag{3.11}$$

Considering that the ratio d/c is usually near to unity, one may observe that conditions (3.5) and (3.11) are similar in effect. As a result, when a core is too compliant to provide a significant contribution to the flexural rigidity of the member, the shear stress may be assumed

nearly constant over the depth of the core. Based on this assumption we can write the constant shear stress in the core as

$$\tau = \frac{Q}{D} \frac{E_f t d}{2} \quad . \tag{3.12}$$

A combination of (3.12) with (3.6) leads to the following:

$$\tau = \frac{Q}{bd} \simeq \frac{Q}{bc} \quad . \tag{3.13}$$

The shear stress distribution is summarized in Fig. 3.2.

3.3 FACE YIELDING

Consider a rectangular sandwich beam under a general loading configuration P as shown in Fig. 3.3. The normal stress distribution at the critical section of the beam (that where the bending moment takes its maximum value) is also shown in Fig. 3.3. The normal stresses are assumed to be uniform over the face thicknesses; this approximation is valid if the faces are thin. The bending moment, M, at the critical section is given as

$$M = \frac{Pl}{c_1} \quad , \tag{3.14}$$

where the constant c_1 depends on the loading arrangement and the support conditions. For the case of a simply supported beam loaded in the middle of its span with a concentrated load P, c_1 takes the value 4. If the beam fails by face yielding, the normal stress in the face at the critical section, σ_f, equals the yield stress of that face, σ_{yf}:

$$\sigma_f = \sigma_{yf} \quad . \tag{3.15}$$

The stress σ_f can be expressed in terms of the bending moment as

$$\sigma_f = \frac{M E_f}{D} \frac{c}{2} \quad . \tag{3.16}$$

According to section 3.2 the flexural rigidity D is approximated as

$$D = E_f \frac{btd^2}{2} \quad , \tag{3.17}$$

where E_f is the Young's modulus for the face material and all other dimensions (b, t and d) are as shown in Fig. 3.1. Substituting equations (3.14) and (3.17) in (3.15) we obtain:

$$\sigma_f = \frac{Plc}{c_1 btd^2} . \tag{3.18}$$

Finally, substitution of (3.18) in (3.15) yields the equation that describes the face yielding failure mode:

$$P = c_1 \sigma_{yf} b \frac{d^2}{c} \frac{t}{l} . \tag{3.19}$$

At this point we should keep in mind that the last equation is valid in all cases where the thin-face and compliant core approximations hold.

3.4 FACE WRINKLING

The compression face of a sandwich beam subject to bending is likely to fail by a particular kind of local instability described as wrinkling. Consider an infinitely long strut attached to an elastic medium which extends to infinity on one side of the strut, as is shown in Fig. 3.4. This is a reasonable idealization for the face of a sandwich member as will be explained later. We can assume a state of plain stress (σ_y=0) provided that the beam's width b is small. The strut is considered to be of rectangular section and of thickness t; it is also described by the differential equation

$$D \frac{d^4 w}{dx^4} + F \frac{d^2 w}{dx^2} = b\sigma_z , \tag{3.20}$$

with D denoting its flexural rigidity, σ_z the normal stress between the strut and the face of the supporting medium (foam) and w the corresponding displacement in the z-direction; F is the axial force.

Assuming buckling into sinusoidal waves (half-wavelength = l) we can write:

$$w = w_m \sin \frac{\pi x}{l} . \tag{3.21}$$

Considering compatibility of displacements, it can be shown [2] that the

stress σ_z which must exist to deform the medium in this manner is

$$\sigma_z = -\frac{a}{l} w_m \sin\frac{\pi x}{l} \quad , \tag{3.22}$$

where

$$a = \frac{2\pi E_c}{(3-\nu_c)(1+\nu_c)} \quad .$$

E_c and ν_c are the modulus of elasticity and Poisson's ratio for the core material, respectively. Combining equations (3.20), (3.21) and (3.22) we obtain:

$$D\frac{\pi^4}{l^4} - F\frac{\pi^2}{l^2} = -\frac{a}{l} \quad . \tag{3.23}$$

F in equation (3.23) is the critical value of the axial load that must exist in the buckled condition. D and F in equation (3.23) can be written as

$$D = \frac{E_f t^3}{12} \quad , \quad F = \sigma bt \quad ,$$

with E_f and σ denoting the modulus of elasticity of the strut and the compressive critical stress in the face, respectively. Therefore, equation (3.23) can now be written as follows:

$$\sigma = \frac{\pi^2 E_f}{12}\left(\frac{t}{l}\right)^2 + \frac{a}{\pi^2}\left(\frac{l}{t}\right) \quad . \tag{3.24}$$

One can observe that the critical stress is a quadratic function of the ratio l/t (Fig. 3.5). Its first derivative with respect to this ratio leads to the following expression for the minimum critical stress:

$$\sigma_{cr} = B_1 E_f^{1/3} E_c^{2/3} \quad \text{where} \quad B_1 = 3\left[12(3-\nu_c)^2(1+\nu_c)^2\right]^{-1/3} \tag{3.25}$$

Variations in the Poisson's ratio of the supporting medium, only slightly affect the values of the constant B_1; a typical value is 0.57.

The stresses in the core which are associated with the sinusoidal disturbance at the surface (z=0) decrease as z increases; at a

sufficiently large value of z they may be regarded as negligible. Consequently, the compression face of a sandwich beam may be idealized in the manner of Fig. 3.4. provided the depth of the core is sufficiently great to allow the effects of the disturbance at one interface to die away before reaching the other.

Equation (3.25) with $B_1 = 0.57$ may therefore be taken as a measure of the stress in the face at which wrinkling occurs, provided the core is thick. We can conclude that a face wrinkling failure mode will take place when the normal stress in the face at the critical section (where the bending moment is maximum), σ_f, becomes equal to the critical stress of equation (3.25):

$$\sigma_f = 0.57 E_f^{1/3} E_c^{2/3} \quad . \tag{3.26}$$

Theoretical work [15] has related the elastic modulus of a foam core, E_c, to the elastic modulus of the solid core material, E_s and to the relative density of the foam, ρ_c/ρ_s:

$$E_c = \left(\frac{\rho_c}{\rho_s}\right)^2 E_s \quad . \tag{3.27}$$

The results of many measurements agree well with this expression. There is small variation in the exponent caused by the distribution of solid between the faces and edges of the cells in the foam. For generality, we assume that this relationship holds as

$$E_c = c_3 \left(\frac{\rho_c}{\rho_s}\right)^A E_s \quad , \tag{3.28}$$

where c_3 and A are constants which are determined experimentally. It should be remembered that ρ_c and ρ_s are the densities of the foamed core and unfoamed solid core materials, respectively. Substituting (3.28) into (3.26) and taking σ_f from (3.16) we find:

$$P = 0.57 c_1 c_3^{2/3} E_f^{1/3} E_s^{2/3} \left(\frac{\rho_c}{\rho_s}\right)^{2A/3} b \frac{d^2}{c} \frac{t}{l} \quad . \tag{3.29}$$

This equation describes the face wrinkling failure mode.

3.5 BOND DECOHESION

A first approach to the debonding mechanism of sandwich members is to consider delamination when the shear stress in a region of the adhesive reaches its shear strength:

$$\tau_{adh} = \tau^{*}_{adh} \quad . \tag{3.30}$$

The shear stress, τ_{adh}, in the adhesive, at a given section, is given by (equation (3.13))

$$\tau_{adh} = \frac{Q}{bc} \tag{3.31}$$

and is maximum at the section where the shear force Q is maximized, i.e., at the critical section. A debonding type of failure will initiate from this section when

$$\frac{Q}{bc} = \tau^{*}_{adh} \quad . \tag{3.32}$$

The shear force, Q, at the critical section is given as

$$Q = \frac{P}{c_2} \quad , \tag{3.33}$$

where the constant c_2 is dependent on the loading arrangement and the support conditions. For the case of a simply supported beam loaded in the middle of its span with a concentrated load P, c_2 takes the value 2. Substituting (3.33) in (3.32) we can derive the failure mode equation for the debonding mechanism considering the adhesive's shear strength approach as

$$P = c_2 \tau^{*}_{adh} bc \quad . \tag{3.34}$$

At this point we should notice that it would be more accurate to compare the adhesive's shear strength with the maximum principal shear stress in the bond, evaluated at the interface between the face and the adhesive. Hence, the formulation followed here is quite simplistic and a more detailed analysis for the debonding mechanism is the subject of future research work.

As we have noticed in Chapter 2, a second, entirely different approach may be used to the delamination problem. The debonding mechanism is theoretically governed by a mixed mode delamination, mode I and mode II, using the well-known fracture mechanics terminology [19]. Mode I is related to normal stresses and mode II is related to the in-plane shear stresses, both occuring in an element of the adhesive. These two modes and the normal and shear stress distribution are depicted in Fig. 3.6. In fact, mixed mode failure is rare. In most engineering materials it is always mode I that governs failure. In our case this can be verified if the ratio of the shear stress in the adhesive, τ_{adh}, over the normal stress, σ_{adh}, is small compared to 1. We consider σ_{adh} to be the maximum normal stress in the adhesive, which implies that this occurs near the boundary with the face, and is therefore equal to σ_f (see Fig. 3.6). As a result (equation (3.18))

$$\sigma_{adh} = \sigma_f = \frac{Plc}{c_1 btd^2} \quad . \tag{3.35}$$

The shear stress in the adhesive is given by

$$\tau_{adh} = \frac{P}{c_2 bc} \tag{3.36}$$

and the τ_{adh}/σ_{adh} ratio becomes

$$\frac{\tau_{adh}}{\sigma_{adh}} = \frac{c_1}{c_2} \frac{t}{l} \left(\frac{d}{c}\right)^2 \quad . \tag{3.37}$$

Equation (3.37) shows that for practical cases the τ_{adh}/σ_{adh} ratio at the critical section of a sandwich member is small enough, thus allowing us to neglect the mode II effects in the fracture of the adhesive. Subsequently, the fracture mechanics approach to the problem predicts debonding failure when

$$\sigma_{adh}\sqrt{\pi a} = K_{ICadh} \quad , \tag{3.38}$$

where K_{ICadh} is the critical stress intensity factor for the adhesive and a is an initial flaw size; inherent in the flaw size is significant uncertainty. Substituting (3.35) in (3.38) we solve for the failure load P which is given as

$$P = c_1 \frac{K_{ICadh}}{\sqrt{\pi a}} b \frac{d^2}{c} \frac{t}{l} \quad . \tag{3.39}$$

This approach is useful in obtaining an approximate solution for the initiation of fracture in the adhesive layer. However, it has several limitations: it does not explain why the crack propagates parallel to the face-core interface and does not account for the contribution of the release of strain energy in the face and core to the driving force to propagate the crack.

In summary, the debonding mechanism, looked upon two different points of view can be described by either equation (3.34) or equation (3.39). The values of the parameters involved in both these equations have to be determined experimentally and which of the two equations is more realistic will be shown from experimental results, as it will be presented in Chapter 4.

3.6 CORE SHEAR

If the cell-wall material of the core has a plastic yield point, which is the case when we deal with rigid polyurethane foams, then the foam as a whole may yield in shear . In other words, the combination of normal and shear stresses in an element of the core is such that the resulting maximum shear stress, $\tau_{c_{max}}$, reaches a critical value, τ_c^*, then the core will fail plastically in shear. The critical value τ_c^* is the shear strength of the core corresponding to significant deviation from linearity and to initiation of a yielding plateau in the shear stress-strain diagram. Therefore, the condition for a shear-type of core failure is

$$\tau_{c_{max}} = \tau_c^* \quad . \tag{3.40}$$

This type of failure will initiate at the "most critical" element of a critical section of a beam. The critical section is the one where the combination of normal and shear stresses is the most severe, while the most critical element is one at the extreme core fibre where the normal stress takes its maximum value (assuming constant shear stress distribution in the core). This is shown in Fig. 3.7. The maximum

shear stress in a core element is given by

$$\tau_{c_{max}} = \sqrt{\frac{\sigma_c^2}{4} + \tau_c^2} \quad . \tag{3.41}$$

The shear strength of the core is related to the solid core material yield stress according to the formula

$$\tau_c^* = c_4 \left(\frac{\rho_c}{\rho_s}\right)^B \sigma_{ys} \quad , \tag{3.42}$$

where c_4 and B are constants which have to be determined experimentally. Recent work [15] has shown that c_4 and B should be approximately equal to 0.30 and 1.50, respectively.

The stresses σ_c and τ_c are given as follows:

$$\sigma_c = \frac{P l E_c c}{c_1 b t d^2 E_f} \quad , \tag{3.43a}$$

$$\tau_c = \frac{P}{c_2 b c} \quad . \tag{3.43b}$$

Using the relationship between E_c and E_s (equation (3.28)), substituting (3.43a) and (3.43b) in (3.41) and equating the right hand side terms of (3.41) and (3.42) we obtain the shear failure criterion for rectangular sandwich beams:

$$P = \frac{c_4 \left(\frac{\rho_c}{\rho_s}\right)^B \sigma_{ys} b}{\sqrt{\left(\frac{c_3 \left(\frac{\rho_c}{\rho_s}\right)^A E_s c}{2 c_1 \frac{t}{l} E_f d^2}\right)^2 + \left(\frac{1}{c_2 c}\right)^2}} \quad . \tag{3.44}$$

3.7 CORE TENSION

Similar arguments as the ones presented for the core shear failure mode apply to the case of tensile failure of the core of a rectangular sandwich beam. When the combination of normal and shear stresses in an element of the core is such that the resulting maximum principal tensile

stress, σ_1, reaches the tensile strength of the core, $\sigma^*_{c,t}$, then the core will fail in tension. Again the tensile strength of the core corresponds to significant deviation from linearity and to initiation of a yielding plateau in the tensile stress-strain diagram. We state that the criterion for a tensile-type failure of the core can be expressed as

$$\sigma_1 = \sigma^*_{c,t} \quad . \tag{3.45}$$

This type of failure will initiate at the most critical element of a critical section in the member. The critical section is the one where the combination of normal and shear stresses is the most severe, and the most critical element is at the extreme core fibre where the normal stress takes its maximum value assuming that the shear stress distribution in the core is constant (Fig. 3.7). The maximum principal stress in a core element is

$$\sigma_1 = \frac{\sigma_c}{2} + \sqrt{\frac{\sigma_c^2}{4} + \tau_c^2} \quad . \tag{3.46}$$

The tensile strength of the core is related to the solid core material yield stress according to the equation

$$\sigma^*_{c,t} = c_5 \left(\frac{\rho_c}{\rho_s}\right)^C \sigma_{ys} \quad . \tag{3.47}$$

where c_5 and C are constants which have to be determined experimentally. For a plastic type of behavior of the core at failure the constants c_5 and C should be approximately equal to 0.30 and 1.50, respectively [15].

The stresses σ_c and τ_c are given by equations (3.43). Taking into account the relationship between E_c and E_f (equation (3.28)), substituting (3.43) in (3.46) and equating the right hand side terms of (3.46) and (3.47) we obtain the tensile failure criterion for rectangular sandwich beams in the form

$$P = \frac{c_5\left(\frac{\rho_c}{\rho_s}\right)^C \sigma_{ys} b}{\frac{c_3\left(\frac{\rho_c}{\rho_s}\right)^A E_s c}{2c_1 \frac{t}{l} E_f d^2} + \sqrt{\left(\frac{c_3\left(\frac{\rho_c}{\rho_s}\right)^A E_s c}{2c_1 \frac{t}{l} E_f d^2}\right)^2 + \left(\frac{1}{c_2 c}\right)^2}} \quad . \qquad (3.48)$$

Sometimes, sandwich members which are properly designed to avoid tensile (plastic) yielding may fail in a catastrophic way by fast fracture. This is possible to happen when we deal with a specific type of rigid foams, known as glassy or brittle foams. The study of the behavior of that particular type of foams is outside the scope of this work.

3.8 CORE COMPRESSION

The mechanism is quite similar to tensile (plastic) failure: when the maximum principal stress, σ_1, reaches the compressive strength of the core, $\sigma^*_{c,c}$, then the core will fail in compression. Following the arguments for the shear and tensile strengths of the core, the compressive strength of the core corresponds to significant deviation from linearity and to initiation of a yielding plateau in the compressive stress-strain diagram. We can now state that the criterion for a compressive-type failure of the core is

$$\sigma_1 = \sigma^*_{c,c} \qquad (3.49)$$

and this type of failure will initiate at the most critical element of a critical section in the member (see comments following equation (3.45)). Fig. 3.7 is relevant but this time failure will initiate in a critical element at the compressive extreme core fibre. The maximum principal stress in a core element is given by equation (3.46) while the compressive strength of the core can be written as

$$\sigma^*_{c,c} = c_6\left(\frac{\rho_c}{\rho_s}\right)^D \sigma_{ys} \quad . \qquad (3.50)$$

Again, the constants c_6 and D are to be determined experimentally.

Performing similar substitutions as previously, the equation describing the core compression failure mode for rectangular sandwich beams is the same as (3.48) with c_6 and D standing for c_5 and C, respectively.

3.9 FAILURE MODE MAPS

For each possible failure mode for rectangular sandwich beams, an equation was obtained describing the load P at which the mode occurs, given the material properties, the beam geometry and the loading and support conditions. By equating pairs of these equations, another set of equations describing the transition from one failure mode to another can be obtained. For example, the failure equations for face yielding and face wrinkling are (3.19) and (3.20), respectively. Transition from one of these two failure modes to the other is described by

$$c_1\sigma_{yf}b\frac{d^2}{c}\frac{t}{l} = 0.57c_1c_3^{2/3}E_f^{1/3}E_s^{2/3}\left(\frac{\rho_c}{\rho_s}\right)^{2A/3}b\frac{d^2}{c}\frac{t}{l} \qquad (3.51)$$

or

$$\frac{\rho_c}{\rho_s} = \left(\frac{\sigma_{yf}}{0.57c_3^{2/3}E_f^{1/3}E_s^{2/3}}\right)^{3/2A} . \qquad (3.52)$$

Given the materials properties the right hand side of equation (3.52) can be evaluated exactly, providing us with information about the foam density, ρ_c, which corresponds to the transition between face yielding and wrinkling.

As a second example, consider the equations for face yielding and core shear failure modes, (3.19) and (3.44) respectively. Transition between these modes occurs when

$$c_1\sigma_{yf}b\frac{d^2}{c}\frac{t}{l} = \frac{c_4\left(\frac{\rho_c}{\rho_s}\right)^B\sigma_{ys}b}{\sqrt{\left[\frac{c_3\left(\frac{\rho_c}{\rho_s}\right)^A E_s c}{2c_1\frac{t}{l}E_f d^2}\right]^2+\left(\frac{1}{c_2 c}\right)^2}} . \qquad (3.53)$$

A more careful examination of the transition equations between pairs of failure modes reveals that if $c \simeq d$ these equations do not include b, c

and d as variables. Therefore, given the material properties and loading and support conditions, the transition equations depend only on the t/l and ρ_c/ρ_s ratios. This implies that we can plot the transition equations on a diagram with axes corresponding to the two above mentioned ratios. The resulting "failure mode map" indicates the regions in which each failure mode is dominant. This is important: for a given rectangular sandwich beam with known loading-support conditions and material properties (i.e. given ρ_c/ρ_s and t/l ratios) we will be able by just looking at the failure mode map to recognize the nature of the imminent mode of failure. Then, by going to the corresponding failure mode equation, we will be in a position to evaluate the maximum load that the member can stand. This is one of the most significant findings of this work.

One can realize that in order to plot a realistic failure mode map we must know the values of all the parameters involved in the equations describing the failure loads for each mode. Such values must be determined experimentally, and this is one of the topics of the subsequent Chapter.

3.10 SUMMARY

Equations describing the face yielding, face wrinkling, debonding, core shear, core tension and core compression failure modes for rectangular sandwich beams have been developed in this Chapter. For the debonding mechanism, two different possible approaches were used yielding in a set of two equations. As it will be presented in Chapter 4, which of the two equations for this failure mode is more realistic, will be experimentally determined. The failure equations are summarized here for convenience:

1) Face yielding:

$$P = c_1 \sigma_{yf} b \frac{d^2}{c} \frac{t}{l} \quad .$$

2) Face wrinkling:

$$P = 0.57 c_1 c_3^{2/3} E_f^{1/3} E_s^{2/3} \left(\frac{\rho_c}{\rho_s}\right)^{2A/3} b \frac{d^2}{c} \frac{t}{l} \quad .$$

3) Debonding:

Adhesive shear strength approach:

$$P = c_2 \tau^*_{adh} bc \quad .$$

Fracture mechanics approach:

$$P = c_1 \frac{K_{ICadh}}{\sqrt{\pi a}} b \frac{d^2}{c} \frac{t}{l} \quad .$$

4) Core shear:

$$P = \frac{c_4 \left(\frac{\rho_c}{\rho_s}\right)^B \sigma_{ys} b}{\sqrt{\left(\frac{c_3 \left(\frac{\rho_c}{\rho_s}\right)^A E_s c}{2c_1 \frac{t}{l} E_f d^2}\right)^2 + \left(\frac{1}{c_2 c}\right)^2}} \quad .$$

5) Core tension:

$$P = \frac{c_5 \left(\frac{\rho_c}{\rho_s}\right)^C \sigma_{ys} b}{\frac{c_3 \left(\frac{\rho_c}{\rho_s}\right)^A E_s c}{2c_1 \frac{t}{l} E_f d^2} + \sqrt{\left(\frac{c_3 \left(\frac{\rho_c}{\rho_s}\right)^A E_s c}{2c_1 \frac{t}{l} E_f d^2}\right)^2 + \left(\frac{1}{c_2 c}\right)^2}} \quad .$$

6) Core compression: same as in 5) with c_6 and D instead of c_5 and C, respectively.

The parameters involved in the above failure equations are also summarized here:

P : failure load

c_1, c_2 : constants depending on the loading-support conditions

b : width of beam

c : depth of core

d : distance between center-lines of opposite faces

t : face thickness

l : span

ρ_c : core density

ρ_s : solid core material density

E_f : elastic modulus for face

E_s : elastic modulus for solid core material

σ_{yf} : yield strength of face

τ^*_{adh} : shear strength of adhesive

K_{ICadh} : fracture toughness of adhesive

a : initial crack half-length

σ_{ys} : yield strength of solid core material

c_3, A : constants in the core-compressive modulus equation

c_4, B : constants in the core shear strength equation

c_5, C : constants in the core tensile strength equation

c_6, D : constants in the core compressive strength equation

Transitions between pairs of failure modes can be described by equating the corresponding equations for the load P. This leads to the idea of constructing a failure mode map with parameters the ρ_c/ρ_s and t/l ratios, providing information about the mode that will occur for given member sizes, materials and loading-support conditions.

The experimental determination of the parameters involved in the failure mode equations and the construction of failure mode maps are presented, among others, in Chapter 4.

CHAPTER 4

EXPERIMENTAL RESULTS - FAILURE MODE MAPS

4.1 GENERAL

The scope of this Chapter is to present the experimental results for the failure of sandwich beams and, using these results, to construct failure mode maps for rectangular sandwich beams. A set of experiments was carried out to determine the parameters relating to the face and core properties in the failure mode equations. Using the values of the measured parameters the failure equations were finalized and used to obtain the failure mode maps. Based on the configuration of these maps and taking into account practical design requirements a series of sandwich beams was designed to be tested to failure, in order to verify the validity of the failure map. These tests and their results are described here; in addition, they are also used to obtain a final failure mode map for rectangular sandwich beams.

4.2 FACE YIELD STRENGTH

The load at which face yielding occurs depends on the yield strength of the face material. The material used as face material throughout this study was aluminium (alloy no. 1100-H14). In order to measure its yield strength five specimens were loaded in tension using an Instron machine [4]. The shape of a typical specimen is shown in Fig. 4.1 along with a typical tensile load-strain curve corresponding to one of the five tests that were conducted.

The yield strength on such a curve corresponds to the first deviation from linearity. The values of the yield stresses measured are summarized below as follows:

Specimen #	Yield stress (psi)
1	11932
2	12545

3	12874
4	12015
5	12975

The mean value of the above values is 12468 psi (86 Mpa). We have thus obtained the face material yield strength, σ_{yf}, which can readily be used in equation (3.19).

4.3 FOAM COMPRESSIVE STRENGTH AND ELASTIC MODULUS

According to the discussion presented in Chapter 3, the foam elastic modulus and compressive strength are related to properties of the solid core material. These relationships are given by equations (3.28) and (3.50) with the observation that the constants c_3, A, c_6 and D are to be determined experimentally. To measure these constants a series of cubic foam specimens 2x2x2 inches^3 were tested in compression, using an Instron machine with a maximum load capacity of 10000 lbs [5]. Four different foam densities were used, 4, 6, 10, and 20 lb/ft^3. Taking the density of the solid polyurethane to be 75 lb/ft^3 [15], this gives ratios of ρ_c/ρ_s of 0.0533, 0.08, 0.13 and 0.27.

The anisotropy in the material was measured by testing cubic specimens in three directions: one parallel to the rise direction and the other two perpendicular, thus examining the material properties in three orthogonal directions (Fig. 4.2).

Typical compressive load-deflection curves for specimens made of all four densities mentioned above and for loading parallel to all three directions are given in Fig. 4.3-4.10. The results of the tests are summarized in Table 4.1. It should be noted that five specimens were tested for each loading case. The elastic moduli were evaluated using the straight portion of the load-deflection curves while the compressive strengths were evaluated at the intersection of the yielding plateau with the straight portion corresponding to linear behavior. By inspection of the values in Table 4.1 one may derive the useful result that the foam has the same properties in both directions perpendicular to the rise and different in the rise direction. We can therefore separate the foam properties using as a basis the rise direction as follows: the properties differ between the rise direction and any other direction perpendicular to that. Taking the average values of Table

4.1, we can now summarize the results obtained from the series of compression tests as follows:

Density ratio, ρ_c/ρ_s	$E_{c_{\parallel}}$ (psi)	$E_{c_{\perp}}$ (psi)	$\sigma^*_{c,c_{\parallel}}$ (psi)	$\sigma^*_{c,c_{\perp}}$ (psi)
0.0533	4418	1897	109.45	39.65
0.08	5289	3610	170.05	133.50
0.13	12174	6850	327.60	244.30
0.27	29677	30807	1082.00	1119.00

The subscript $\parallel$ denotes the rise direction while the subscript $\perp$ denotes any other perpendicular to that. In order to avoid any confusion regarding the loading directions, we make the pre-agreement to treat the case where stresses develop perpendicular to the rise direction only. That means that in a typical flexural loading condition of a rectangular beam the rise has to be parallel to the height of the beam. Based on this pre-agreement, we can now continue taking into account properties of the core material only perpendicular to the rise direction.

The results of the compression tests are now plotted in log-log scale as shown in Fig. 4.11 and 4.12. The linear regression analysis based on the test results yields the following equations for the elastic modulus and compressive strength of the foam:

$$\frac{E_c}{E_s} = 1.13\left(\frac{\rho_c}{\rho_s}\right)^{1.71} , \tag{4.1}$$

$$\frac{\sigma^*_{c,c}}{\sigma_{ys}} = 0.82\left(\frac{\rho_c}{\rho_s}\right)^{1.98} . \tag{4.2}$$

The lines corresponding to these equations are shown in Fig. 4.11 and 4.12 respectively. The subscripts denoting the loading direction have been dropped under the assumption that we will no longer deal with the direction of rise. The values of 232 Ksi (1600 Mpa) and 18.4 Ksi (127 Mpa) were used for the elastic modulus, E_s, and the yield strength, σ_{ys}, of the unfoamed solid core material, respectively [25].

If we compare equations (4.1) and (4.2) with (3.28) and (3.50) we

find that we have experimentally obtained the values of the constants c_3, A, c_6 and D involved in the failure mode equations. These are:

$$c_3 = 1.13 \ , \ A = 1.71$$
$$c_6 = 0.82 \ , \ D = 1.98$$

Data in the literature suggest values of c_3 and c_6 of 1 and 0.3. A and D theoretically found to be 2 and 1.5 [15]. One can thus consider the experimental procedure and results presented in this section reliable.

4.4 FOAM SHEAR STRENGTH

As it was discussed in Chapter 3, we need to relate the shear strength of the rigid foam to its density, after doing some normalization with respect to the properties of the solid core material (see equation (3.42)). The constants c_4 and B involved in equation (3.42) have to be determined experimentally. For this purpose, it was decided that five specimens of each of the densities of 4, 6, 10 and 20 lb/ft^3 be tested in direct shear [6]. In order to simulate a pure shear condition the specimens were tested as is shown in Fig. 4.13. All specimens were identically formed as parallelepiped prisms with dimensions 1x1x3 inches. They were rigidly supported by means of 0.5x1x5 inch steel plates bonded to the facings as shown in the above Figure. The load was applied at the ends of the rigid plates in tension, using an Instron machine. As we were interested only in evaluating the maximum strength from the shear stress-strain curves, the measurement of displacements was not accurate (horizontal axis). A typical curve is shown qualitatively in Fig. 4.14 together with the definition of maximum (or ultimate) shear strength.

In the experimental procedure we are interested in shear stresses developed in the plane of the rise direction (see discussion in paragraph 4.4). In order to achieve this, the foam specimens were bonded to the steel plates in such a manner that the rise direction was perpendicular to the face of the plates. Therefore we should keep in mind that all the results obtained correspond to development of shear stresses in the plane of the rise direction. All experimental results from foam shear tests are summarized in Table 4.2. Taking the average of the values in this Table we have the following results:

Density ratio, ρ_c/ρ_s	0.0533	0.08	0.133	0.267
τ_c^* (psi)	72	112.8	246	801.8

The findings of the shear tests can now be plotted in log-log scale as shown in Fig. 4.15, where a linear regression line is passed through the points of experimentally measured values for the shear strength.

Finally, a linear regression analysis based on these values yields the following equation for the shear strength of the rigid polyurethane foam:

$$\frac{\tau_c^*}{\sigma_{ys}} = 0.31\left(\frac{\rho_c}{\rho_s}\right)^{1.52} \quad . \tag{4.3}$$

Again here, the values of 18.4 Ksi (127 Mpa) and 75 lb/ft^3 were used for the solid foam material yield strength and density, respectively.

Comparing equation (4.3) with (3.42) we are now in a position to know the values of the constants c_4 and B involved in the failure mode equations. These are:

$$c_4 = 0.31 \ , \ D = 1.52$$

Data available in the literature suggest that c_4=0.3. In theory D is equal to 1.50 [15]. Therefore, one could obviously recognize an extremely good agreement of experimental results with theory.

4.5 FOAM TENSILE STRENGTH

Equation (3.47) relates the foam tensile strength, $\sigma_{c,t}^*$, to its density, ρ_c, and to properties of the unfoamed, solid core material. The unknown parameters c_5 and C involved in equation (3.47) were determined experimentally. To do this, the foam specimens were tested in tension, using an Instron machine with gripping devices [7]. The testing apparatus with a typical specimen is shown in Fig. 4.16. Four different foam densities were used, 4, 6, 10 and 20 lb/ft^3, resulting in ρ_c/ρ_s ratios of 0.0533, 0.08, 0.13, 0.27 respectively. For each density value five specimens were cut. Therefore the total number of foam tensile tests that were performed was twenty. In the experimental

procedure we were interested for stresses developed perpendicular to the rise direction. Considering this, all specimens were appropriately cut.

Typical tensile load-deflection curves are given in Fig.4.17-4.20, one for each different foam density. Based on the values of the ultimate loads obtained from such curves the foam tensile strength was then computed, and the results for all specimens are summarized in Table 4.3. Taking the average of the values in this Table, for each density, we obtain the following results for the tensile strength:

Density ratio, ρ_c/ρ_s	0.0533	0.08	0.133	0.267
$\sigma^*_{c,t}$ (psi)	98.56	158.39	354.38	892.04

The results of the foam tensile tests can now be plotted in log-log scale as shown in Fig. 4.21, where a linear regression line is passed through the points of experimentally measured values for the tensile strength.

Finally, a linear regression analysis based on these results yields the following equation for the tensile strength of the rigid polyurethane foam:

$$\frac{\sigma^*_{c,t}}{\sigma_{ys}} = 0.31\left(\frac{\rho_c}{\rho_s}\right)^{1.39} \quad . \tag{4.4}$$

The values of 18.4 Ksi (127 Mpa) and 75 lb/ft^3 were used for the solid foam material yield strength and density, respectively.

A comparison of equations (3.47) and (4.4) reveals that the values of the parameters c_5 and C involved in the failure mode equations are 0.31 and 1.39, respectively. The expected values [15] for c_5 and C are 0.30 and 1.50, respectively. We can therefore visualize that the agreement of experimental results with theory is quite satisfactory.

4.6 ADHESIVE SHEAR STRENGTH

The shear strength of the adhesive, τ^*_{adh}, used in the equation describing the debonding mechanism, is a property of the specific adhesive used at the interface between the face and the foam. Any time

a new adhesive is used for bonding the two materials, one has to determine experimentally its shear strength. The adhesive employed in this study was polyester resin and its shear strength was measured as shown in Fig. 4.22. Steel plates were sand-blasted and glued with polyester resin and then subjected to tension after a cure of two days. In a way similar to that presented in section 4.4 for the foam shear strength, eight tests were carried out and the results obtained are summarized here:

Test, #	Adhesive shear strength, τ^*_{adh} (psi)
1	1973
2	1982
3	1804
4	2135
5	1771
6	1767
7	1993
8	2201

The mean value of these results is 1953 psi (13.5 Mpa) and the standard deviation 153 psi, resulting in a coefficient of variation of 8%. Therefore, for the adhesive used in this study we will consider:

$$\tau^*_{adh} = 1953 \text{ psi}$$

4.7 ADHESIVE CRITICAL STRESS INTENSITY FACTOR

Based on the fracture mechanics approach for the debonding mechanism in sandwich beams, in order to define the failure load (see equation (3.39)), we must evaluate the fracture toughness, K_{ICadh}, of the adhesive used. Fig. 4.23 shows the experimental configuration of a typical test for evaluating the toughness, G_{Cadh} of the adhesive [8]. The parameters in Fig. 4.23 are related with the formula

$$G_{Cadh} = \frac{T}{3BEI}\left[3(a+a_0)^2 + h^2\right] ,$$

with $I=Bh^3/12$ and $a_0=0.6h$. For each test for the evaluation of the

fracture properties of the adhesive two steel plates were glued together with polyester resin of thickness 2h, having an initial flaw size a, according to Fig. 4.23. The plates were appropriately gripped and subject to tension with an Instron machine. The load T corresponding to the propagation of the crack, a, was recorded and used in equation (4.5) for the evaluation of the product $G_{Cadh}E$.

Five different series of tests were conducted, with the parameter a taking values 0.197 inch (0.005m), 5.906 inch (0.15m), 7.874 inch (0.20m), 9.842 inch (0.25m) and 11.811 inch (0.30m). For each value of a ten tests were performed. In each test the following values for B and h were considered:

B = 0.787 inch (0.02m) , h = 0.118 inch (0.003m).

The results of all series of tests are summarized in Table 4.4. For each of the five different test series the critical stress intensity factor, K_{ICadh}, was evaluated as the square root of the product $G_{Cadh}E$ obtained by equation (4.5). Fig. 4.24 shows the variation of K_{ICadh} with the initial crack length a. It is summarized as follows:

a (in)	0.197	5.906	7.874	9.842	11.811
K_{ICadh} (Ksi·in$^{1/2}$)	0.381	0.424	0.398	0.378	0.417

Finally, the mean value for the critical stress intensity factor for the adhesive was obtained based on all the experimental results, and is K_{ICadh}=0.40 Ksi·in$^{1/2}$ (0.44 MNm$^{-3/2}$).

4.8 SUMMARY OF EXPERIMENTAL RESULTS

All series of tests presented so far aimed at evaluating the parameters involved in the failure mode equations which were obtained analytically in Chapter 3. Mean values, standard deviations and coefficients of variation for all these parameters are given below for convenience:

Parameter	Mean value	Standard deviation	Coeff. of variation
σ_{yf}	12468 psi	435 psi	3.5%
τ^*_{adh}	1953 psi	153 psi	8%

K_{ICadh}	0.40 Ksi·in$^{1/2}$	0.038 Ksi·in$^{1/2}$	9.6%
c_3	1.13	0.09	8%
A	1.71	0.14	8.2%
c_4	0.31	0.027	8.7%
B	1.52	0.13	8.5%
c_5	0.31	0.036	11.6%
C	1.39	0.11	7.9%
c_6	0.82	0.08	9.7%
D	1.98	0.17	8.6%

Other parameters used in the failure equations were assumed as follows:

$$\rho_s = 75 \text{ lb/ft}^3$$
$$E_f = 10153 \text{ Ksi}$$
$$E_s = 232 \text{ Ksi}$$
$$\sigma_{ys} = 18.4 \text{ Ksi}$$

4.9 FAILURE MODE MAPS

In Chapter 3 we developed a set of equations describing each possible failure mode for a rectangular sandwich beam. Each equation gives the load P at which the corresponding failure mode will occur, given the material properties, the beam geometry and the loading and support conditions. The parameters involved in the failure mode equations were determined experimentally and the results were presented in previous sections of this Chapter. Substituting for these parameters, the failure equations can be written as functions of the ratios t/l and ρ_c/ρ_s.

We have a total of seven failure mode equations. However, the debonding mechanism is described by two alternate expressions (equations (3.34) and (3.39)). Therefore, we have two possible sets of failure equations for rectangular sandwich beams, each one containing six equations. Moreover, upon substitution of the experimentally determined parameters into the failure equations one finds that the load which corresponds to the core compression failure is always higher than the load which describes the core tension failure. This happens because the parameters c_6 and D are larger than the parameters c_5 and C,

respectively. This implies that a core compression failure mode is not expected to occur, because the core tension failure mode will develop first. Under this observation we will not consider the core compression failure equation further. As a result, we finally have two possible sets of equations with five equations each. The only difference between the two sets is the expression for the debonding failure. Following the procedure of section 3.9 we can now obtain a failure mode map for each set of equations.

Considering the approach which uses the shear strength of the adhesive to describe the debonding mechanism, we developed the failure mode map shown in Fig. 4.25 for a simply supported beam loaded at mid-span with a concentrated load. The adhesive fracture mechanics approach for the debonding mechanism resulted in the construction of failure mode maps such as those shown in Fig. 4.26-4.27, for different initial crack lengths, a. We must emphasize that each failure mode map corresponds to a specific loading and support configuration. The experimentally obtained mean values of the parameters involved in the failure equations were used for the construction of the maps presented here and the influence of the variation in these parameters to the failure mode maps is discussed in the subsequent Chapter.

The failure maps in Fig. 4.26-4.27 predict that failure mostly happens by debonding, which, as we will discuss later, was not verified by the experimental results. However, we should notice that the fracture approach used here is quite simplistic and needs additional work. Alternatively, the failure mode map in Fig. 4.25 is divided in four regions, each one corresponding to a failure mode. This map provides qualitative information regarding the imminent mode of failure for simply supported rectangular sandwich beams. We can clearly observe that face failure is expected for small t/l ratios. More specifically, the face is expected to wrinkle when we deal with small ρ_c/ρ_s ratios (weak core) and is expected to yield when the ρ_c/ρ_s ratio is larger. For t/l increasing, when ρ_c/ρ_s is small (weak core) the core is expected to fail in shear, while when ρ_c/ρ_s is larger the face is expected to yield; for very large t/l and ρ_c/ρ_s ratios a debonding type of failure is expected. These observations are intuitively justified. Indeed, as experimental results will reveal at subsequent sections, the failure mode map in Fig. 4.25 seems to be quite reliable, giving thus a

"preference" to the adhesive shear strength approach for the debonding mechanism between the face and the core.

Usual design requirements [2] imply that the face thickness over span ratio, t/l, vary in the range 0.0002-0.01. A slightly wider range has been used for the construction of failure mode maps in this study (0.0001-0.1). Moreover, the ρ_c/ρ_s ratio was assumed to vary in the range 0.01-1, which covers all feasible core densities. The validity of a possible failure mode map is now questionable. Do test results, in general, agree with one of the failure mode maps shown in Fig. 4.25-4.27? This is discussed in the subsequent Chapter. The need of test data lead to a series of tests described next.

4.10 BEAM TESTS-EXPERIMENTAL METHOD

In order to check the failure equations and the failure mode maps developed above we decided to test a series of sandwich beams with rigid polyurethane foam cores to failure. The beams were designed with varying core densities and face thickness to span ratios. A list of the beam designs used is given in Table 4.5. Four beams of each geometry were made by cutting the foam and aluminium to the correct size and then bonding them together with polyester adhesive resin. Before the bonding procedure the aluminium faces were sand-blasted. The specimens were clamped together using weights and the adhesive was cured overnight.

The beams were tested in three-point bending using roller supports and a screw jack to apply the load. In order to avoid any local crushing of the core near the region of the concentrated load, P, a steel plate was used to distribute this load. The load-deflection behavior of each beam was plotted using an X-Y recorder. Photographs were taken of each beam at the first deviation from linearity in the load-deflection curve and as the failure progressed.

4.11 RESULTS OF BEAM TESTS

The tests on the sandwich beams produced three main modes of failure: face yielding, face wrinkling and core shear. Out of 124 beams tested 3 failed by debonding and 4 failed by local crushing of the core. Each failure mode gave a distinct load-deflection curve; typical examples of such curves are shown in Fig. 4.28. All curves are linear elastic initially.

The load-deflection curves of beams that failed by face yielding showed a flattening corresponding to yield followed by eventual face wrinkling after extensive yielding. Strong indication of face yielding was the presence of Luders bands on the tensile face of the specimens observed after unloading. Beams with higher density cores yielded more extensively than ones with lower density cores before face wrinkling occured; this was expected since the resistance provided by the higher density cores is greater. In order to be consistent with the development of the failure equation for the face yielding and with the measured yield strength of the aluminium, we measured the failure loads at the first deviation from linearity in the load-deflection curves.

The load-deflection curves of the beams that failed by plastic shearing of the core are similar to those for failure by plastic yield of the face; this was expected since the yielding in the core material results in a yield plateau. Since Luders bands were not observed in the face, there should be no confusion with the face yielding failure mode. In this case, the yielding is generally less extensive before the load-deflection curve is terminated by the formation of a diagonal shear crack in the specimen. The development of the equation that describes the core shear failure mode is based on the ultimate shear strength of the core. Therefore, for the core shear case, we measured the failure loads corresponding to the yield plateau in the load-deflection curves.

The beams that failed by face wrinkling behaved linearly-elastically up to the load at which wrinkling occured. Wrinkling resulted in a sudden drop in the load carried by the beam. This is where the failure load was measured.

Typical photographs of each failure mode are given in Fig. 4.29. Table 4.6 summarizes the measured failure loads and modes for all specimens tested and the coresponding calculated failure loads according to the equations developed in Chapter 3. The results indicate that the simplistic fracture mechanics approach for the debonding mechanism of the adhesive does not lead to results in agreement with the experiments. Hence, the failure mode maps given in Fig. 4.26-4.27 will not be considered any more in the present work. However, additional work needs to be done on a more accurate fracture mechanics approach to the debonding mechanism. The failure map in Fig. 4.25 turns out to be in a good agreement with the test results; further discussion of the

agreement between the analytical and experimental work will be presented in Chapter 5. All test results are now plotted on the failure map based on the adhesive shear strength approach for the debonding mechanism. This is illustrated in Fig. 4.30. Fig. 4.31 shows the failure mode map under consideration with load contours which were constructed based on the failure load equations; in order to compare the validity of these contour lines with test results, their construction corresponds to sandwich beams with width b=1" and core depth c=1", which was the case for most of the beam designs that were tested to failure (d is assumed equal to c). On the failure map of Fig. 4.31 the average values of the measured failure loads are also plotted; this plot indicates excellent agreement between predicted and measured failure loads.

4.12 SUMMARY

In this Chapter the experimental procedures are described and results are given for the evaluation of all parameters involved in the failure mode equations. The parameters obtained are in a quite satisfactory agreement with theoretically derived values for the material properties. These parameters are then used together with the failure mode equations given at the end of Chapter 3 for the construction of failure mode maps. These maps are diagrams which show the transitions between the failure modes. Assuming for a sandwich beam that its face is thin compared to its depth (i.e. $c \simeq d$), the failure mode maps can be constructed with variables the ratios of t/l and ρ_c/ρ_s only. Because we developed two possible equations for the debonding mechanism of the adhesive in sandwich beams, two sets of failure maps were constructed.

In order to check the failure equations and the failure loads, a set of beams with rigid polyurethane foams were tested to failure. Based on the test results the adhesive shear strength approach to the debonding mechanism of the adhesive seems to be justified; for this case results are in very good agreement with expected loads and failure modes. Three failure modes were produced by the beam tests: face yielding, face wrinkling and core shear. Further discussion and comparisons are the subject of Chapter 5.

CHAPTER 5

DISCUSSION

5.1 GENERAL

The consistency of all the experimental results related to the study of the failure modes of rectangular sandwich beams is discussed in this Chapter. In addition, the agreement between the analysis and measured loads and failure modes is also discussed. Based on the results, a simplification of the analysis is presented. Finally, the effect of the variation in the parameters involved in the failure equations, on the failure mode map is presented and some comments are given for the construction of failure maps for other cases.

5.2 DISCUSSION

Tests on the foam to be used in the core gave almost all the parameters involved in the failure equations. The results are summarized in section 4.8 together with the coefficients of variation for each parameter. The variation is of the order of 8% which is considered reasonable and acceptable. The conclusion is that the derivation of these parameters was done in a rather reliable manner.

Table 4.6 lists the calculated and average measured failure loads for each sandwich beam tested along with the mode of failure. The results are also plotted on the failure maps of Fig. 4.30 and 4.31. There is close agreement between the calculated and measured failure loads and in the mode of failure. The agreement is still good if we approximate the flexural rigidity of the member with $D = E_f btc^2/2$, except for the beams with large t/l ratio. However, using the more exact formula $D = E_f btd^2/2$, most of the calculated failure loads are within 10% of the measured loads, and all but 4 out of the 124 beams tested are within 15%.

Out of all the beams tested only 3 failed by debonding; no systematic trend in the design of the beams that failed by debonding could be detected. Most probably these beams had significant defects

introduced into the adhesive when the beams were prepared. It is interesting to note that in two out of the three cases in which debonding occurred, the failure load was close to that calculated for the predicted load. Since the beams tested cover most of the practical range of t/l and ρ_c/ρ_s we conclude that if some care is taken to avoid introducing defects into the adhesive when making sandwich beams, debonding is unlikely to occur. More work needs to be done on the debonding mechanism to fully understand it. A general observation is that the failure of sandwich beams with rigid foam cores is most likely to occur under face yield or face wrinkling or core shear. In comparison with the test results, the analytical formulas give excellent results for the face yield mode, are slightly unsafe for the face wrinkling mode and slightly conservative for the core shear mode. Given the structural sandwich beam the designer can predict the imminent mode of failure using the failure map, and then using the corresponding equation given at the end of Chapter 3 he should be able to evaluate the failure load. At this point, a safety factor could also be applied, depending on the member's importance.

5.3 MODIFICATION OF THE ANALYSIS

For small t/l (and t/c) ratios one can approximate the equivalent flexural rigidity of a sandwich beam as $E_f btc^2/2$. Relevant comments are given in section 3.2.

Moreover, the failure equation for the core shear can be simplified. For the combinations of core density, ρ_c/ρ_s, and the ratio of face thickness to span length, t/l, for which core shear is the dominant failure mode, the normal stresses in the core are negligible compared to the shearing stresses. In this case, the failure equation for core shear becomes simply:

$$P = c_2 c_4 (\rho_c/\rho_s)^B \sigma_{ys} bc \quad . \tag{5.1}$$

Using this simplified equation for core shear failure, and considering $c \simeq d$ in all failure equations, closed form solutions for the equations describing the transition between one failure mode and another can be found; for the modes shown on the failure map (Fig. 4.33) they are

listed in Table 5.1. This suggests that a simpler way of plotting the failure map for a sandwich panel would be to first assume that the normal stresses in the core are insignificant in the region in which core shear is the dominant failure mode. The map can then be plotted using the closed form solutions for the transition equations. Finally, the region in which core shear is the dominant failure mode should be checked to ensure that the normal stresses are small relative to the shearing stresses in the core.

As we noticed before, none of the foam cores failed in tension or compression. Normal stresses in the core are largest, relative to the shearing stresses, when the face thickness to span ratio, t/l, is small and the core relative density is high. But in this region of the failure mode map, normal stresses in the faces are also high. Tensile yield failure in the core precedes yield in the faces if:

$$\frac{\sigma^*_{c,t}}{\sigma_{c,t}} < \frac{\sigma_{yf}}{\sigma_f} \quad .$$

Using equations (3.7) for the normal stresses in the face and the core, and the general relationships for foam properties [15]:

$$\sigma_{c,t}/\sigma_f = E_c/E_f \quad ,$$

$$\sigma^*_{c,t} = 0.3(\rho_c/\rho_s)^{3/2}\sigma_{ys} \quad ,$$

$$E_c = (\rho_c/\rho_s)^2 E_s \quad ,$$

we observe that tensile yield failure of the core precedes tensile yield failure of the face if:

$$0.3(\rho_c/\rho_s)^{1/2}\frac{\sigma_{ys}}{E_s} < \frac{\sigma_{yf}}{E_f} \quad .$$

Foams used in the cores of sandwich panels generally have a relative density greater than 0.05, and the ratio of σ_{ys}/E_s for polymeric materials used to make the foam cores is generally about 1/20. The ratio σ_{ys}/E_f for metal face materials is usually about 1/1000 so that, in practice, tensile yielding of the face always precedes that of the

core.

5.4 VARIATIONS IN THE FAILURE MODE MAP

In this section we discuss the effect of the variation in all parameters involved in the failure mode equations, on the failure mode map. To study this effect, we constructed maps using the mean values of these parameters plus and minus one standard deviation. The maps thus obtained are given in Fig. 5.1-5.8.

The largest source of variation in the failure maps arises from the variability in the properties of the foam used in the core. In general, the maps have the same form as those shown in Chapter 4. The boundaries on the failure mode map are most sensitive to the parameters A and B, as might be expected as they act as exponents in the failure equations. All these effects are shown in Fig. 5.1-5.8. It is interesting to notice that core tension appears as a failure mode if C or c_5 varies. With solid lines we represent the boundaries based on the mean values of the parameters. Dashed and dotted lines represent the boundaries for the parameters plus and minus one standard deviation respectively.

5.5 FAILURE MAPS FOR OTHER CASES

The formulation given for the construction of failure maps for rectangular sandwich beams is general. For other loading and support conditions one only needs to change the parameters c_1 and c_2. As an example, we give a map for a simply supported beam with two concentrated loads applied at 1/3 and 2/3 of the span. This is shown in Fig. 5.9. The general form of this map is the same as that shown in Chapter 4.

Failure mode maps can also be constructed for sandwich plates with foam cores. The procedure is the same as that followed here: using the equations describing the normal and shearing stresses in the faces and the core of a sandwich plate and the equations describing how the core properties depend on core density, a set of failure equations for each mode of failure can be developed. The failure mode map can then be constructed by equating pairs of failure equations.

The maps developed here are useful in the minimum weight analysis of a sandwich beam of a given strength. This is the subject of the next Chapter.

CHAPTER 6

MINIMUM WEIGHT DESIGN FOR A GIVEN STRENGTH REQUIREMENT

6.1 GENERAL

In most applications, sandwich construction is used to reduce the weight of structural components. In this Chapter we describe how the weight of a sandwich beam with a foam core can be minimized for a given strength requirement. The analysis that follows assumes that both the face and core materials yield plastically and makes use of the failure mode map developed in Chapter 4. The analysis gives the thicknesses of the face and the core and the density of the core which minimize the weight of a rectangular sandwich beam of a given strength. The ideas developed here can also be applied to sandwich panels made from materials that fracture. However, failure equations for face and core fracture are required to do this.

6.2 ANALYSIS

Our purpose is to minimize the weight of a sandwich beam for a given strength. We assume that both the face and solid unfoamed core materials are known and that they yield plastically. We aim to find the values of the face thickness, t_{opt}, the core thickness, c_{opt}, and of the relative density of the core, $\rho_{c_{opt}}/\rho_s$, which minimize the weight of the beam for a given strength.

In Chapter 4 we developed a failure mode map for rectangular sandwich beams with aluminium faces and rigid polyurethane foam cores. This map is divided into four regions, each one corresponding to a failure mode. The modes that are shown are: face yielding, face wrinkling, core plastic shear and debonding. The results of tests on a wide range of sandwich beams verified the validity of the failure map. Debonding was not found to be a significant failure mode in the tests conducted. The equations describing each mode of failure are given in

Chapter 3. As we discussed in Chapter 5, the equations for the modes of failure that appear on the failure map can be simplified. For convenience, we list them in Table 6.1. Consider now the optimum design of the sandwich beam. One approach to the optimization analysis is to use each of the four failure equations of Table 6.1 in turn as the constraint equation and to optimize the beam design for each. A comparison of the four "optima" corresponding to the four failure modes would then give the minimum weight design. This beam design could then be plotted on the failure mode map to ensure that it failed in the assumed mode. Another approach is based on the observation that at the optimum design, the face and core will fail at the same load. If this were not the case, the unfailed component would be overdesigned and the weight of the member could be reduced further by reducing the weight of the unfailed component. Beam designs which give simultaneous face and core failure are those corresponding to one of the transition lines on the failure mode map. Based on this observation, we now proceed with the minimum weight analysis. We have to consider the analysis of two cases: first, simultaneous failure by face yielding and core shear, and then simultaneous failure by face wrinkling and core shear.

6.2.1 Simultaneous failure by face yielding and core shear

The load at which failure occurs by face yielding is P_{fy}:

$$P_{fy} = c_1 \sigma_{yf} bc \frac{t}{l} \quad . \tag{6.1}$$

Rearranging this to obtain the face thickness, t, in terms of the core thickness, c:

$$t = \frac{P_{fy}}{b} \frac{l}{c_1 \sigma_{yf} c} \quad . \tag{6.2}$$

The load at which failure occurs by core shear, P_{cs}, is given as:

$$P_{cs} = c_2 c_4 (\rho_c/\rho_s)^B \sigma_{ys} bc \quad . \tag{6.3}$$

Solving this equation for the relative density of the core, ρ_c/ρ_s, in terms of the core thickness, c:

$$\rho_c/\rho_s = \left(\frac{P_{cs}}{c_2 c_4 \sigma_{ys} bc}\right)^{1/B} . \qquad (6.4)$$

The expressions for face thickness and core density ((6.2) and (6.4)) can be substituted into the equation for the weight of the beam:

$$W = 2\rho_f blt + \rho_c blc \qquad (6.5)$$

or

$$W = 2\rho_f \frac{P_{fy} l^2}{c_1 \sigma_{yf} c} + \left(\frac{P_{cs}}{c_2 c_4 \sigma_{ys}}\right)^{1/B} (bc)^{1-1/B} l\rho_s . \qquad (6.6)$$

The optimum core thickness, c_{opt}, can now be found by setting the derivative of the weight equation with respect to the core thickness equal to zero:

$$\frac{\partial W}{\partial c} = 0 . \qquad (6.7)$$

Doing this, we find:

$$c_{opt} = \left[2 \frac{\rho_f}{\rho_s} \frac{P}{b} \frac{1}{c_1 \sigma_{yf}} \left(\frac{bc_2 c_4 \sigma_{ys}}{P}\right)^{1/B}\right]^{\frac{B}{2B-1}} . \qquad (6.8)$$

Note that we set $P_{cs} = P_{fy} = P$. Optimum values of t and ρ_c which minimize the weight of the beam are found by substituting equation (6.8) into equations (6.2) and (6.4). The result is:

$$t_{opt} = \frac{P}{b} \frac{1}{c_1 \sigma_{yf} \left[2 \frac{\rho_f}{\rho_s} \frac{P}{b} \frac{1}{c_1 \sigma_{yf}} \left(\frac{bc_2 c_4 \sigma_{ys}}{P}\right)^{1/B}\right]^{\frac{B}{2B-1}}} , \qquad (6.9)$$

$$\rho_{c_{opt}} = \rho_s \left(\frac{P}{bc_2 c_4 \sigma_{ys}}\right)^{\frac{1}{B}} \frac{1}{\left[2 \frac{\rho_f}{\rho_s} \frac{P}{b} \frac{1}{c_1 \sigma_{yf}} \left(\frac{bc_2 c_4 \sigma_{ys}}{P}\right)^{1/B}\right]^{\frac{1}{2B-1}}} . \qquad (6.10)$$

6.2.2 Simultaneous face wrinkling and core shear

The analysis for simultaneous face wrinkling and core shear is analogous. Face wrinkling occurs at a load, P_{fw}:

$$P_{fw} = 0.57 c_1 c_3^{2/3} E_f^{1/3} E_s^{2/3} (\rho_c/\rho_s)^{2A/3} bc(t/l) \qquad (6.11)$$

from which

$$t = \frac{P_{fw} l}{0.57 c_1 c_3^{2/3} E_f^{1/3} E_s^{2/3} (\rho_c/\rho_s)^{2A/3} bc} \quad . \qquad (6.12)$$

Using equation (6.3) for failure by core shear, we find:

$$\frac{\rho_c}{\rho_s} = \left(\frac{P_{cs}}{c_2 c_4 \sigma_{ys} bc}\right)^{1/B} \quad . \qquad (6.13)$$

Again, substituting these two expressions into the weight equation gives:

$$W = 2\rho_f blt + \rho_c blc =$$

$$= 2\rho_f \left[\frac{P_{fw} l^2}{0.57 c_1 c_3^{2/3} E_f^{1/3} E_s^{2/3} (\rho_c/\rho_s)^{2A/3} c}\right] + \left(\frac{P_{cs}}{c_2 c_4 \sigma_{ys}}\right)^{\frac{1}{B}} (bc)^{\left(1-\frac{1}{B}\right)} l \rho_s . \qquad (6.14)$$

The optimum design is again found by setting the derivative of the weight equation with respect to the core thickness equal to zero. Doing this we find:

$$c_{opt} = \left[-\frac{\rho_s}{2\rho_f}\left(\frac{3B-3}{2A-3B}\right)\left(\frac{P}{c_2 c_4 \sigma_{ys} b}\right)^{\frac{2A}{3B}+\frac{1}{B}} \frac{zb}{Pl}\right]^{\left(\frac{2A}{3B}-2+\frac{1}{B}\right)^{-1}} \qquad (6.15)$$

where $z = 0.57 c_1 c_3^{2/3} E_f^{1/3} E_s^{2/3}$.

The optimum values of the core density and the face thickness can be found by substituting equation (6.15) into equations (6.12) and (6.13). The result is:

$$\rho_{c_{opt}} = \rho_s \left(\frac{P}{c_2 c_4 \sigma_{ys} b c_{opt}} \right)^{1/B} \tag{6.16}$$

$$t_{opt} = \frac{Pl}{z(\rho_{c_{opt}}/\rho_s)^{2A/3} b c_{opt}} \tag{6.17}$$

The optimum design is now given comparing the resulting beam weight for the two cases. This should then be checked to ensure that the optimum beam design fails in the way assumed.

The ratio of the weight of the faces to that of the core is 1 for simultaneous face yielding and core shear and (3-3B)/(2A-3B) for simultaneous face wrinkling and core shear.

6.2.3 Other cases

One might argue that we have neglected the debonding failure mode in the analysis. The whole region in the failure map that corresponds to the debonding mode of failure, is associated with only one value of the failure load,

$$P_d = c_2 \tau^*_{adh} b c \quad . \tag{6.18}$$

This implies that the minimum weight design corresponds to a point within the debonding region for which both ρ_c/ρ_s and t/l are minimized. This point is the end of the face yielding-core shear transition line, towards the top and right of the failure map. In other words, the analysis in this case is exactly the same as that of section 6.2.1 with the restriction that

$$c_{opt} = \frac{P}{c_2 \tau^*_{adh} b} \quad . \tag{6.19}$$

We should also cover the possibility of simultaneous failure of the face by both yielding and wrinkling. The analysis in this case is analogous to that presented in sections 6.2.1 and 6.2.2. However, the weight that is obtained in this case is higher than the weight produced

by simultaneous failure by face wrinkling and core shear. This verifies the statement that for minimum weight design the face and core should fail simultaneously.

6.3 DISCUSSION

The analysis described above gives closed form solutions for the optimum weight design of sandwich beams subject to a strength constraint. It gives values of the face and core thicknesses and of the core density which minimize the weight of the sandwich beam assuming that the loading configuration is known and that the face and solid core materials fail plastically and are known.

The success of the method described above suggests that the analysis can be extended to other, more complex cases. In particular, it would seem possible to develop failure maps and a minimum weight analysis for face and core materials that fracture instead of yield; this would be useful in designing beams with fibre composite faces. In addition, it should also be possible to develop failure maps and a minimum weight analysis for sandwich plates.

In some applications, the design of the sandwich member must satisfy more than one constraint; for example, it may be required to have a given stiffness and strength. The analysis developed here suggests that this optimization problem can be solved by considering the minimum weight design for four different constraint conditions: stiffness and failure by face yielding; stiffness and failure by face wrinkling; stiffness and failure by core shear; and stiffness and failure by debonding. A comparison of the weights of the four resulting beam designs would then give the optimum design. Finally, the failure mode of the optimum design would have to be checked to ensure that it corresponded to the assumed failure mode for the optimization.

CHAPTER 7

SUMMARY-CONCLUSIONS

7.1 GENERAL

Structural members made of two thin stiff faces separated by a light-weight core are known as sandwich panels. The separation of the faces by the core increases the moment of inertia of the panel with little increase in weight, producing an efficient member for resisting bending and buckling loads. Because of this they are often used in applications where minimizing the weight of the panel is critical.

The scope of the present research work was first to identify and model the modes of failure in structural sandwich beams made of rigid polyurethane foam cores and aluminium faces, and to apply the results to the minimum weight design of composite members for a strength requirement.

Sandwich beams loaded in bending can fail in several ways. The tension and compression faces may fail uniaxially. Using aluminium faces this failure is characterized by yielding. The compression face may also buckle locally by "wrinkling". The core, too, can fail, although this seems to have attracted less attention than face failure. The most common mode of core failure is shear. Other possible modes are tensile or compressive yield. Finally the bond between the face and core can fail.

For each possible mode of failure, an equation was derived describing the load at which a sandwich beam with given geometry, loading and support conditions would fail. The analytical formulation of these equations was based on non-linear relationships between the foam and the solid core material properties. Another assumption was that the faces are thin relative to the core.

Two different approaches were considered for the formulation of the equation describing the debonding mechanism. One was based on the shear strength of the adhesive and another on the fracture mechanism

associated with the propagation of cracks at the face-core interface.

Each failure equation depends on three sets of variables: those relating to the loading configuration; those relating to the material properties of the face and the solid from which the core is foamed and those relating to the beam design. The beam design at which two failure modes occur simultaneously can be found by equating the failure equations for the two modes. For a given loading configuration and set of face and solid core properties, this produces a failure mode transition equation which can then be plotted on a diagram with axes for each of the beam design parameters to show the combinations of design parameters which give each failure mode. This is known as a failure mode map.

The parameters involved in the failure equations which are related to materials properties were determined experimentally. Such parameters were the face yield strength, the foam compressive strength, tensile strength and elastic modulus, and the adhesive shear strength and critical stress intensity factor. It was thus possible to construct two different failure mode maps, one corresponding to each debonding mechanism assumed.

Sandwich beams with rigid polyurethane foam cores and aluminium faces were made and tested to check the failure equations and the failure mode maps developed. The beams were tested in three-point bending. The load-deflection behavior of each beam was plotted and used to identify the failure load. Three main failure modes were produced by the beam tests: face yielding, face wrinkling and core shear. Out of 124 beams tested 3 failed by debonding and 4 by indentation of the core.

A comparison of the analytical and experimental results indicated that the failure equations can be simplified. This was done, and the new set of equations was used for the minimum weight design of sandwich beams for a strength requirement.

The optimum weight analysis was based on the observation that at the optimum design, the face and core will fail at the same load. If this were not the case, the unfailed component would be overdesigned. Beam designs which give simultaneous face and core failure are those corresponding to one of the transition lines on the failure mode map.

The analysis gave closed form solutions for the optimum design of composite beams subject to a strength constraint. It gave values of the face and core thicknesses and of the core density which minimize the weight of the beam assuming that the loading configuration is known and that the face and solid core materials fail plastically and are known. This was done for the first time, using realistic (non-linear) relationships between moduli and densities of the foam and unfoamed core material.

7.2 CONCLUSIONS

The failure modes that characterize the behavior of rectangular sandwich beams in bending can be described by analytical expressions for the load that corresponds to failure.

These expressions lead to the construction of failure mode maps which allow the designer to recognize the nature of the imminent failure mode of a given structural member with known loading conditions. Then, the corresponding equation yields the maximum load that the member can safely carry.

Two different expressions for the debonding mechanism were developed. None of the expressions was verified, since debonding was not observed as a mode of failure in the experimental procedure that was carried out. Further work is required to characterize debonding in sandwich beams.

A simplified way of constructing the failure mode map has been suggested based on the assumption that within the core shear failure regime the normal stresses in the core are small relative to the shearing stresses.

The non-linear relationships between the rigid polyurethane foam and the solid core material moduli and strengths were experimentally verified. Measured values were found in good agreement with these theoretically derived.

The polyurethane foam material was not found to be isotropic; different properties were measured in directions parallel and perpendicular to the rise.

The equation developed for the compressive failure of the core

gives always a higher load than that is predicted by the equation for the tensile failure of the core. That means that a core compressive type of failure is not expected to occur.

Tests on sandwich beams produced three main modes of failure: face yielding, face wrinkling and core shear. The failure equations for these three modes were found to accurately describe the load at failure.

Measured and expected failure loads were found in very good agreement, especially when the beam's flexural rigidity was approximated as $E_f btd^2/2$.

The failure mode map that was constructed based on the adhesive shear strength was verified by test results. However, debonding was not found to be an important mode of failure in the sandwich beams tested. Therefore, the boundaries of the debonding region within the failure mode map are not yet accurately determined.

If some care is taken to avoid introducing defects into the adhesive when making sandwich beams, debonding is rather unlikely to occur.

At the optimum weight design, the face and core will fail at the same load. This allows to obtain closed form solutions for the minimum weight design of sandwich beams subject to a strength constraint.

7.3 RECOMMENDATIONS FOR FUTURE RESEARCH

The mechanics of the debonding type of failure are not well understood. No satisfactory solution of this problem exists. Further research is required to understand the debonding mechanism and describe the load at which bond failure occurs in sandwich beams.

Other failure modes are possible for materials that fracture (brittle materials). The ideas presented in this work can be extended to such cases.

Similar failure equations and failure mode maps can be constructed for sandwich plates with foam cores. The procedure is the same as that followed here: using the equations describing the normal and shearing stresses in the faces and the core of a sandwich plate and the equations describing how the core properties depend on core density, a set of

failure equations for each mode of failure can be developed. The failure mode map can then be constructed by equating pairs of failure equations; the resulting equations describe the transition from one failure mode to another. In practice, the transition equations will probably be more complicated than those for beams.

The optimization analysis can be extended to multiple constraint conditions; one can impose both stiffness and strength requirements. In this case, the equations for stiffness, strength and weight should be appropriately combined to obtain the minimum weight design. The complexity of the equations will probably demand numerical solution of the resulting equations.

REFERENCES

1. Ackers, P. (1945), The efficiency of sandwich struts utilizing a calcium alginate core, R&M 2015 (U.K. Aeronautical Research Council, Farnborough, Hants.).

2. Allen, H.G. (1969), Analysis and Design of Structural Sandwich Panels. Pergamon, Oxford.

3. Ashby, M.F. and Jones, D.R.H. (1980), Engineering Materials: an Introduction to their Properties and Applications. Pergamon, Oxford.

4. ASTM Designation B557-84.

5. ASTM Designation D1621-73.

6. ASTM Designation C273-61.

7. ASTM Designation D1623-78.

8. ASTM STP 876 (1983), Delamination and Debonding of Materials. W.S. Johnson ed.

9. Benjamin, J.R. and Cornell, C.A. (1970), Probability, Statistics, and Decision for Civil Engineers. McGraw-Hill.

10. Bitner, J.L., Rushford, J.L., Rose, W.S., Huston, D.L. and Riew, C.K. (1981), Viscoelastic fracture of structural adhesives, J. Adhesion 13, 3-28.

11. CIBA-GEIGY Composites (Jan. 1980), Instruction sheet no. AGC. 33a (part 2).

12. Demsetz, L.A. and Gibson, L.J. (1986), Minimum weight design for stiffness in sandwich plates with rigid foam cores, Research Report No. R86-04, Department of Civil Engineering, M.I.T.

13. Easterling, K.E., Harrysson, R., Gibson, L.J. and Ashby, M.F. (1982), On the mechanics of balsa and other woods, Proc. R. Soc. London, Ser. A, 383, 31-41.

14. Gibson, L.J., Ashby, M.F., Schajer, G.S. and Robertson, C.I. (1982), The mechanics of two-dimensional cellular materials,

Proc. R. Soc. London, Ser. A, 382, 25-42.

15. Gibson, L.J. and Ashby, M.F. (1982), The mechanics of three-dimensional cellular materials, Proc. R. Soc. London, Ser. A, 382, 43-59.

16. Gibson, L.J. (1984), Optimization of stiffness in sandwich beams with rigid foam cores, J. Materials Science and Engineering, 67, 125-135.

17. Gibson, L.J. (1986), Class notes, Department of Civil Engineering, M.I.T.

18. Hall, D.J. and Robson, B.L. (1984), A review of the design and materials evaluation programme for the GRP/foam sandwich composite hull of the RAN minehunter, Composites 15, 266-276.

19. Hertzberg, R.W. (1983), Deformation and Fracture Mechanics of Engineering Materials. Wiley (2nd edition), New york.

20. Huang, S.N. and Alspaugh, D.W. (1974), Minimum weight sandwich beam design, AIAA J., 12, 1617-1618.

21. Kinloch, A.J. and Shaw, S.J. (1981), The fracture resistance of a toughened epoxy adhesive, J. Adhesion, 12, 59-77.

22. Kuenzi, E.W. (1951), Edgewise compression strength of panels and flatwise flexural strength of strips of sandwich construction, FPL Report 1827.

23. Kuenzi, E.W. (1965), Minimum weight structural sandwich, U.S. For. Serv. Res. Note FPL-086 (Forest Products Laboratory, Madison, WI).

24. March, H.W. (1944), Buckling loads of panels having light cores and dense faces, FPL Report 1504.

25. Patel, M.R. and Finnie, I. (1970), Structural features and mechanical properties of rigid cellular plastics, J. Mater. 5, 909-932.

26. Timoshenko & Young (1968), Elements of Strength of Materials, 5th edition, D. Van Nostrand.

27. Ueng, C.E.S. and Liu, T.L. (1979), Least weight of a sandwich

panel. In R.R. Craig (ed.), Proc. ASCE, Engineering Mechanics Division, 3rd Specialty Conf., University of Texas at Austin, Sept. 17-19, ASCE, New York, 41-44.

28. U.S. Department of Defence (1974), Structural Sandwich Composites, MIL HDBK-23A.

29. Wittrick, W.H. (1945), A theoretical analysis of the efficiency of sandwich construction under compressive end load, R&M 2016 (U.K. Aeronautical Research Council, Farnborough, Hants.).

30. Wrzecioniarz, P.A. (1983), Stability investigations of variable core sandwich, J. Eng. Mech. 109, 1460-1471.

Table 4.1 Results of compression tests using cubic foam specimens.

$\frac{\rho_c}{\rho_s}$	Spec. #	E_{c_1} (psi)	σ^*_{c,c_1} (psi)	Spec. #	E_{c_2} (psi)	σ^*_{c,c_2} (psi)	Spec. #	E_{c_3} (psi)	σ^*_{c,c_3} (psi)
0.0533	1	4054	105.7	6	2083	40.6	11	1705	39.5
	2	4411	110.7	7	1786	38.2	12	2027	39.7
	3	4430	111.5	8	1705	38.0	13	2045	40.5
	4	4950	109.7	9	1875	40.6	14	2041	39.2
	5	4240	109.5	10	1852	40.0	15	1852	40.0
0.08	1	5000	165.0	6	3448	121.7	11	3571	123.2
	2	5063	172.5	7	3846	142.5	12	3333	128.0
	3	5263	166.7	8	3849	145.0	13	3846	137.5
	4	5714	173.0	9	3636	138.7	14	3571	131.2
	5	5405	173.0	10	3773	142.0	15	3225	125.0
0.13	1	11765	336.0	6	7407	246.2	11	6669	236.5
	2	13043	343.0	7	6667	247.5	12	6896	246.7
	3	13158	343.5	8	7143	250.0	13	6780	243.2
	4	11364	303.0	9	6896	246.5	14	6899	247.5
	5	11538	312.5	10	6667	233.7	15	6452	245.0
0.27	1	28571	1046.9	6	31579	1090.0	11	30769	1106.2
	2	30769	1150.0	7	32086	1117.5	12	28591	1162.5
	3	29630	1062.5	8	30000	1168.7	13	30020	1081.2
	4	30723	1068.7	9	32432	1168.7	14	28572	1050.0
	5	28692	1081.2	10	32436	1175.0	15	31579	1070.0

E_{c_1}, E_{c_2}, E_{c_3}: elastic moduli in directions parallel to rise (1) and perpendicular (2,3).

σ^*_{c,c_1}, σ^*_{c,c_2}, σ^*_{c,c_3}: compressive strengths in directions parallel to rise (1) and perpendicular (2,3).

Table 4.2 Results of shear tests using foam specimens.

$\frac{\rho_c}{\rho_s}$	Spec. #	τ_c^* (psi)
0.0533	1	69
	2	74
	3	68
	4	73
	5	76
0.08	1	109
	2	117
	3	121
	4	104
	5	113
0.13	1	229
	2	258
	3	249
	4	243
	5	251
0.27	1	798
	2	806
	3	813
	4	787
	5	805

Table 4.3 Results of tension tests using foam specimens.

$\frac{\rho_c}{\rho_s}$	Spec. #	$\sigma^*_{c,t}$ (psi)
0.0533	1	100.00
	2	92.70
	3	104.65
	4	98.67
	5	96.77
0.08	1	157.40
	2	151.00
	3	163.27
	4	170.23
	5	150.05
0.13	1	377.91
	2	361.10
	3	341.58
	4	360.75
	5	330.57
0.27	1	943.70
	2	857.68
	3	915.20
	4	873.89
	5	869.75

Table 4.4 Results of tests for the evaluation of the adhesive fracture toughness, K_{ICadh}.
Tabulated values correspond to fracture load, T (lbs).

Test,#	Initial crack length a (mm)				
	5	15	20	25	30
1	11.9	4.9	4.4	3.1	2.9
2	12.9	5.7	3.9	2.9	2.8
3	13.2	6.3	4.3	4.1	3.3
4	13.6	6.2	5.2	3.2	3.1
5	12.7	5.9	5.1	2.8	3.9
6	12.1	5.2	4.2	3.3	2.7
7	13.4	6.4	4.3	3.6	2.8
8	11.7	6.4	3.2	3.5	3.2
9	13.1	6.3	3.8	3.4	3.0
10	13.0	5.6	4.3	3.2	3.1

Table 4.5 Design of sandwich beams tested.

t/l (-)	t (in)	l (in)	c (in)	b (in)	t/c (-)	d (in)
0.00040	0.016	40.00	2.0	2.0	0.008	2.016
0.00070	0.016	22.86	1.0	1.0	0.016	1.016
0.00125	0.025	20.00	1.0	1.0	0.025	1.025
0.00200	0.032	16.00	1.0	1.0	0.032	1.032
0.00400	0.050	12.50	1.0	1.0	0.050	1.050
0.00700	0.080	11.43	1.0	1.0	0.080	1.080
0.01000	0.080	8.00	0.8	1.0	0.100	0.880

For each ratio of t/l, beams were made with the following core densities (and corresponding relative densities):

ρ_c (lb/ft^3)	4	6	10	20
ρ_c/ρ_s (-)	0.0533	0.08	0.13	0.27

In addition, for ratios of t/l = 0.0007, 0.00125, 0.002 and 0.004, beams were made with a core density of 2 lb/ft^3 (ρ_c/ρ_s = 0.027).

Table 4.6 Measured and calculated failure loads for sandwich beams.

t/l ρ_c/ρ_s	Avg. measured failure load (lbs)	Measured failure mode	Calculated failure load (lbs)				
			Face yield	Face Wrinkling	Debonding Shear#fracture	Core shear	Core tension
0.27							
0.00040	83.3	Face yield	81.1	732.5	15560 # $0.23/\sqrt{a}$	3174.1	2005.0
0.00070	39.3	..	36.0	323.0	3915 # $0.10/\sqrt{a}$	1134.2	781.5
0.00125	74.5	..	65.5	581.9	3915 # $0.18/\sqrt{a}$	1383.3	928.4
0.00200	121.2	..	106.2	937.4	3915 # $0.29/\sqrt{a}$	1481.6	1126.0
0.00400	245.2	..	219.9	1907.6	3915 # $0.58/\sqrt{a}$	1540.0	1391.0
0.00700	429.0	..	407.2	3433.6	3915 # $1.01/\sqrt{a}$	1555.3	1679.0
0.01000	493.5	..	482.8	3996.8	3132 # $1.15/\sqrt{a}$	1246.3	1382.0
0.13							
0.00040	80.3	Face yield	81.1	318.2	15560 # $0.23/\sqrt{a}$	1849.0	1681.2
0.00070	40.7	..	36.0	140.3	3915 # $0.10/\sqrt{a}$	496.2	514.0
0.00125	74.5	..	65.5	252.8	3915 # $0.18/\sqrt{a}$	507.9	579.4
0.00200	118.2	..	106.2	407.3	3915 # $0.29/\sqrt{a}$	511.6	610.1
0.00400	216.7	..	219.9	828.8	3915 # $0.58/\sqrt{a}$	514.3	639.2
0.00700	396.7	..	407.2	1491.8	3915 # $1.01/\sqrt{a}$	514.9	652.3
0.01000	483.5	Core shear	482.8	1736.5	3132 # $1.15/\sqrt{a}$	411.0	526.1
0.08							
0.00040	80.0	Face yield	81.1	182.9	15560 # $0.23/\sqrt{a}$	961.2	1334.2
0.00070	40.0	..	36.0	80.7	3915 # $0.10/\sqrt{a}$	243.9	301.9
0.00125	70.0	..	65.5	145.3	3915 # $0.18/\sqrt{a}$	245.1	318.7
0.00200	109.5	..	106.2	234.1	3915 # $0.29/\sqrt{a}$	245.5	326.9
0.00400	186.2	..	219.9	476.4	3915 # $0.58/\sqrt{a}$	245.7	333.9
0.00700	263.5	Core shear[1]	407.2	857.4	3915 # $1.01/\sqrt{a}$	245.7	337.0
0.01000	272.0	.. [2]	482.8	998.1	3132 # $1.15/\sqrt{a}$	196.6	270.6
0.0533							
0.00040	79.7	Face yield	81.1	115.1	15560 # $0.23/\sqrt{a}$	527.0	697.6
0.00070	36.3	.. [3]	36.0	50.8	3915 # $0.10/\sqrt{a}$	132.3	182.7
0.00125	64.5	..	65.5	91.4	3915 # $0.18/\sqrt{a}$	132.4	187.6
0.00200	100.0	.. [4]	106.2	147.3	3915 # $0.29/\sqrt{a}$	132.5	189.9
0.00400	120.2	Core shear	219.9	299.7	3915 # $0.58/\sqrt{a}$	132.5	191.9
0.00700	136.7	.. [5]	407.2	539.6	3915 # $1.01/\sqrt{a}$	132.5	192.9
0.01000	142.7	.. [6]	482.8	629.1	3132 # $1.15/\sqrt{a}$	106.1	154.6
0.0267							
0.00070	20.2	Wrinkling	36.0	23.0	3915 # $0.10/\sqrt{a}$	46.3	72.9
0.00125	33.4	..	65.5	41.5	3915 # $0.18/\sqrt{a}$	46.3	73.5
0.00200	40.5	Core shear[7]	106.2	66.8	3915 # $0.29/\sqrt{a}$	46.3	73.9
0.00400	47.2	..	219.9	135.6	3915 # $0.58/\sqrt{a}$	46.3	74.0

Notes to Table 4.6

All specimens of each beam design failed in the mode indicated in the table with the following exceptions:

1. One beam failed by debonding at 225 lbs and one failed by local crushing at 240 lbs.
2. One beam failed by local crushing at 195 lbs.
3. One beam failed by debonding at 28 lbs.
4. One beam failed by core shear at 90 lbs.
5. One beam failed by local crushing at 138 lbs.
6. One beam failed by debonding at 112 lbs.
7. One beam failed by face wrinkling at 39 lbs and one failed by local crushing at 31 lbs.

Beam stresses were calculated using $D = E_f bt(c+t)^2/2$.

Table 5.1 Transition equations for failure mode map.

Failure modes	Transition equation
Face yield-face wrinkling	$\rho_c/\rho_s = \left(\frac{\sigma_{yf}}{0.57 c_3^{2/3} E_f^{1/3} E_s^{2/3}}\right)^{\frac{3}{2A}}$
Face yield-core shear	$t/l = \frac{c_2 c_4}{c_1} (\rho_c/\rho_s)^B \frac{\sigma_{ys}}{\sigma_{yf}}$
Face wrinkling-core shear	$t/l = \frac{c_2 c_4}{0.57 c_1 c_3^{2/3}} \left(\frac{\rho_c}{\rho_s}\right)^{B-\frac{2A}{3}} \frac{\sigma_{ys}}{E_f^{1/3} E_s^{2/3}}$
Face yield-debonding	$t/l = \frac{c_2}{c_1} \frac{\tau^*_{adh}}{\sigma_{yf}}$
Core shear-debonding	$\rho_c/\rho_s = \left(\frac{\tau^*_{adh}}{c_4 \sigma_{ys}}\right)^{\frac{1}{B}}$

Note:
These transition equations are based on the assumptions that $c \simeq d$ and that normal stresses in the core are insignificant in the core shear failure mode.

Table 6.1 Simplified failure mode equations

Failure mode	Equation
Face yielding	$P_{fy} = c_1 \sigma_{yf} bc(t/l)$
Face wrinkling	$P_{fw} = 0.57 c_1 c_3^{2/3} E_f^{1/3} E_s^{2/3} (\rho_c/\rho_s)^{2A/3}\ bc(t/l)$
Core shear	$P_{cs} = c_2 c_4 (\rho_c/\rho_s)^B\ \sigma_{ys} bc$
Debonding	$P_d = c_2 T^*_{adh} bc$

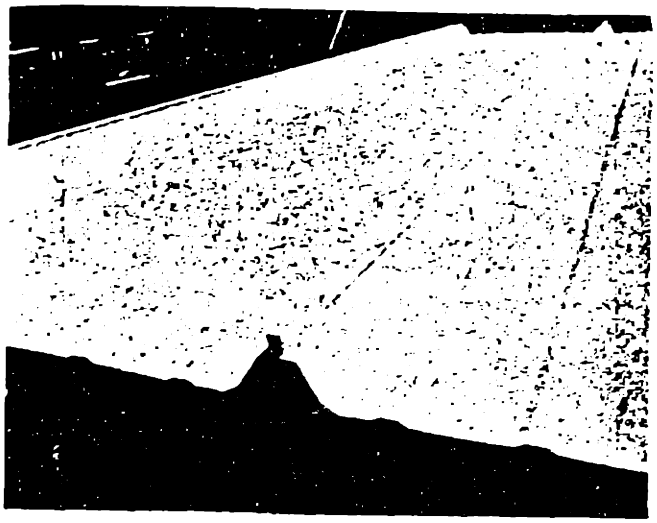

(a)

(b)

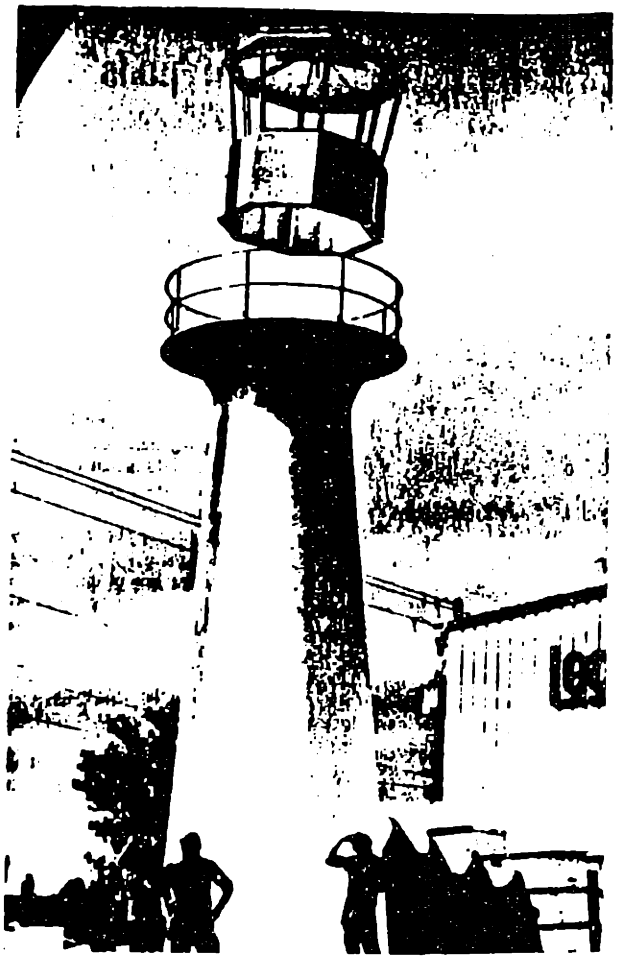

(c)

Fig. 1.1 Some applications of sandwich panel construction.
(a) roofing panel
(b) pre-fabricated housing
(c) lighthouse tower.

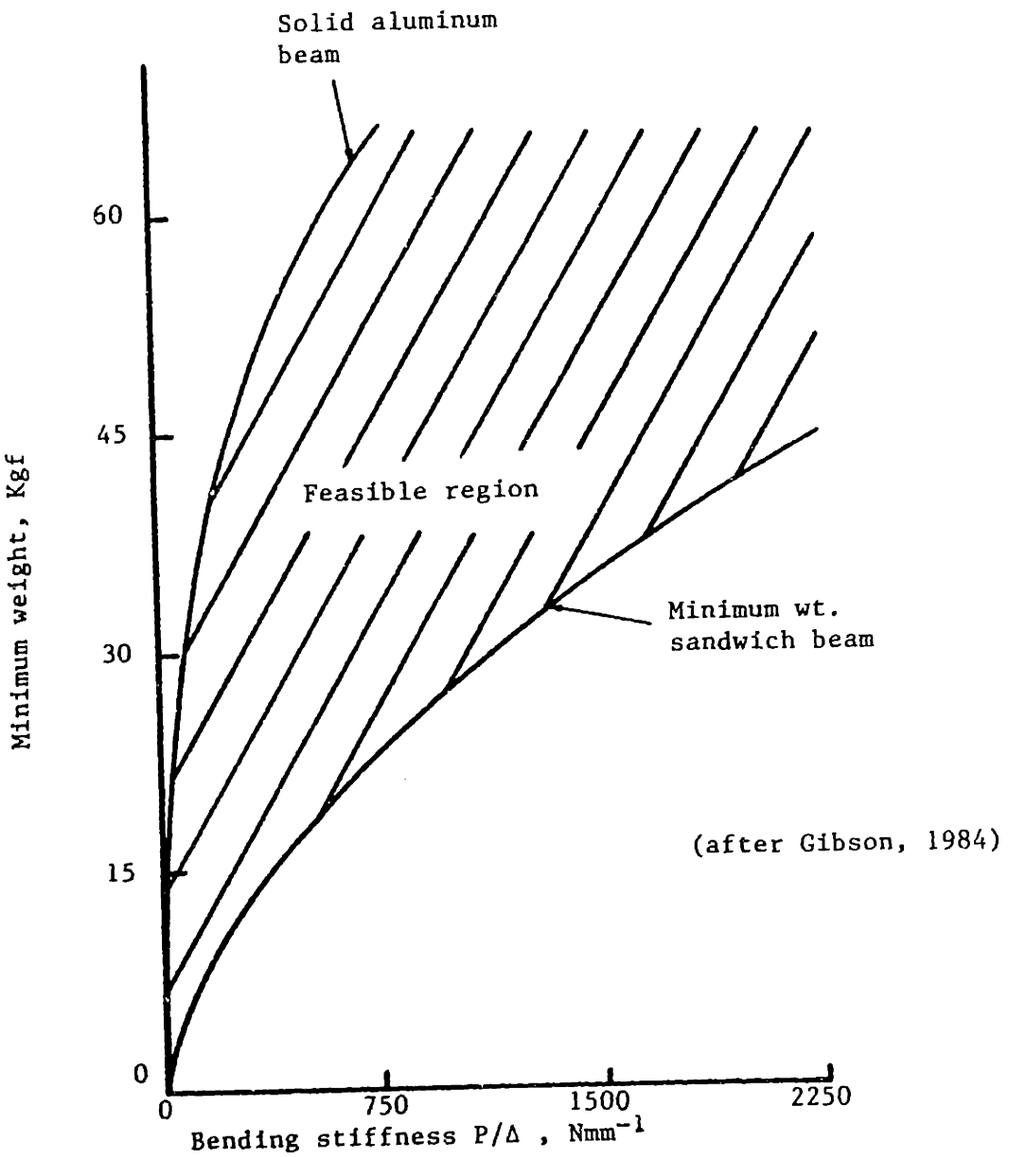

Fig. 1.2 Minimum weight as a function of stiffness for a sandwich beam with aluminum faces (ρ_f = 2700 Kgm^{-3}; E_f = 70 GNm^{-2}) and a foamed polyurethane core (ρ_s = 1200 Kgm^{-3}, E_s = 1.6 GNm^{-2}) in three point bending (ℓ = 2438.4mm; b = 160 mm).

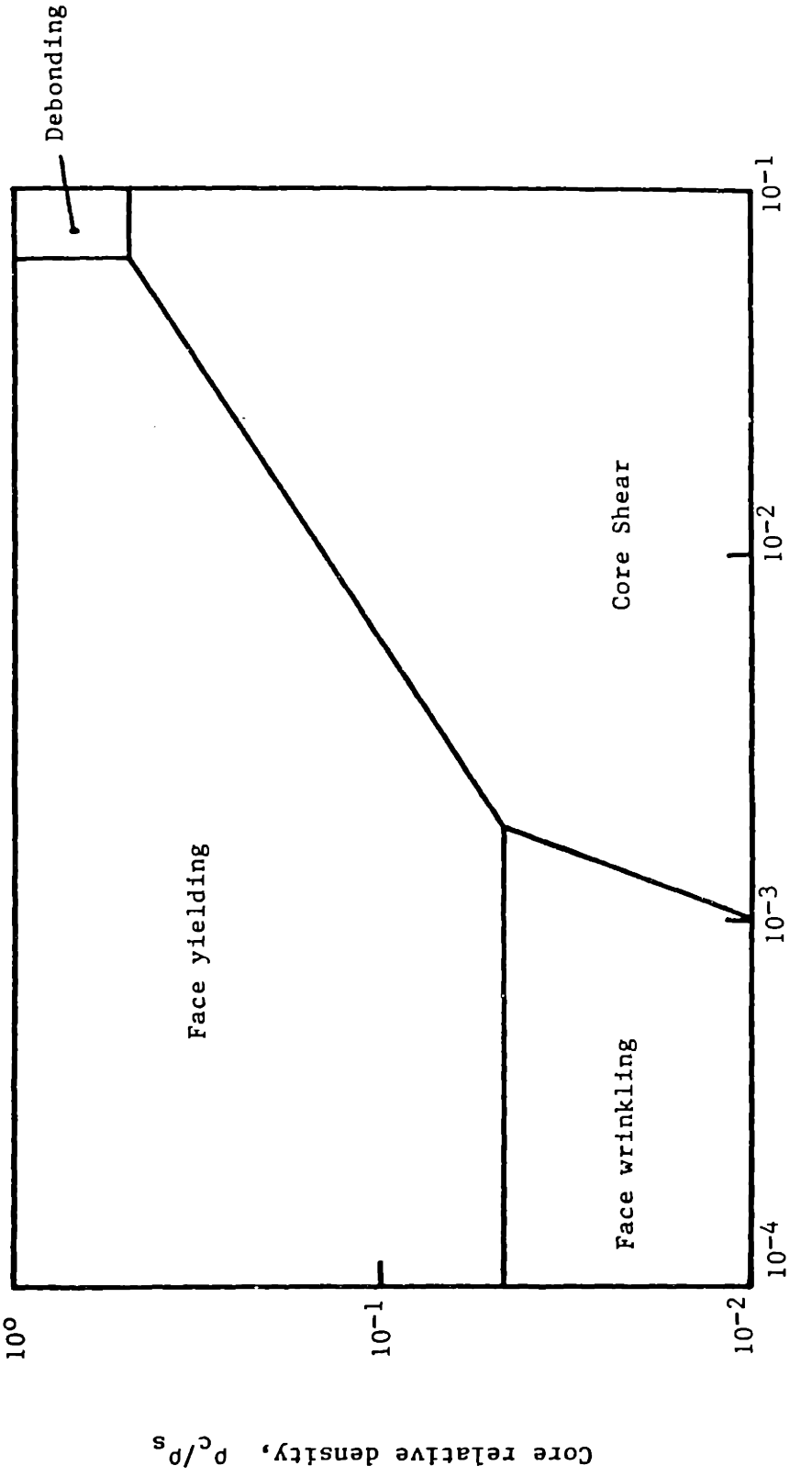

Fig. 1.3 A typical failure mode map for simply supported rectangular sandwich beams with rigid foam cores loaded at mid-span.

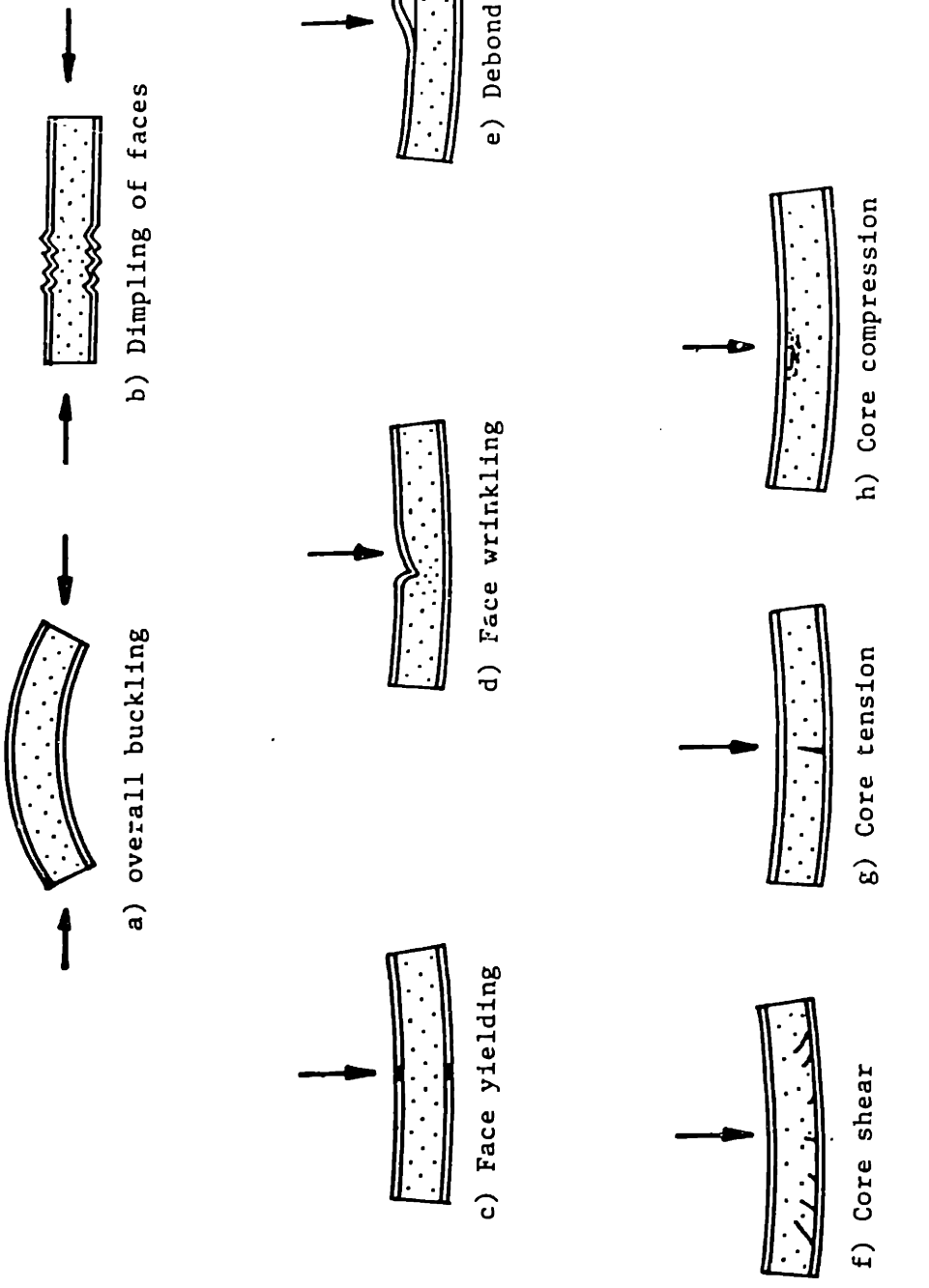

Fig. 2.1 Some possible failure modes of sandwich beams.

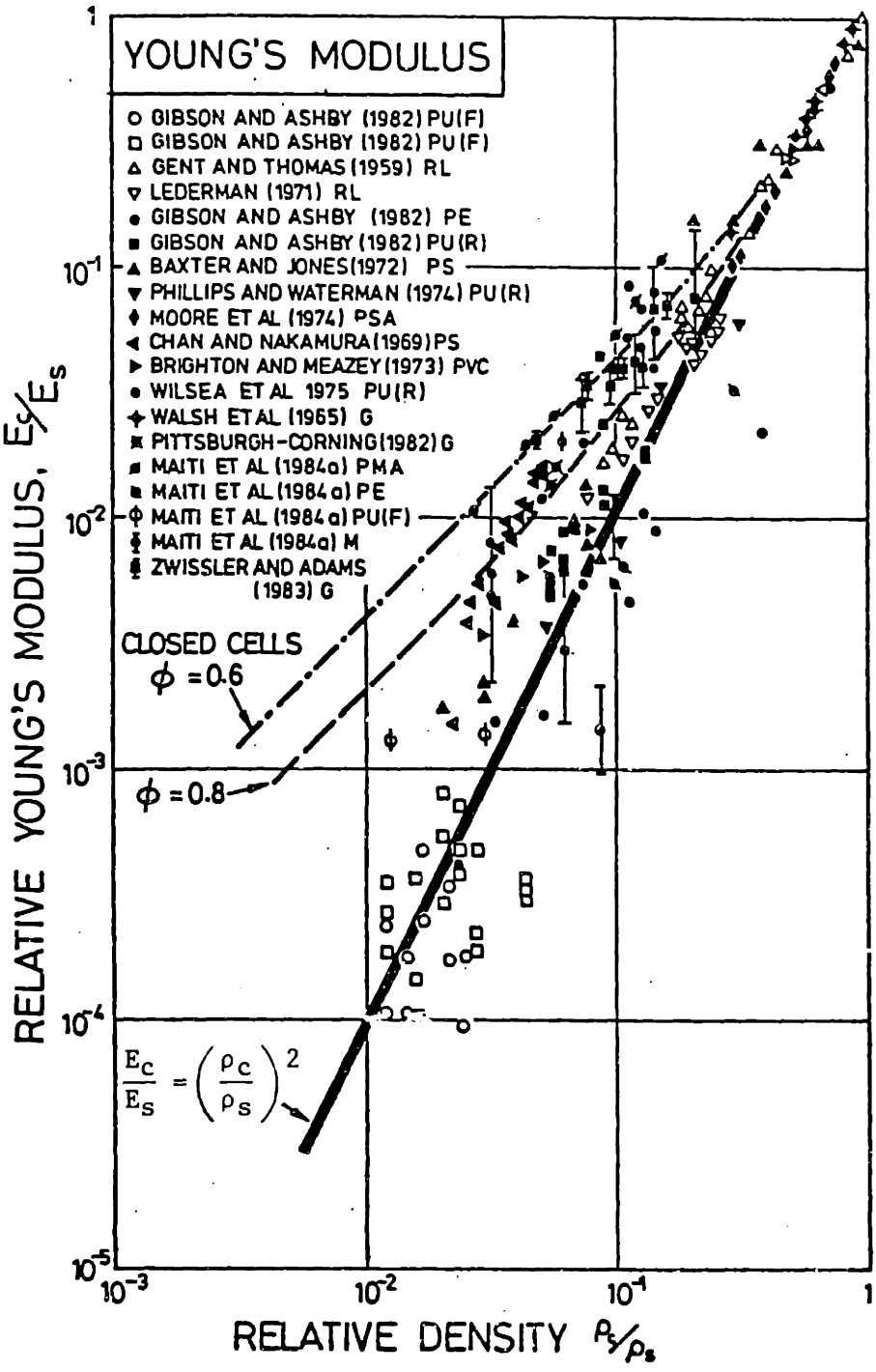

Fig. 2.2 Relative Young's modulus, E_c/E_s, against relative density, ρ_c/ρ_s.

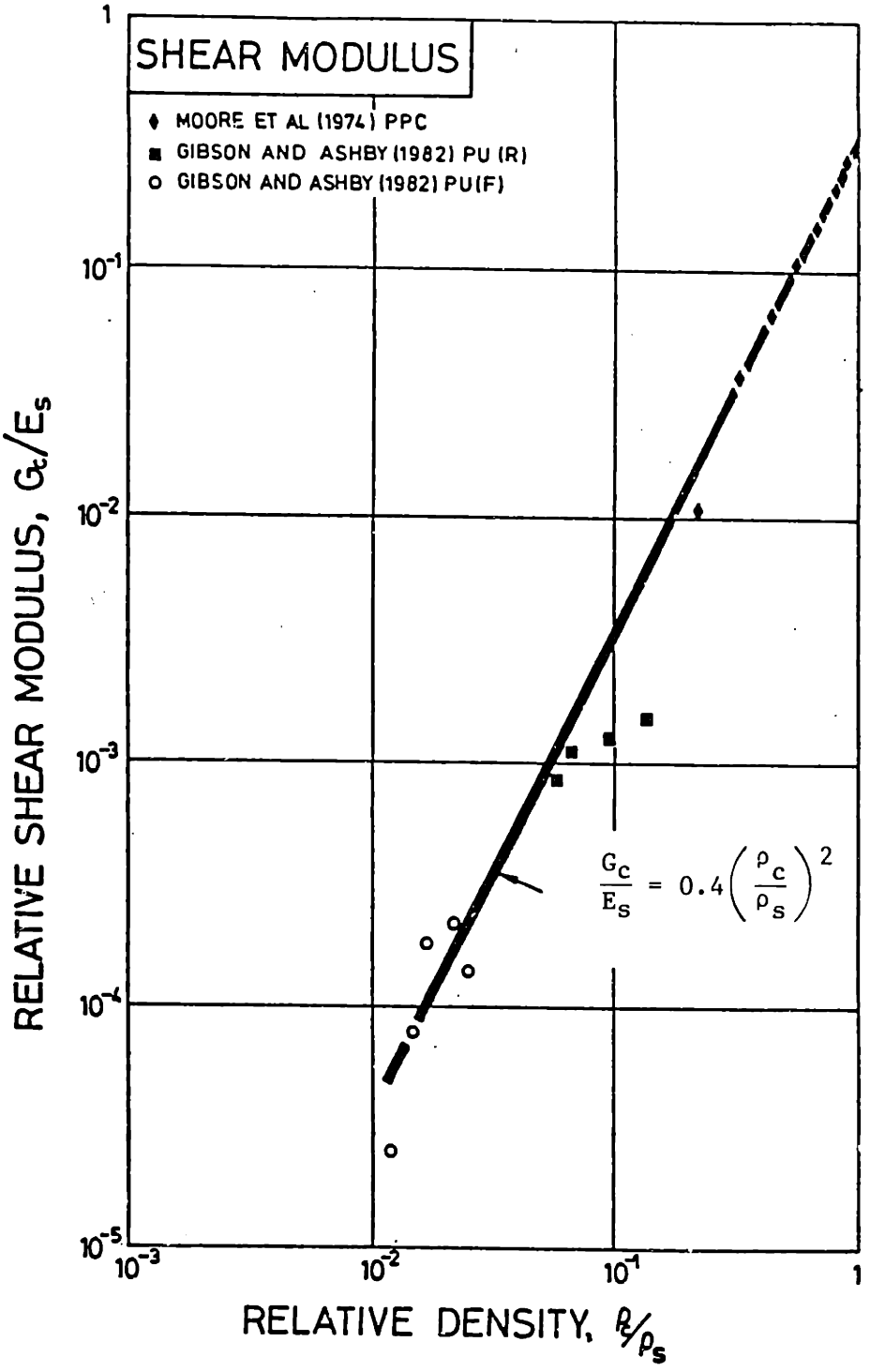

Fig. 2.3 Relative shear modulus, G_c/E_s, against relative density, ρ_c/ρ_s.

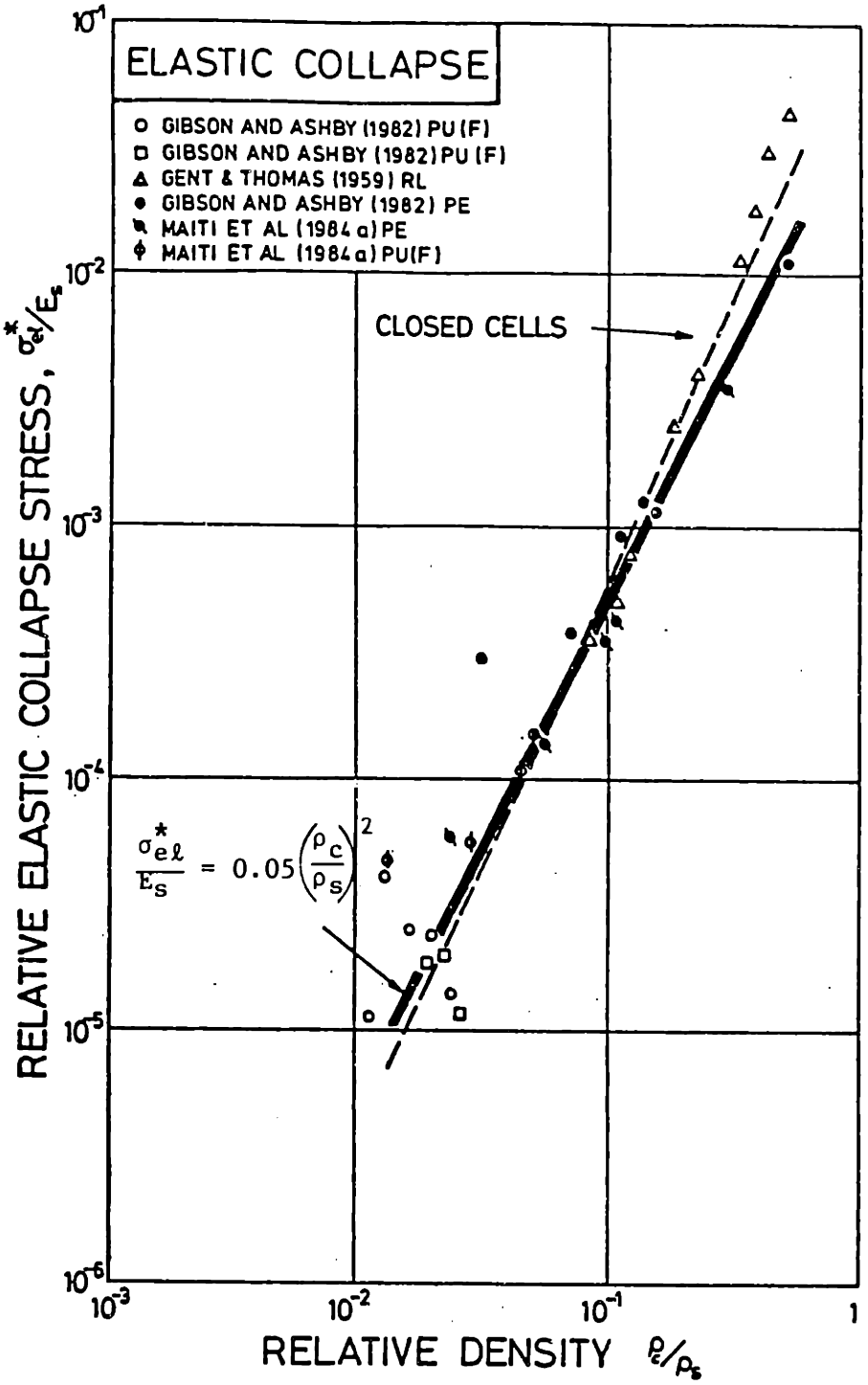

Fig. 2.4 Relative elastic collapse stress, σ^*_{el}/E_s, against relative density, ρ_c/ρ_s.

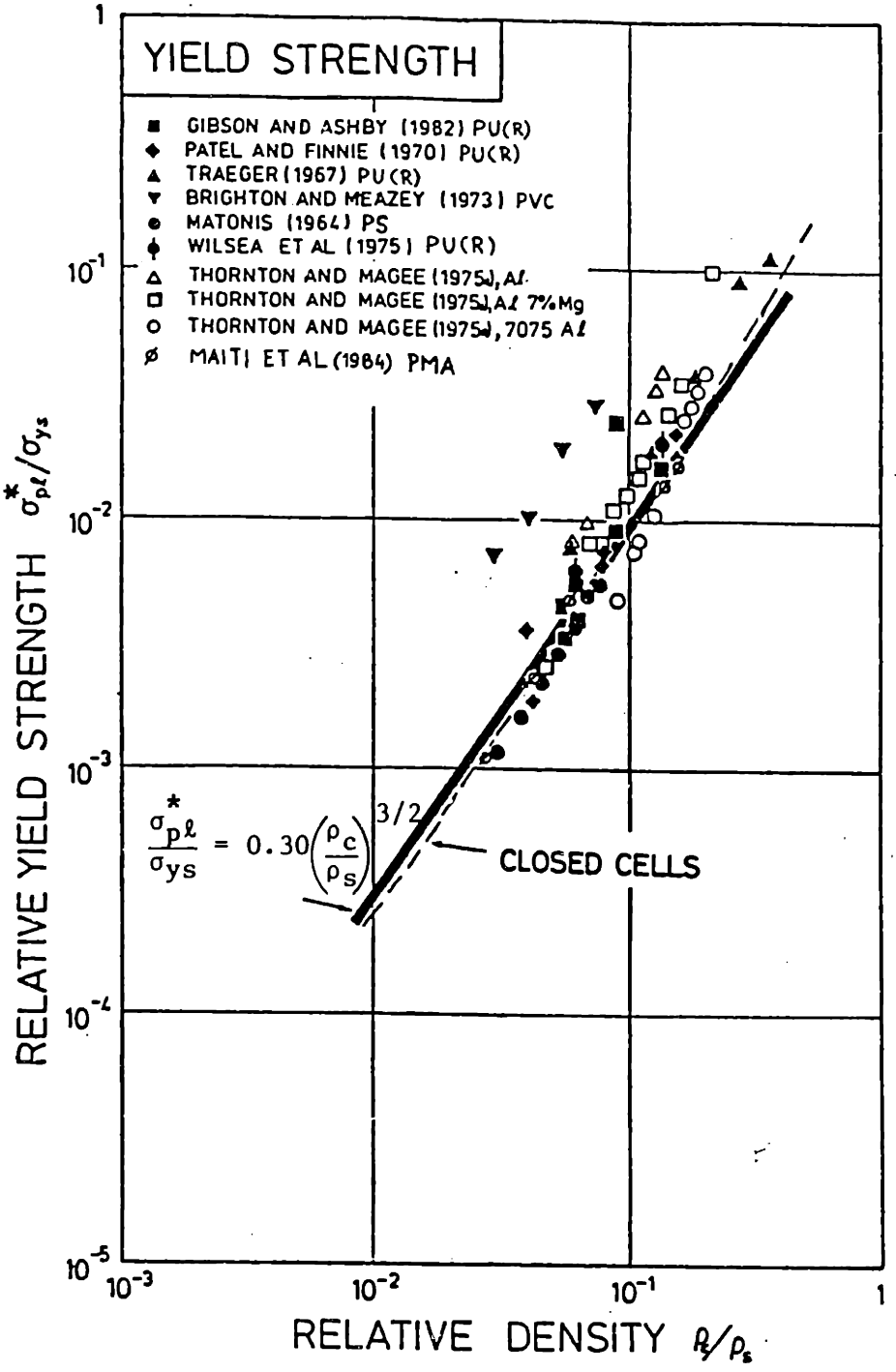

Fig. 2.5 Relative plastic collapse stress, $\sigma^*_{pl}/\sigma_{ys}$, against relative density, ρ_c/ρ_s.

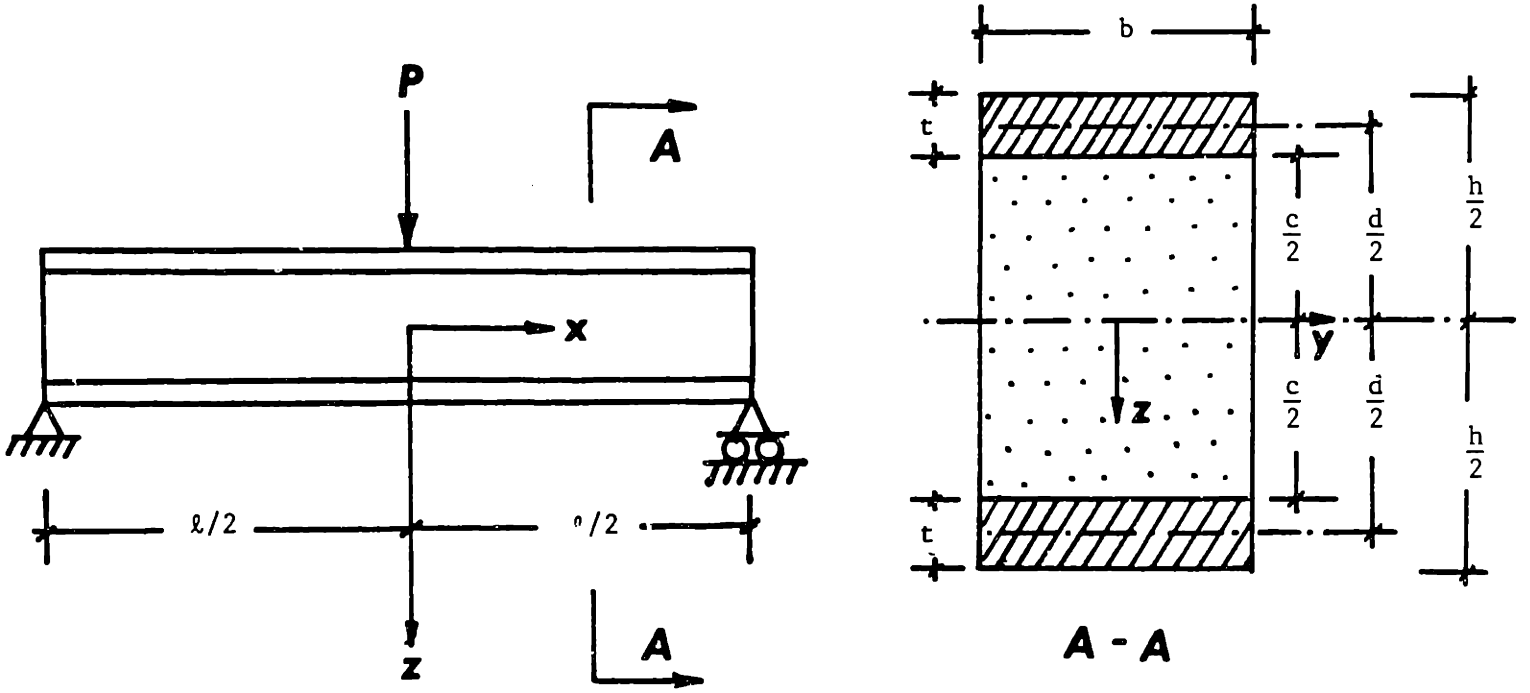

Fig. 3.1 Dimensions of a sandwich beam.
(after Allen, 1969)

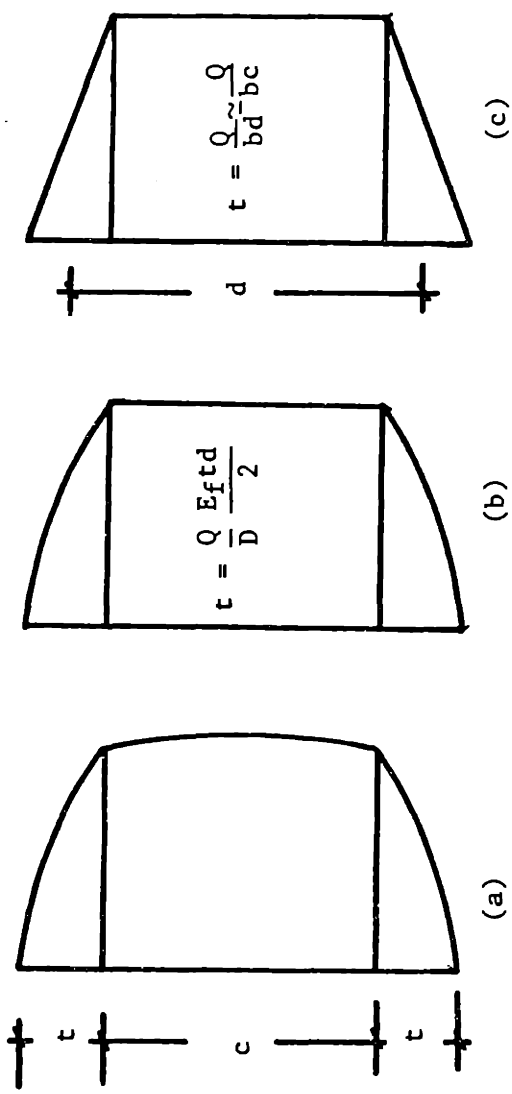

Fig. 3.2 Shear stress distribution in sandwich beam.

(a) True distribution
(b) Effect of weak core
(c) Effect of weak core in addition with the thin face approximation (after Allen, 1969).

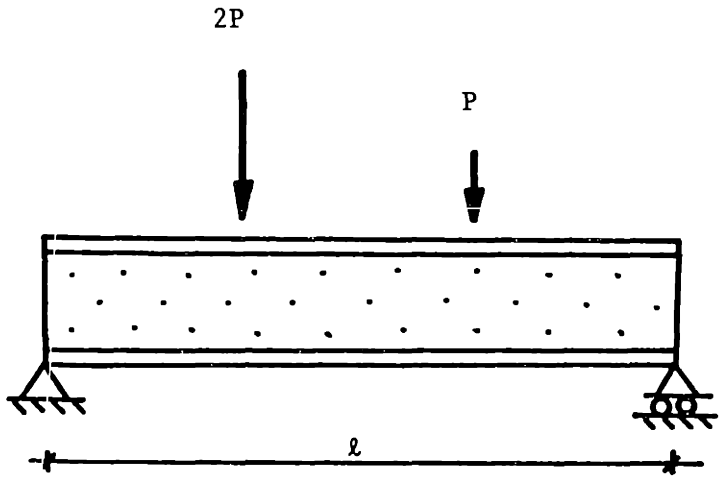

$$M = \frac{P\ell}{c_1}, \quad Q = \frac{P}{c_2}$$

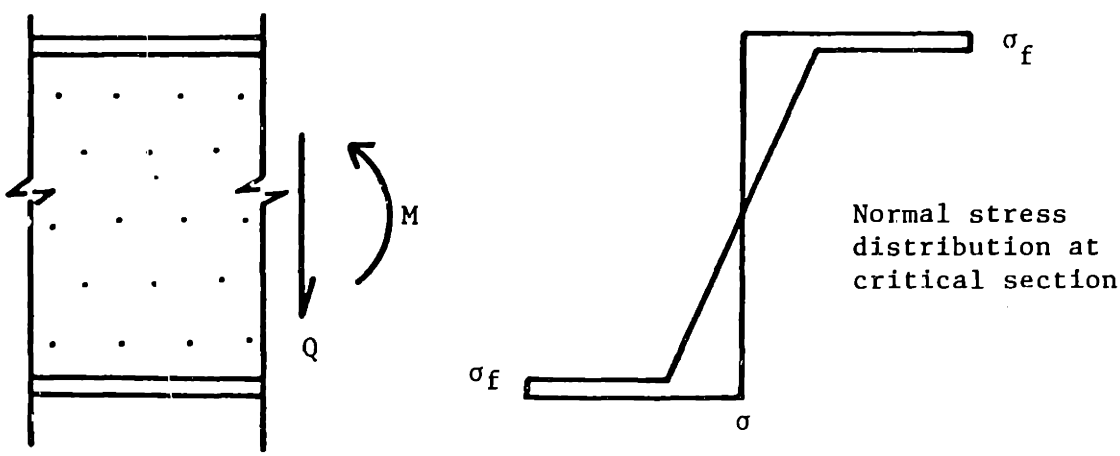

Fig. 3.3 A rectangular sandwich beam under loading and the normal stress distribution at the critical section.

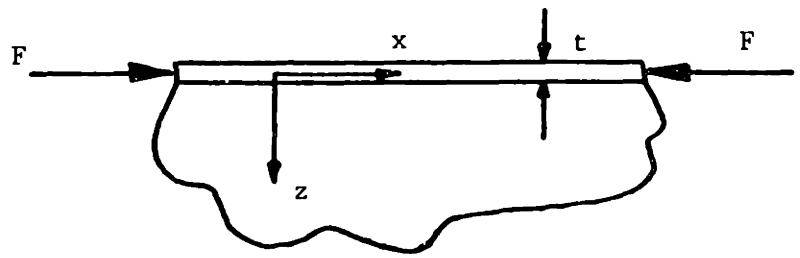

Fig. 3.4 Axially loaded long strut attached to an elastic medium.

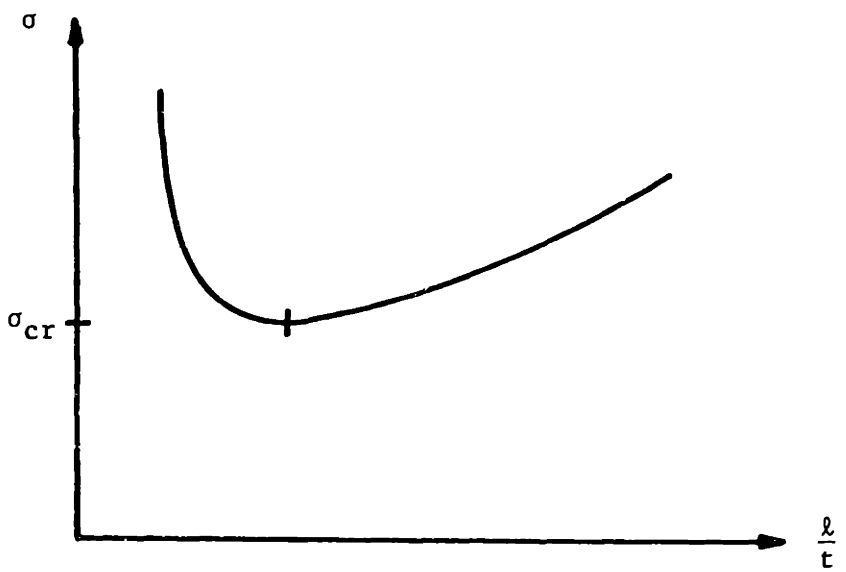

Fig. 3.5 Typical variation of critical stress with ℓ/t (equation (3.24)).

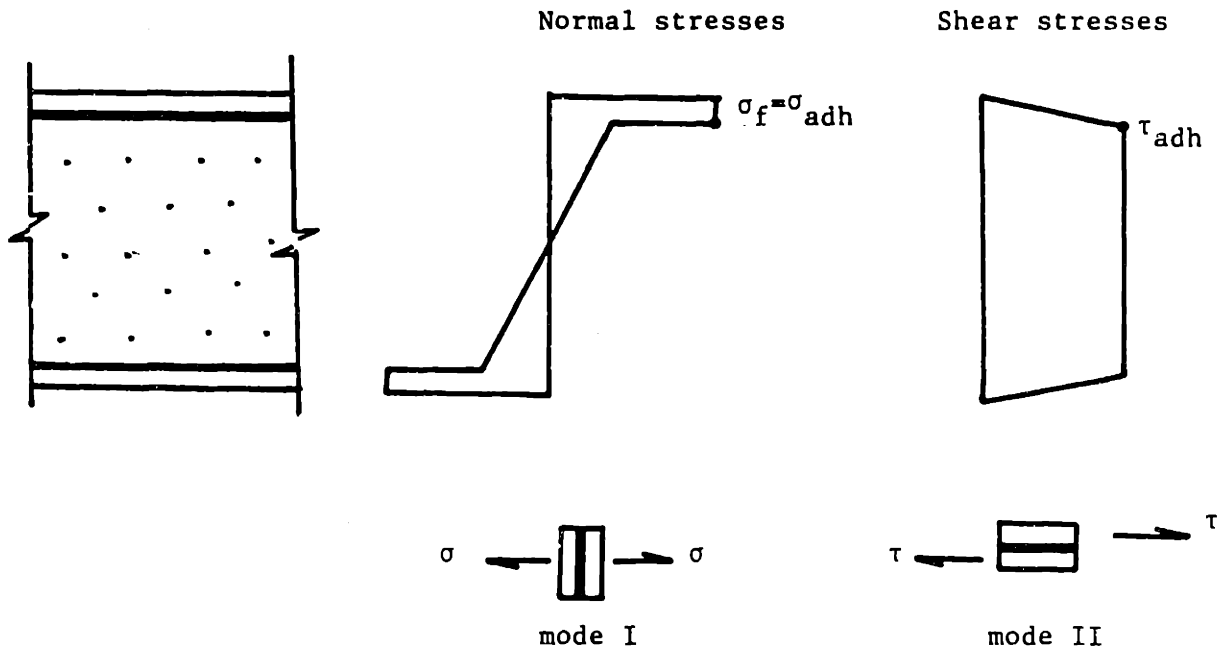

Fig. 3.6 Normal and shear stresses in the adhesive and related fracture modes I and II.

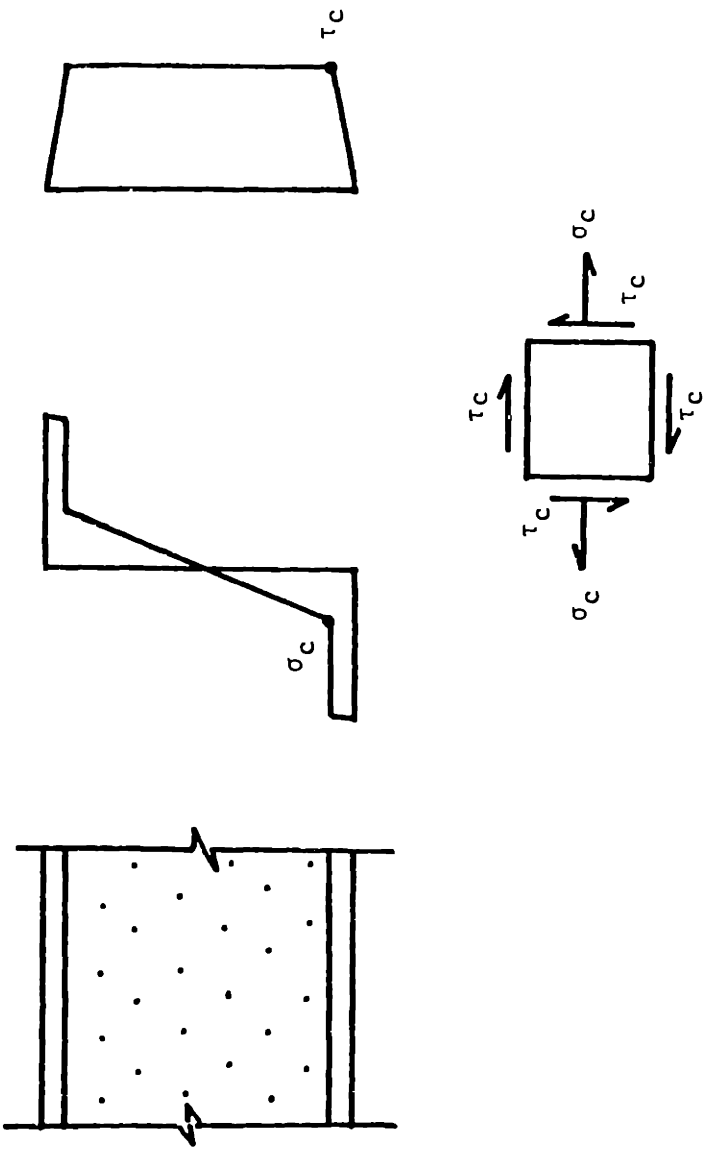

Fig. 3.7 Stresses acting on an element of the core at the extreme fibre.

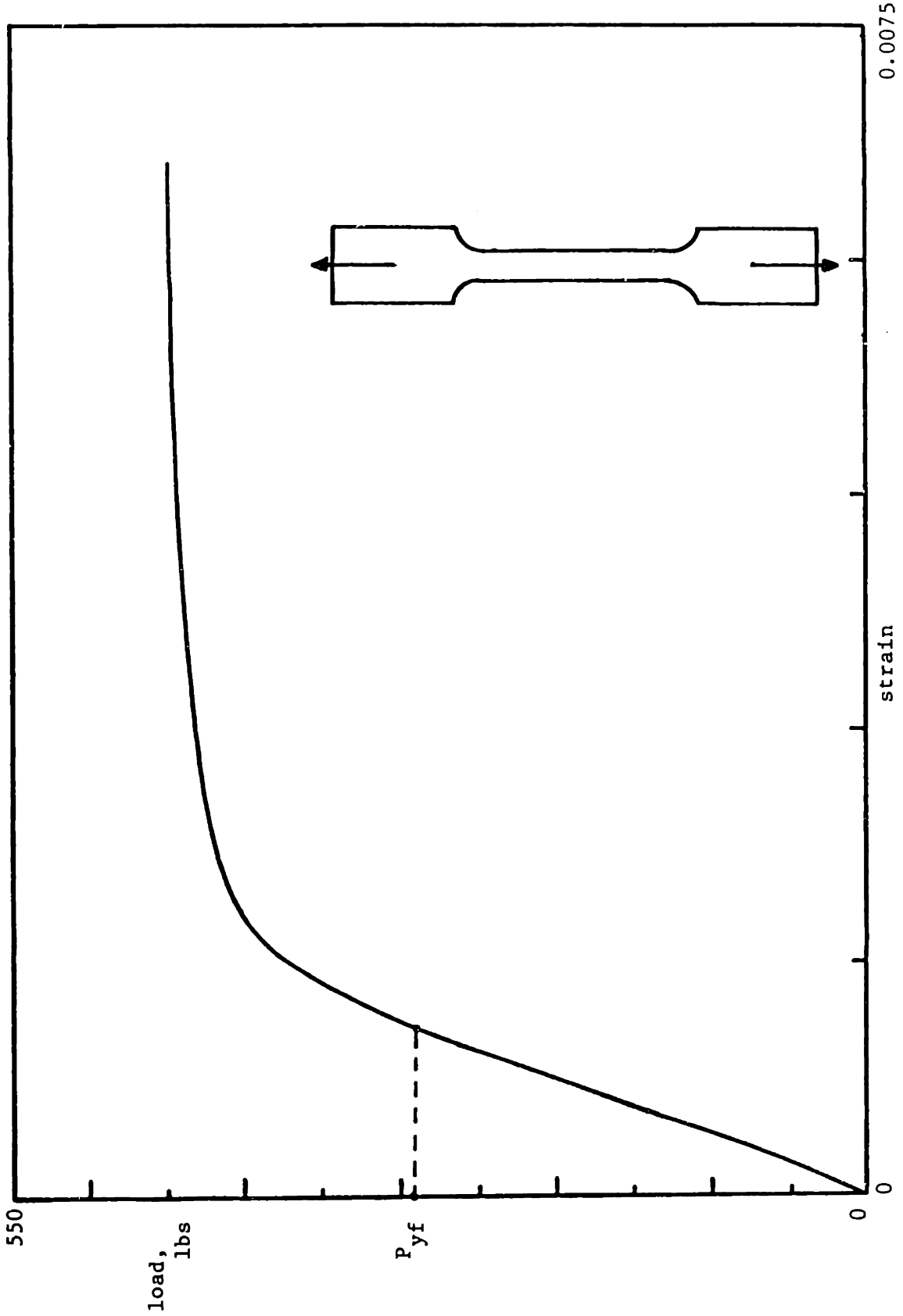

Fig. 4.1 A typical tensile load-strain curve of axially loaded aluminum specimens.

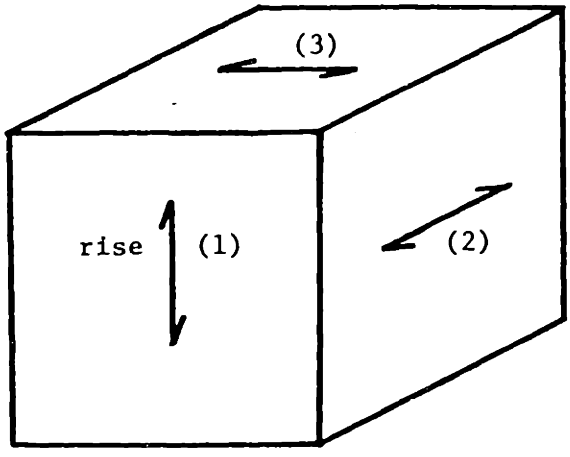

Fig. 4.2 A cubic foam specimen with the rise direction and both directions perpendicular to his, marked by (1), (2) and (3).

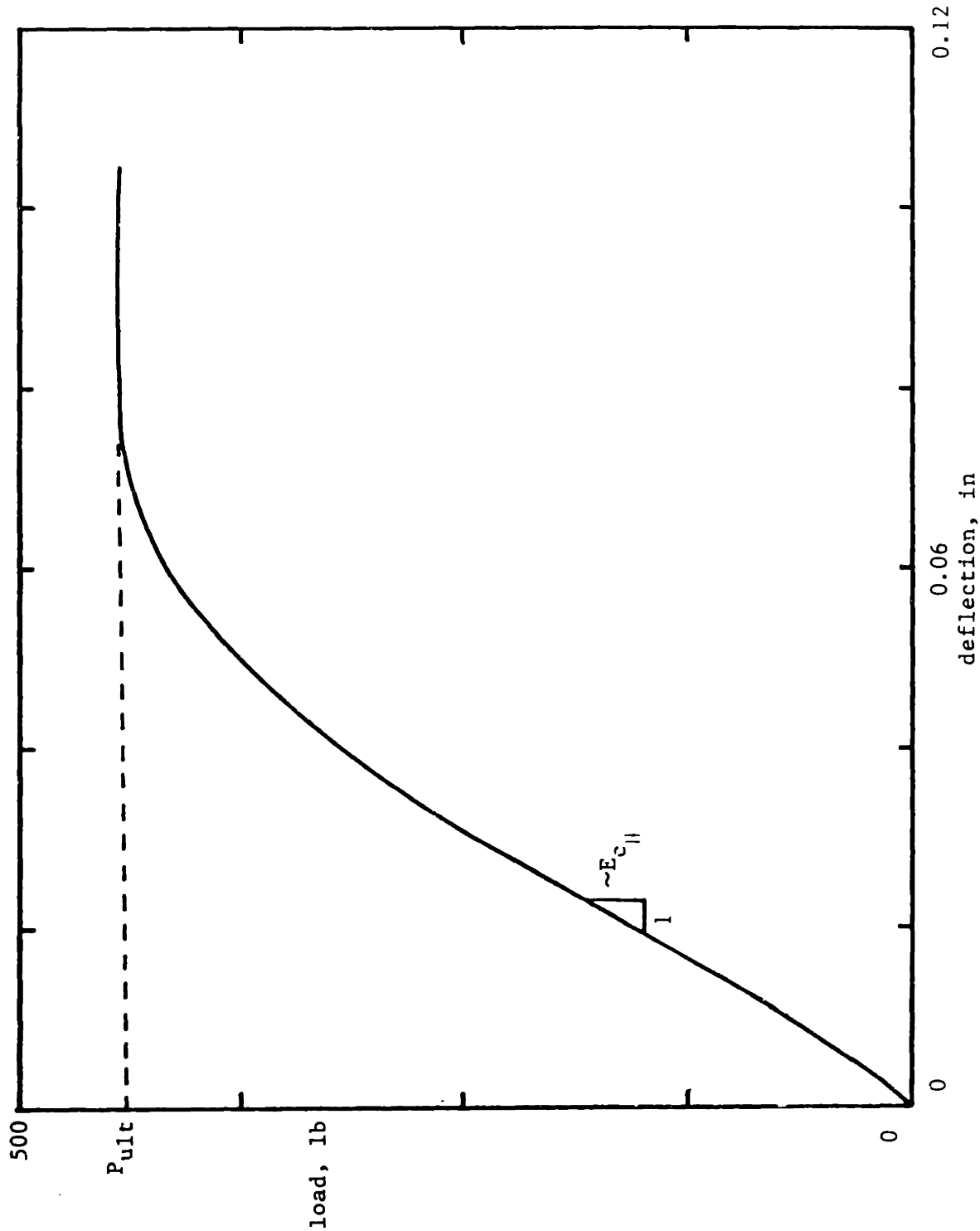

Fig. 4.3 A typical load-deflection curve for cubic foam specimens loaded parallel to the rise direction, $\rho_c/\rho_s = 0.0533$.

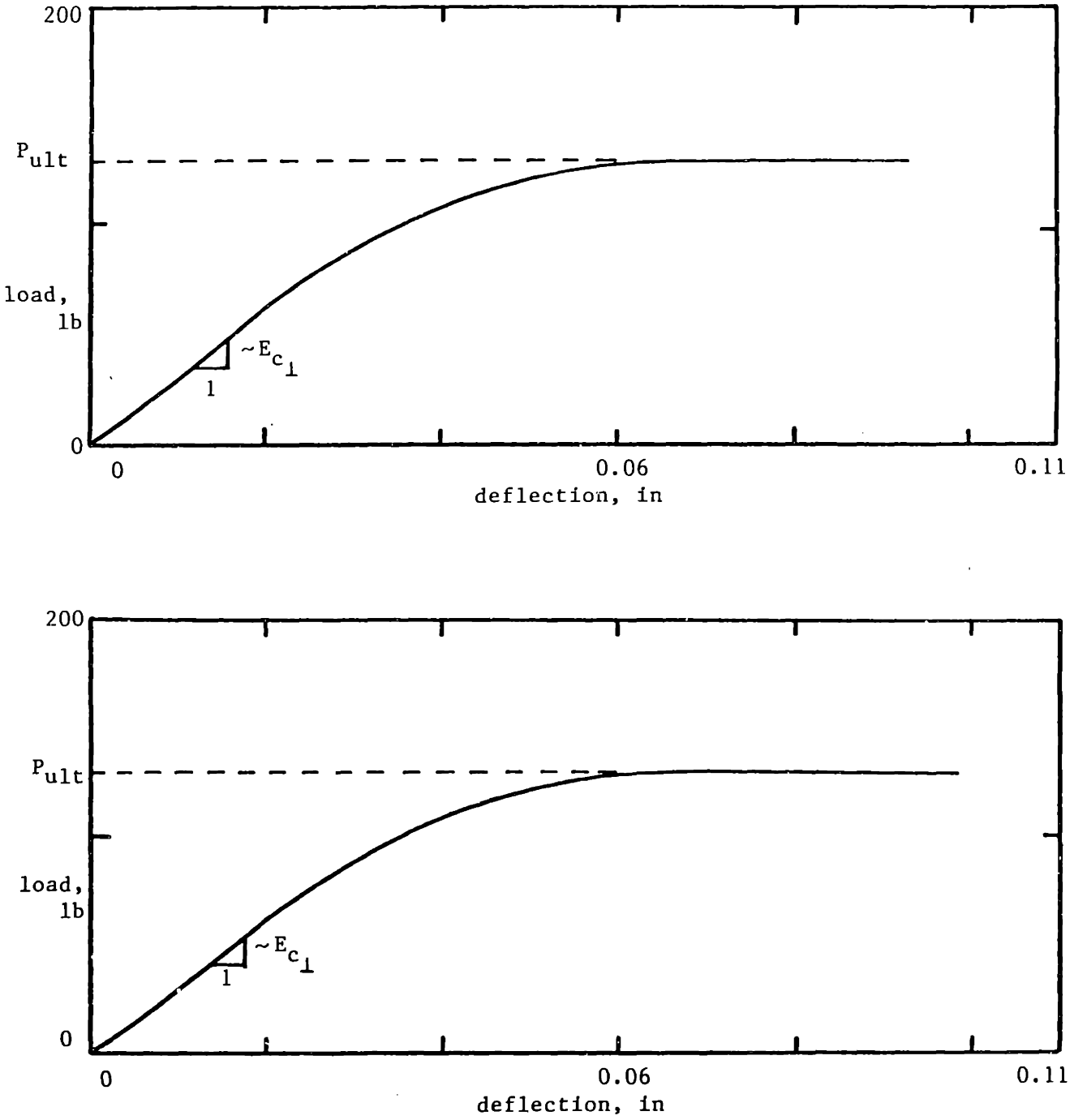

Fig. 4.4 Typical load-deflection curves for cubic foam specimens loaded in two different directions perpendicular to the rise, $\rho_c/\rho_s = 0.0533$.

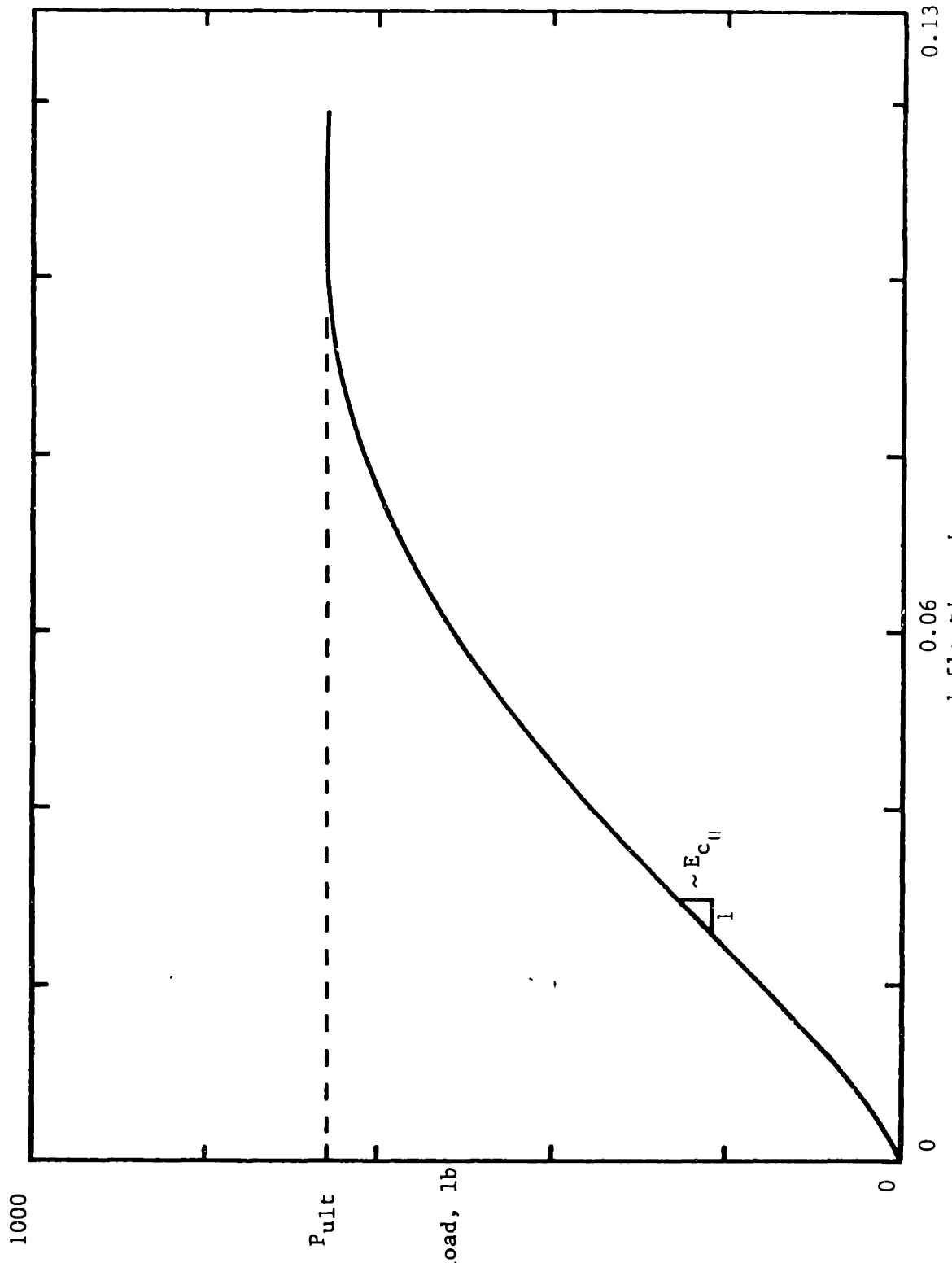

Fig. 4.5 A typical load-deflection curve for cubic foam specimens loaded parallel to the rise direction, $\rho_c/\rho_s = 0.08$.

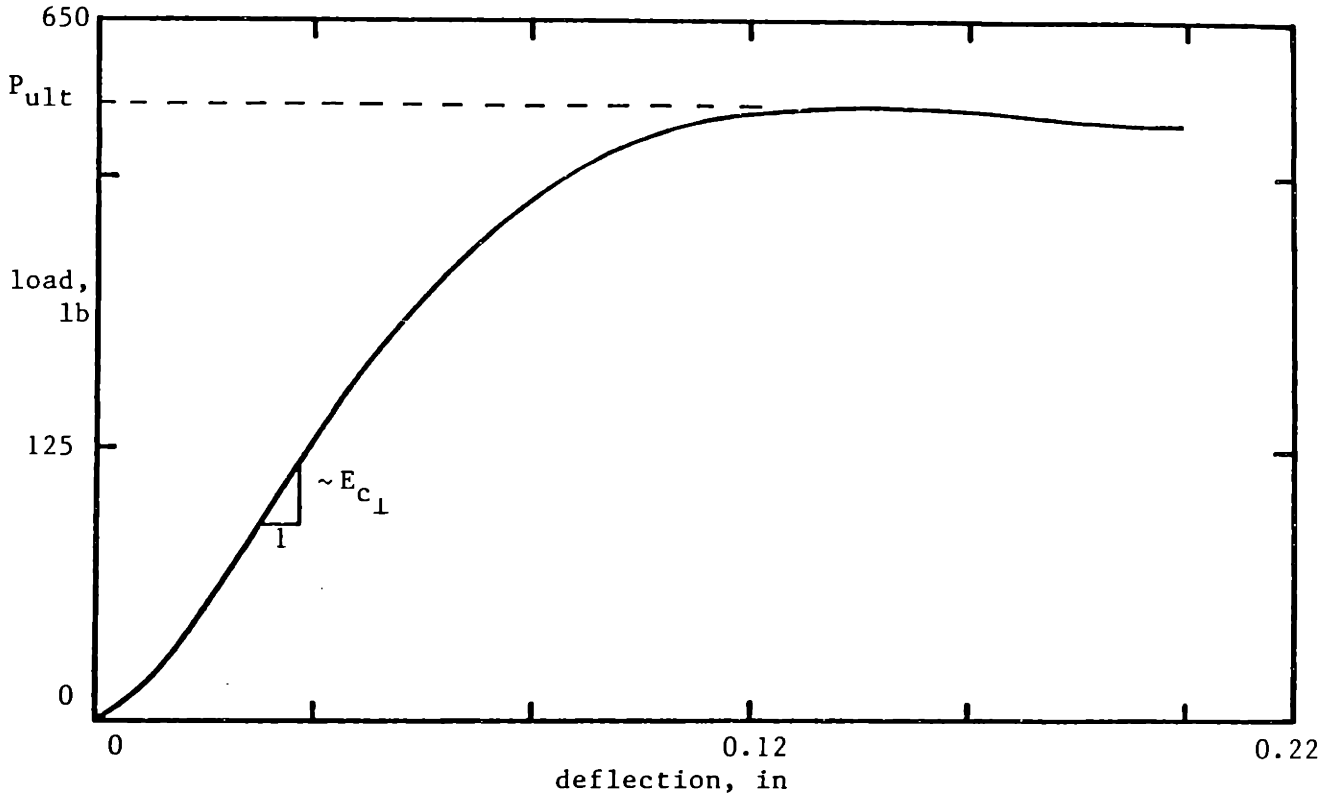

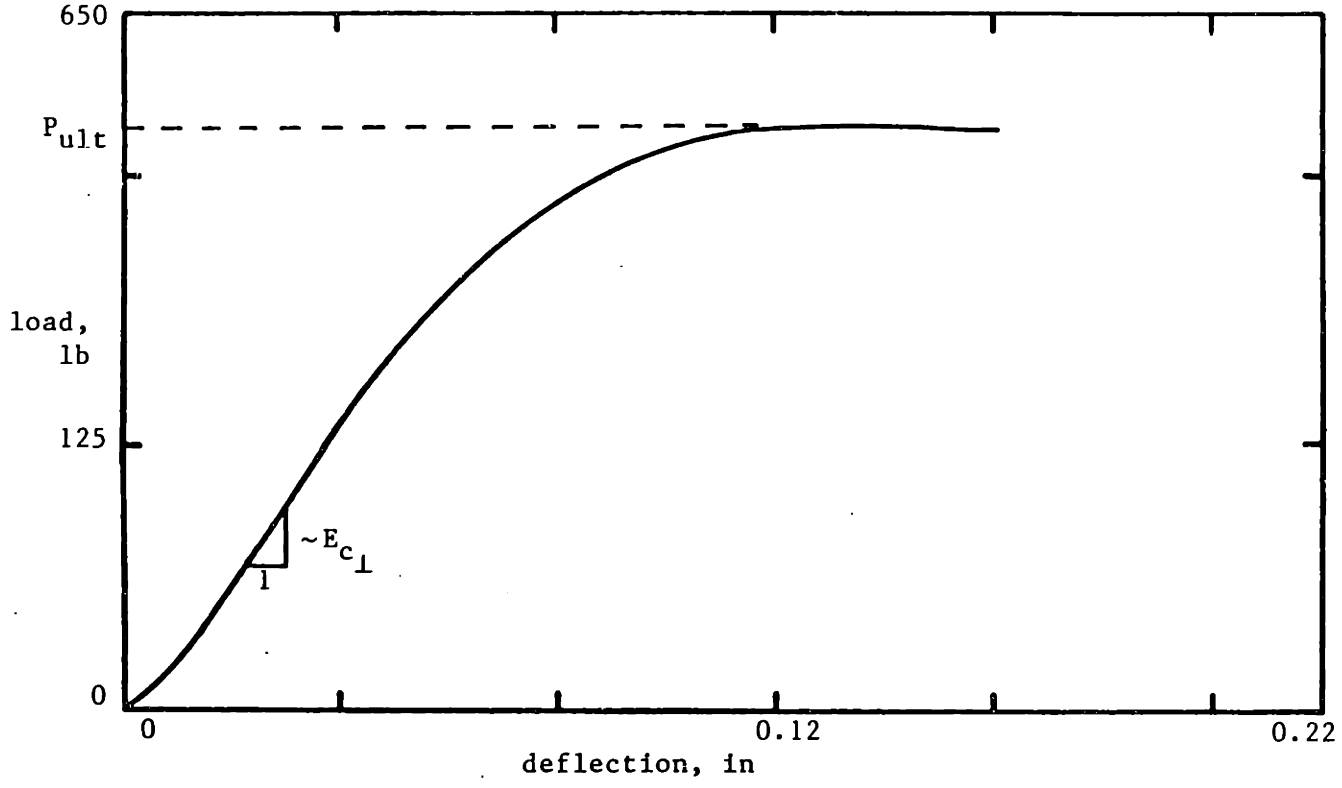

Fig. 4.6 Typical load-deflection curves for cubic foam specimens loaded in two different directions perpendicular to the rise, $\rho_c/\rho_s = 0.08$.

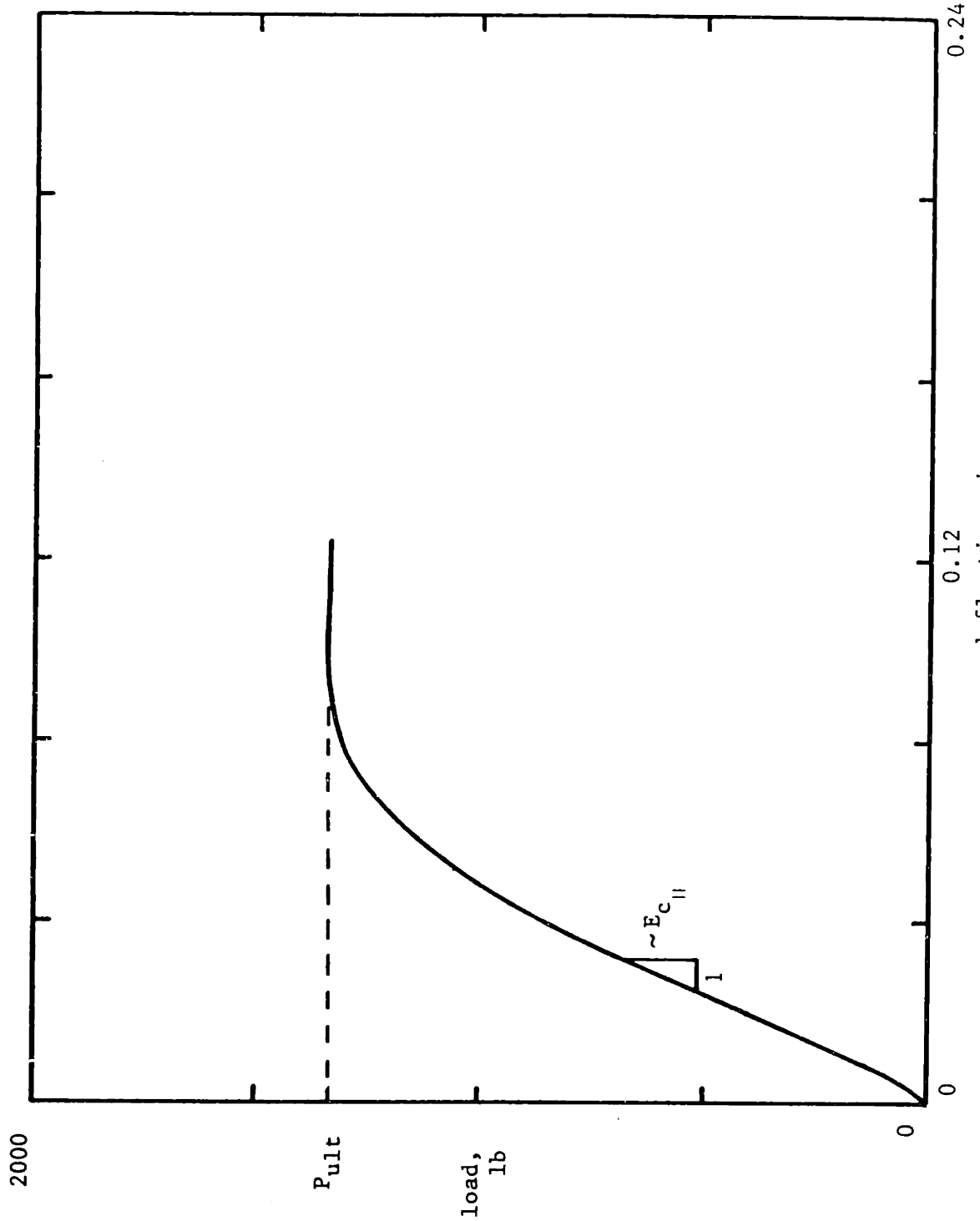

Fig. 4.7 A typical load-deflection curve for cubic foam specimens loaded parallel to the rise direction, $\rho_c/\rho_s = 0.13$.

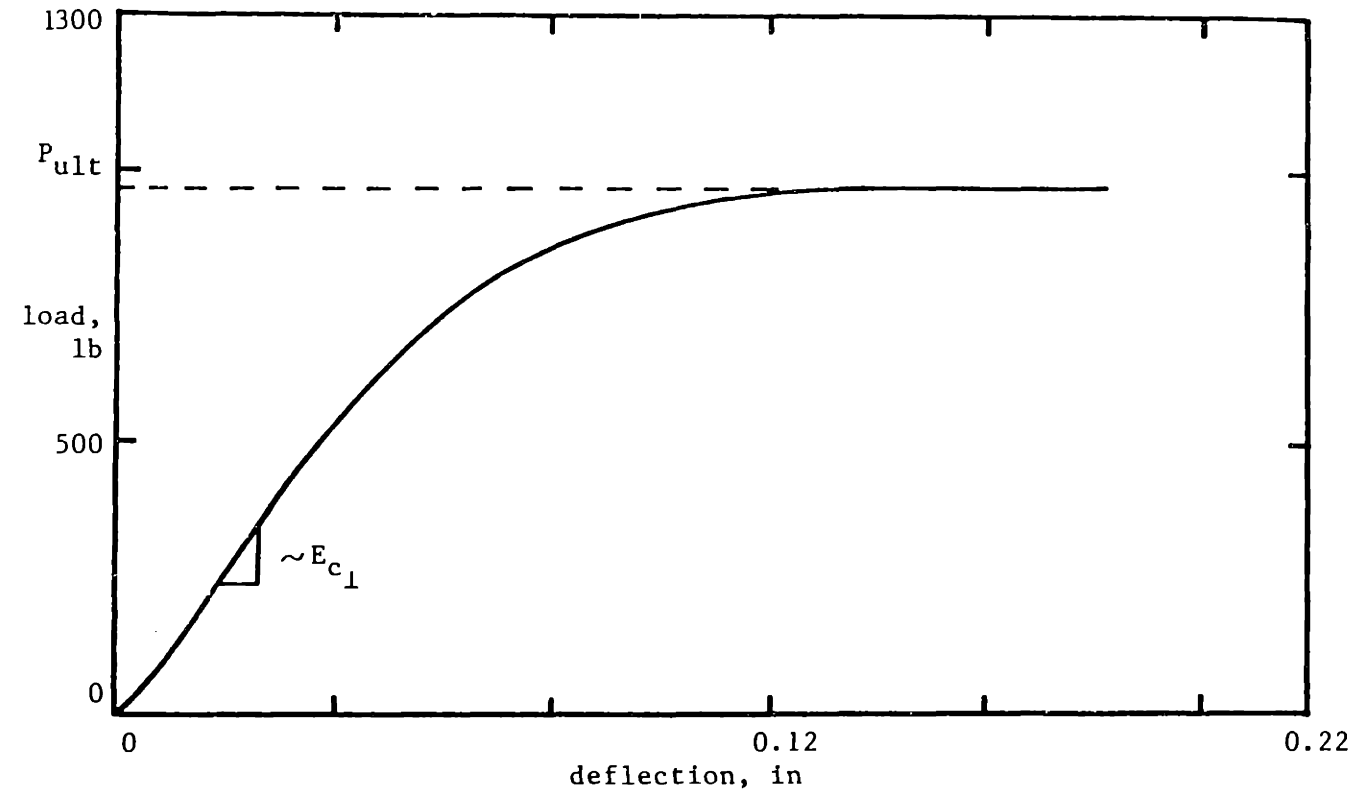

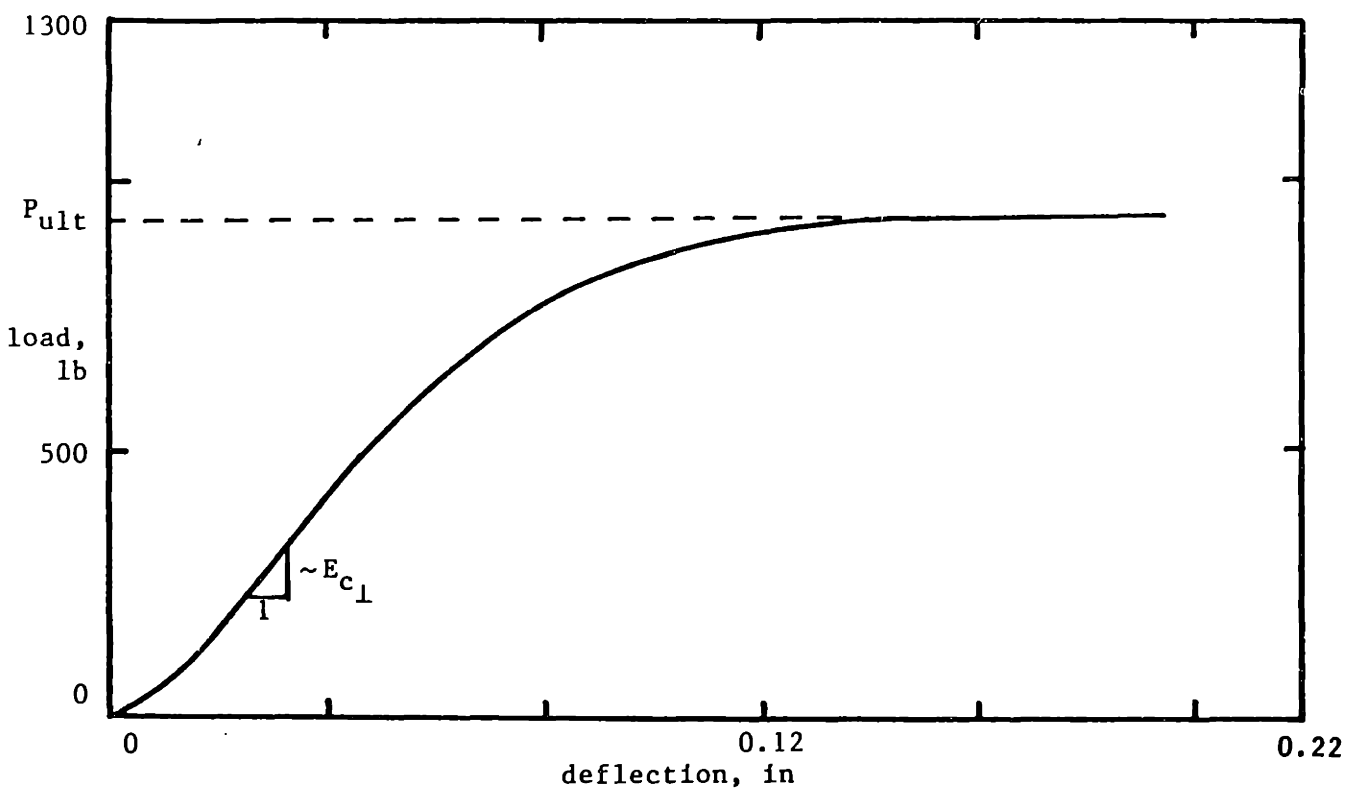

Fig. 4.8 Typical load-deflection curves for cubic foam specimens loaded in two different directions perpendicular to the rise, $\rho_c/\rho_s = 0.13$.

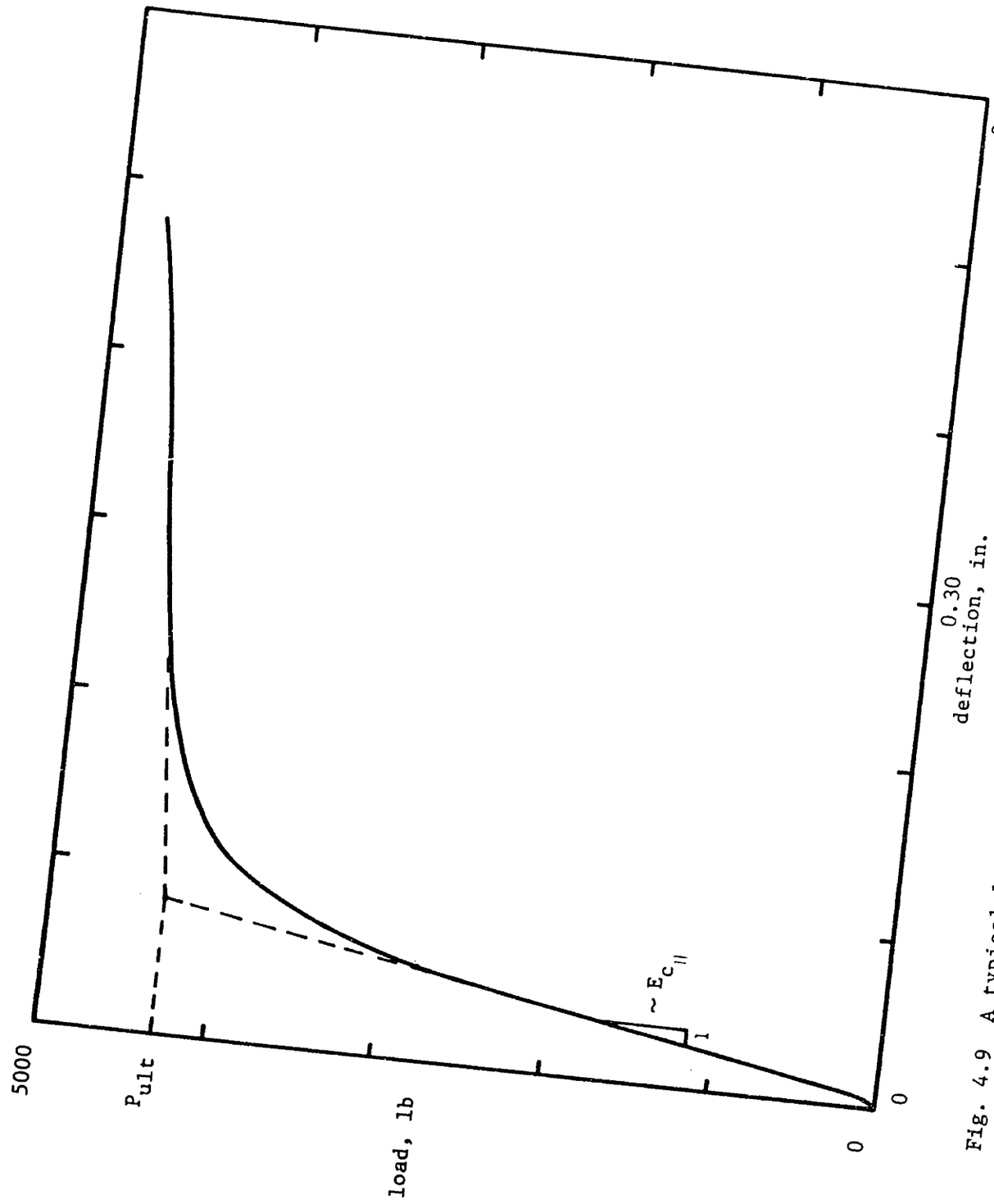

Fig. 4.9 A typical load-deflection curve for cubic foam specimens loaded parallel to the rise direction, $\rho_c/\rho_s = 0.27$.

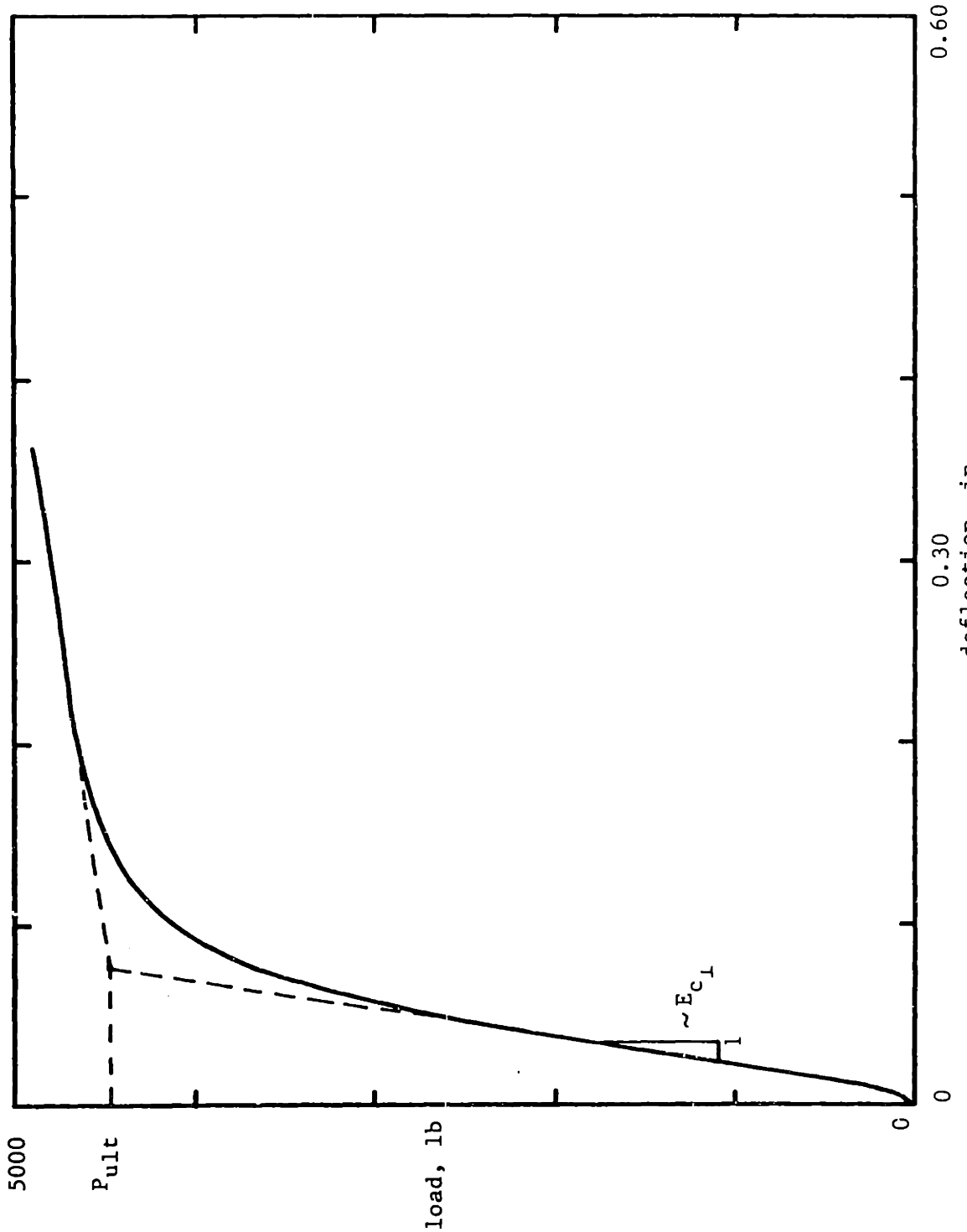

Fig. 4.10 Typical load-deflection curves for cubic foam specimens loaded in two different directions perpendicular to the rise, $\rho_c/\rho_s = 0.27$.

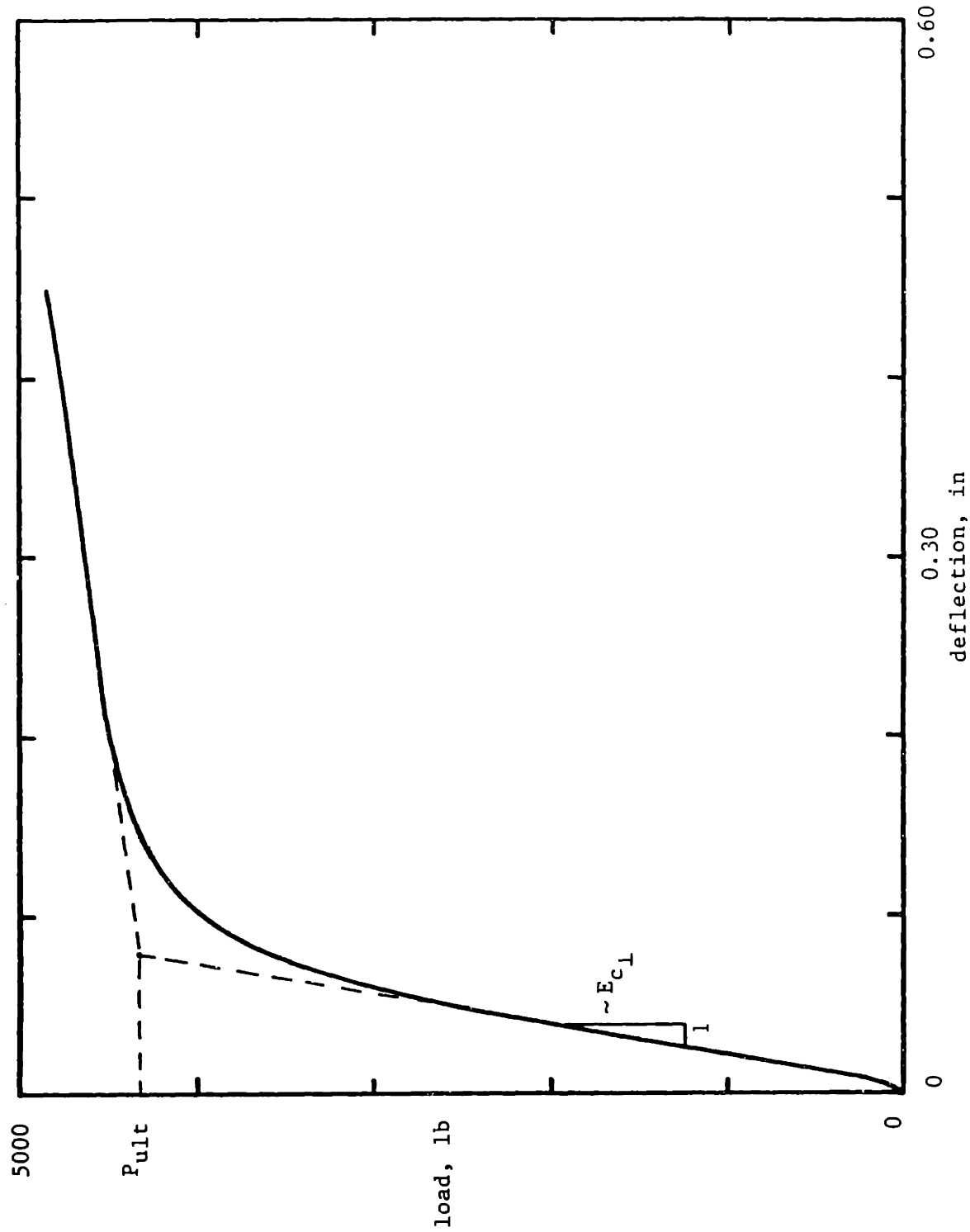

Fig. 4.10 continued.

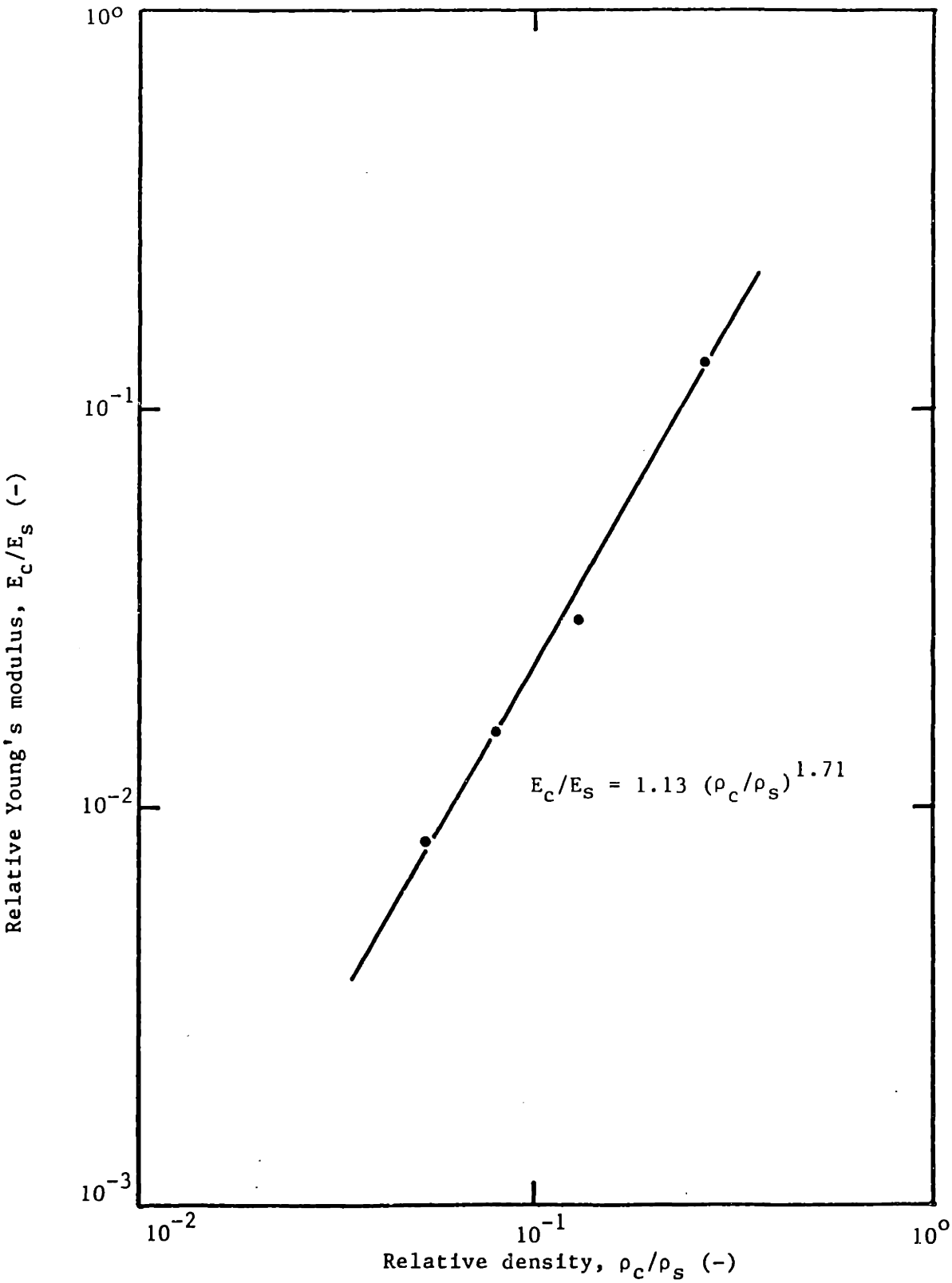

Fig. 4.11 The elastic modulus of the polyurethane foams tested. Data are presented for loading perpendicular to the rise direction.

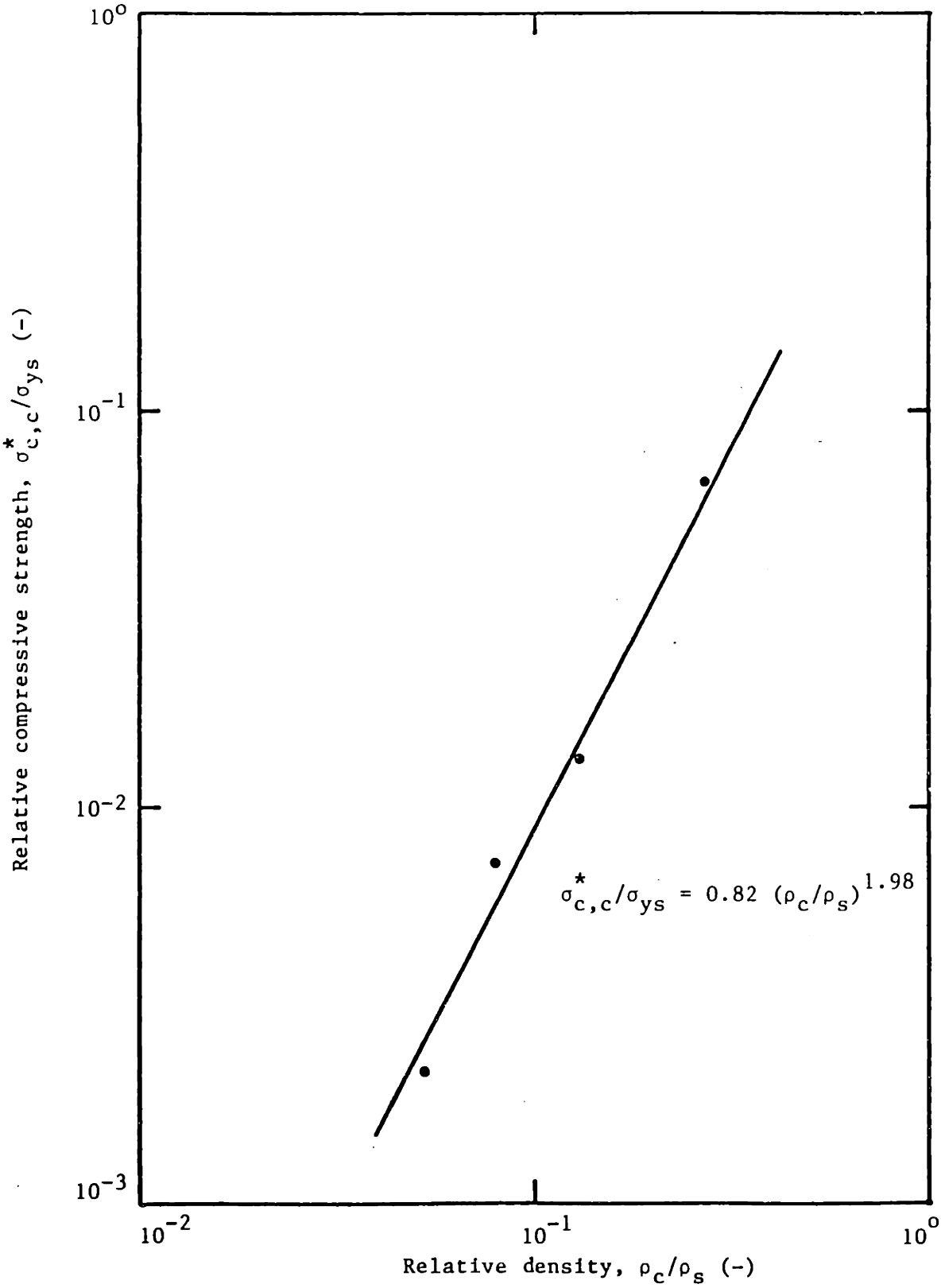

Fig. 4.12 The compressive strength of the polyurethane foams tested. Data are presented for loading perpendicular to the rise direction.

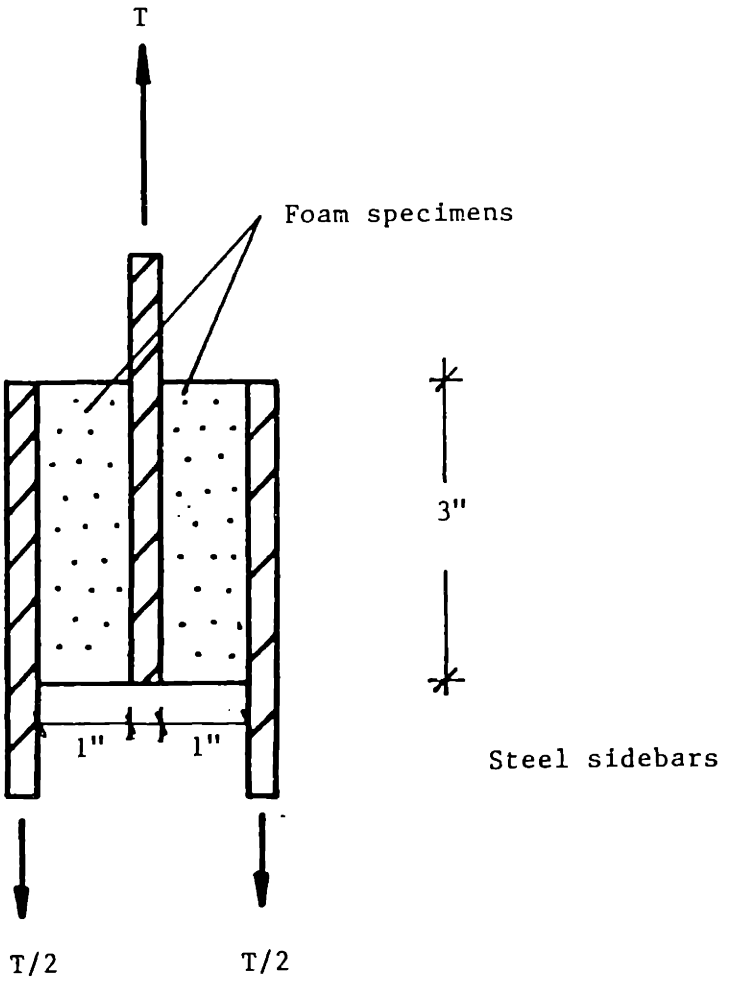

Fig. 4.13 The loading arrangement for measuring the shear strength of the foam specimens.

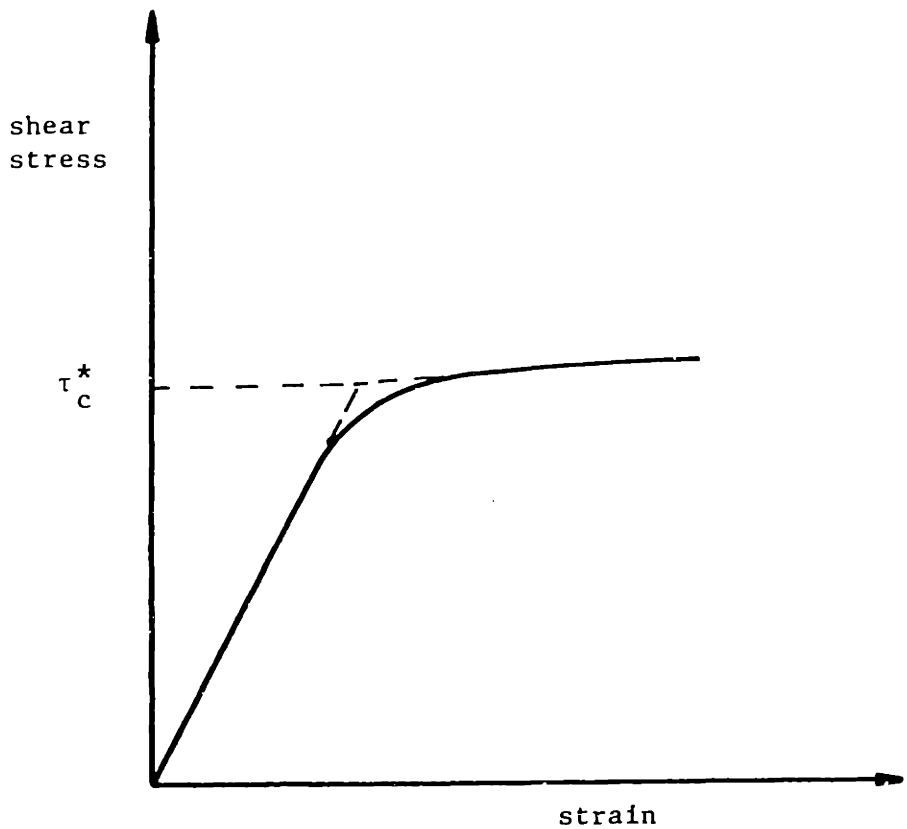

Fig. 4.14 Definition of the core shear strength.

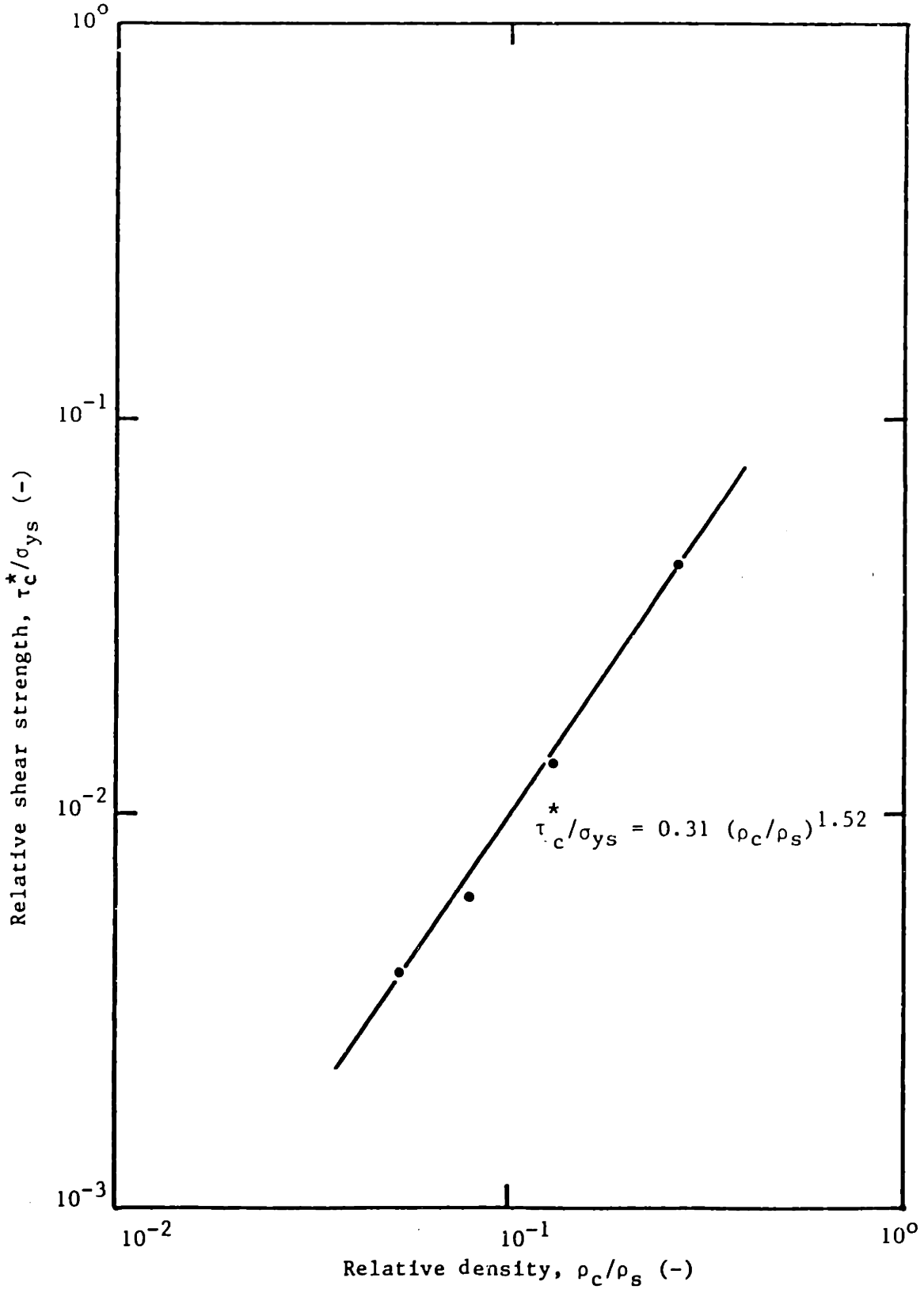

Fig. 4.15 The shear strength of the polyurethane foams tested. Data are presented for loading perpendicular to the rise direction.

foam specimen

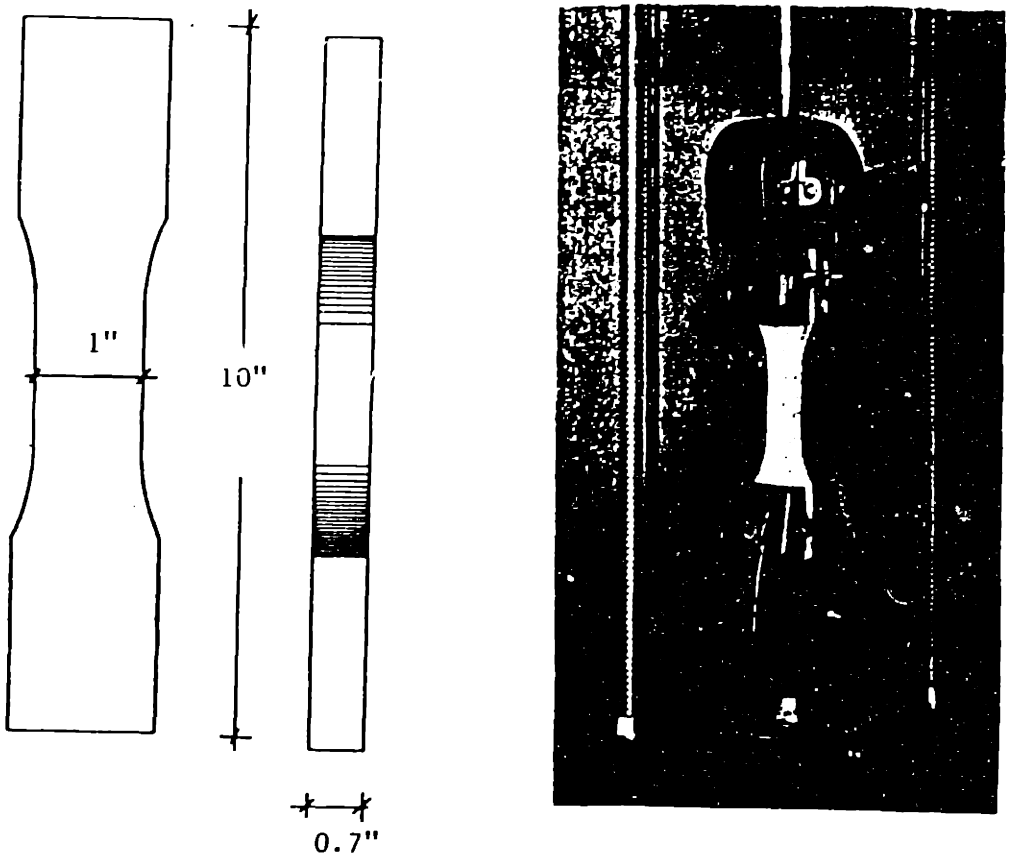

Fig. 4.16 Assembly for tension tests.

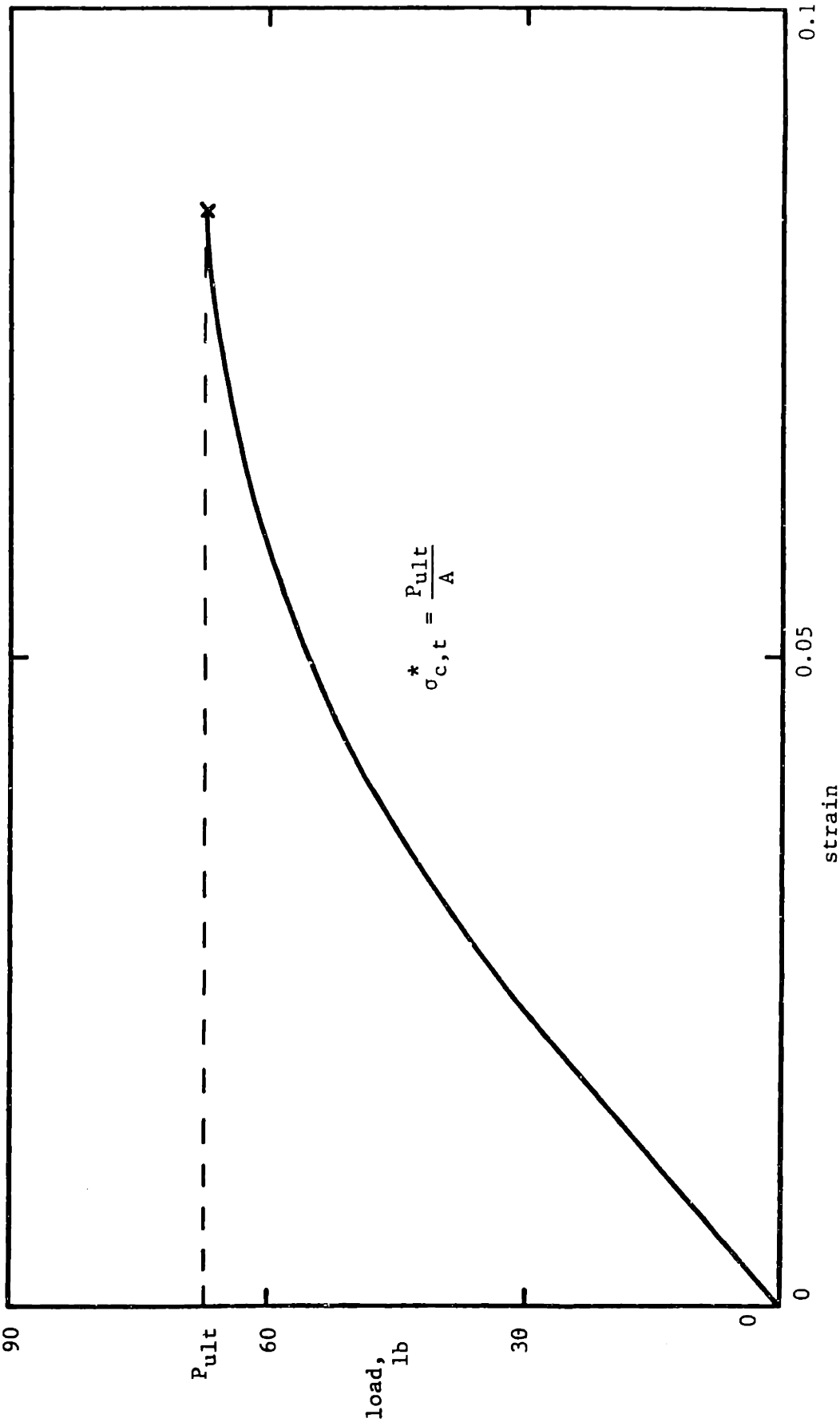

Fig. 4.17 A typical load-strain curve for foam specimens subject to tension, $\rho_c/\rho_s = 0.0533$.

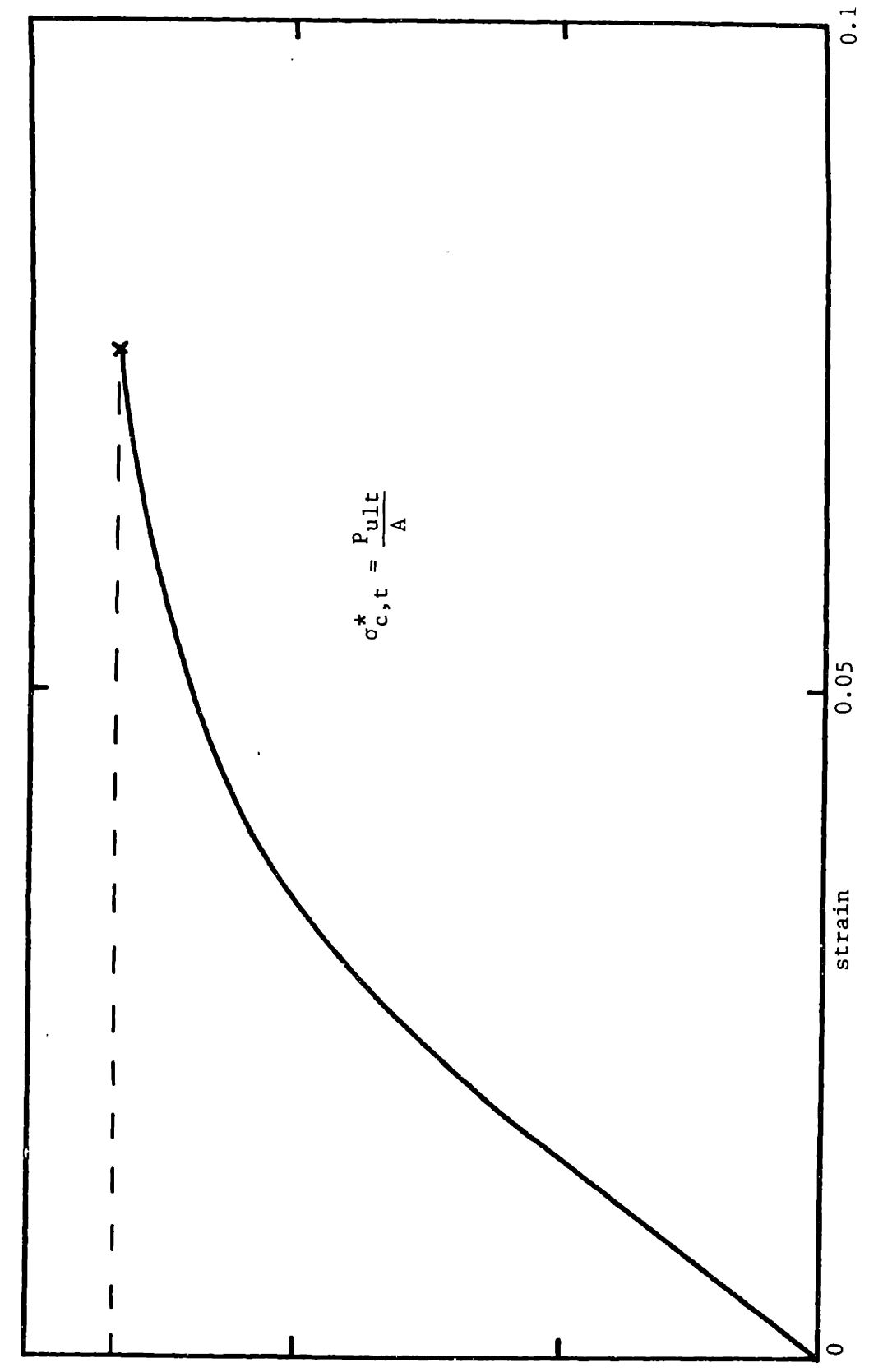

Fig. 4.18 A typical load-strain curve for foam specimens subject to tension, $\rho_c/\rho_s = 0.08$.

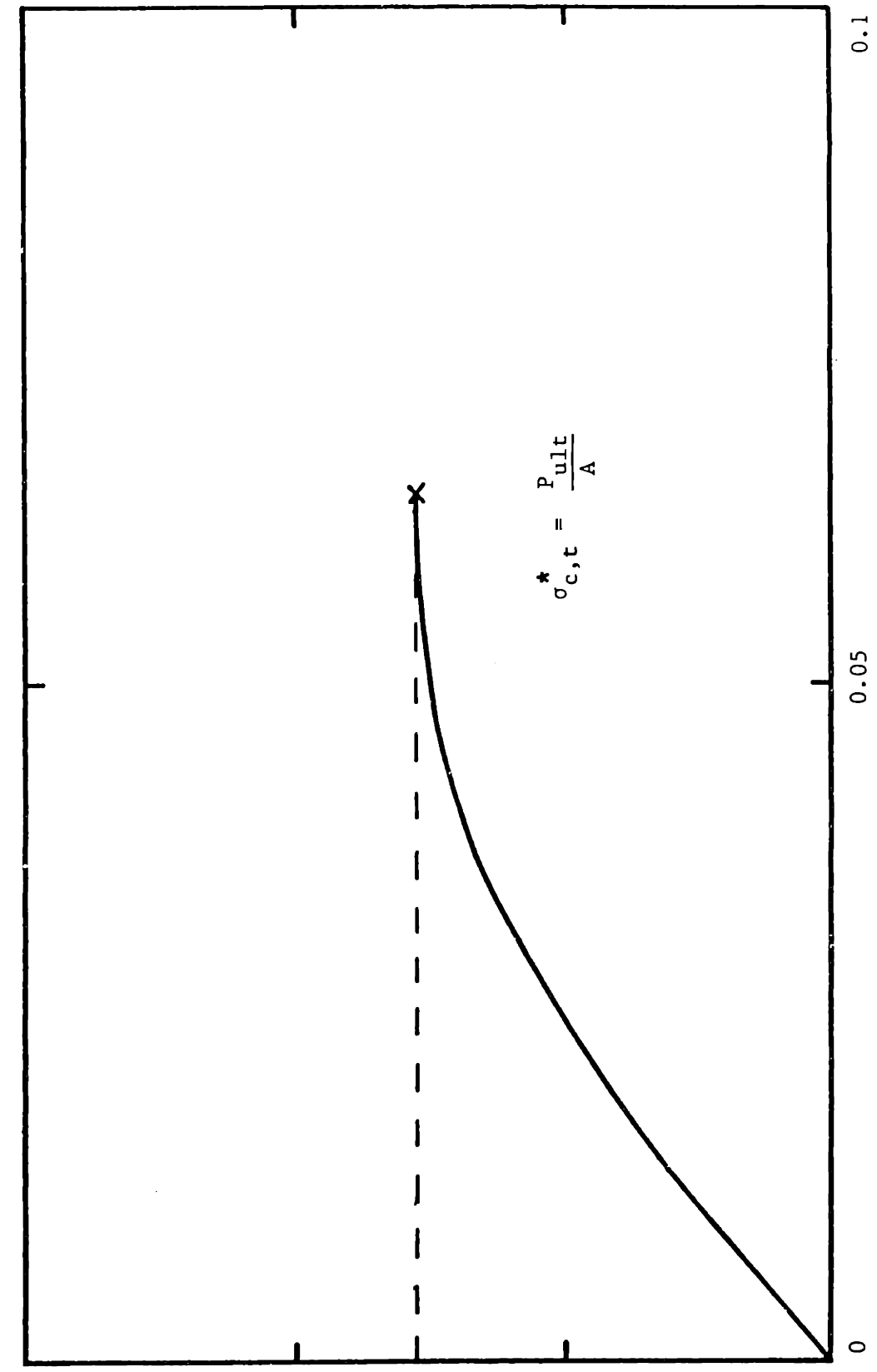

Fig. 4.19 A typical load-strain curve for foam specimens subject to tension, $\rho_c/\rho_s = 0.13$.

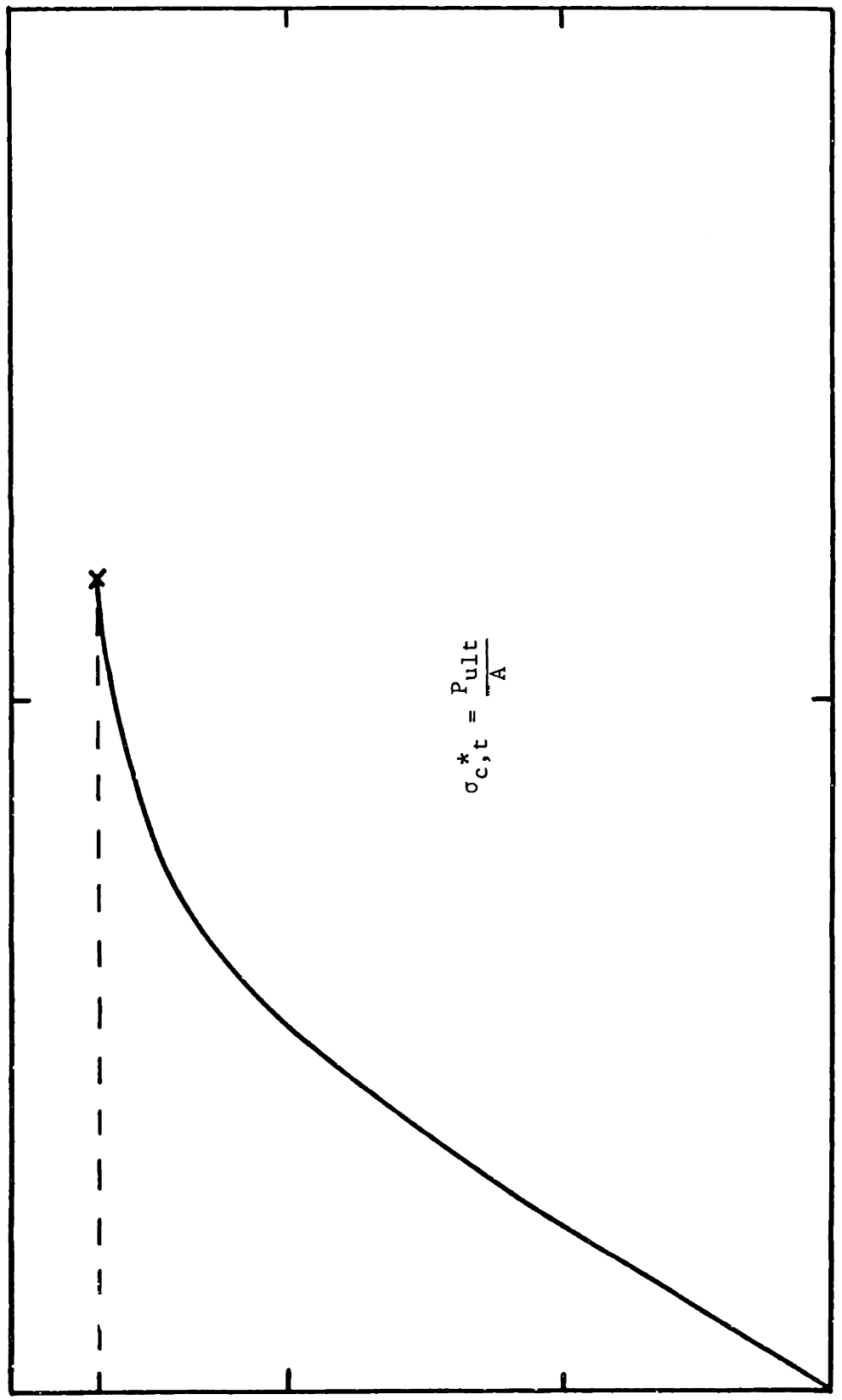

Fig. 4.20 A typical load-strain curve for foam specimens subject to tension, $\rho_c/\rho_s = 0.27$.

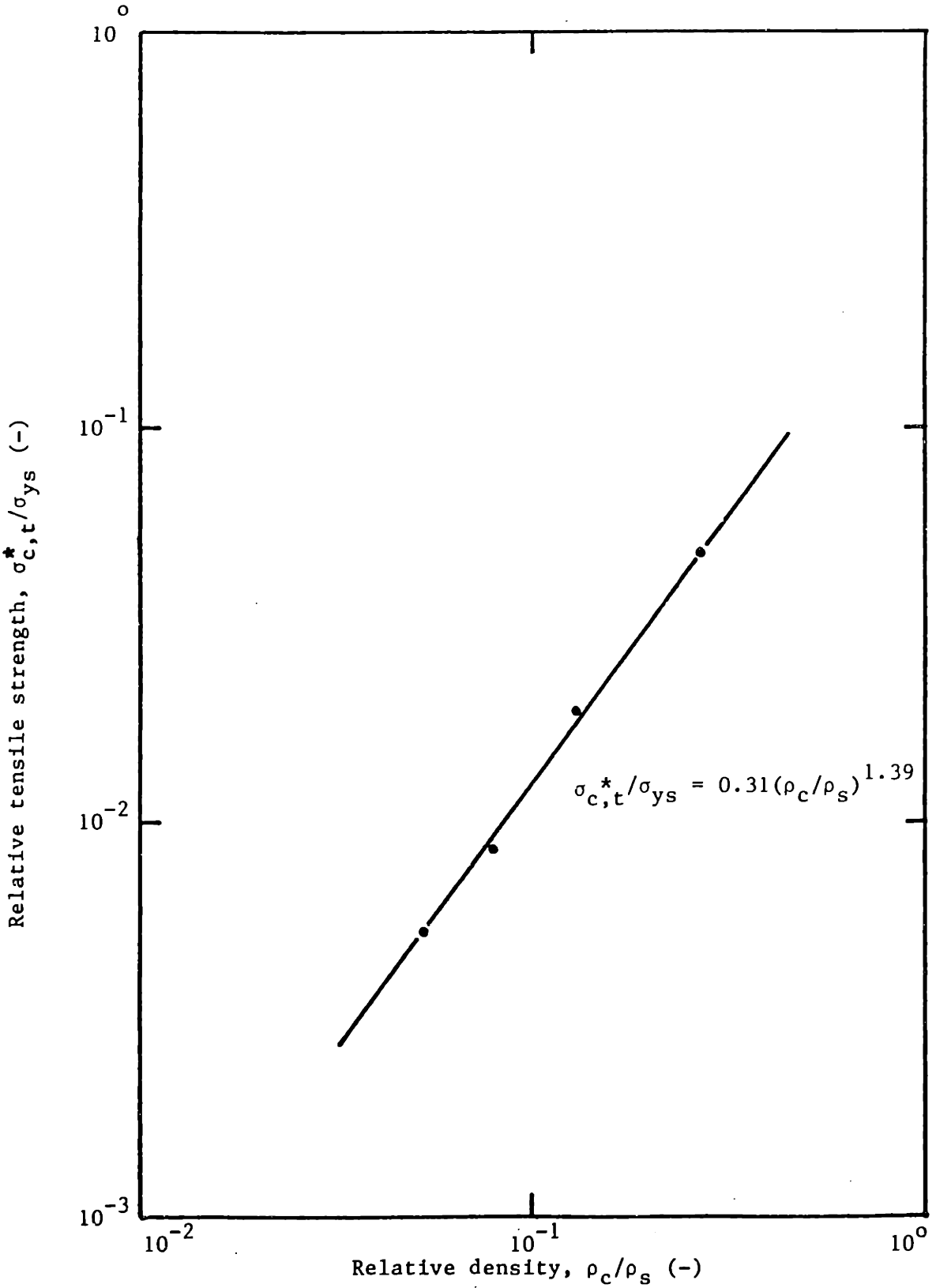

Fig. 4.21 The tensile strength of the polyurethane foams tested. Data are presented for loading perpendicular to the rise direction.

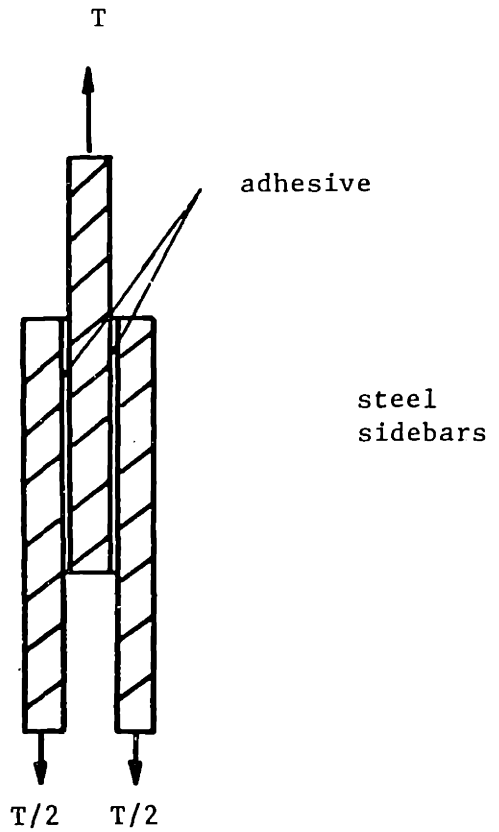

Fig. 4.22 Assembly for measuring the shear strength of the adhesive.

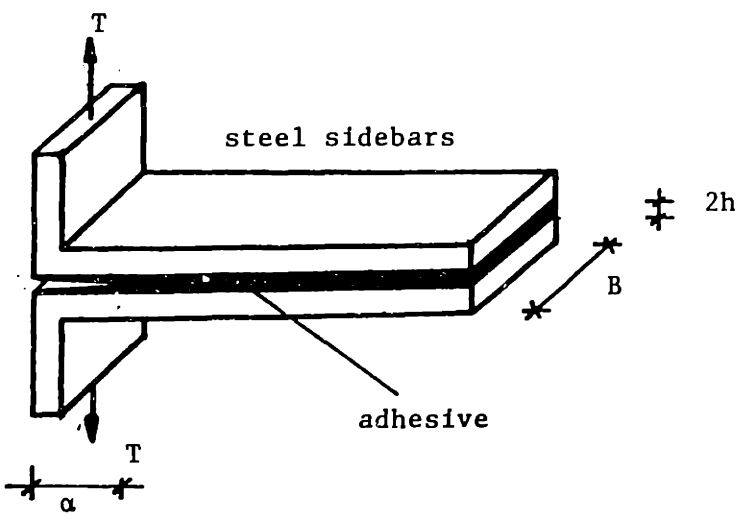

Fig. 4.23 Assembly for measuring the adhesive critical stress intensity factor.

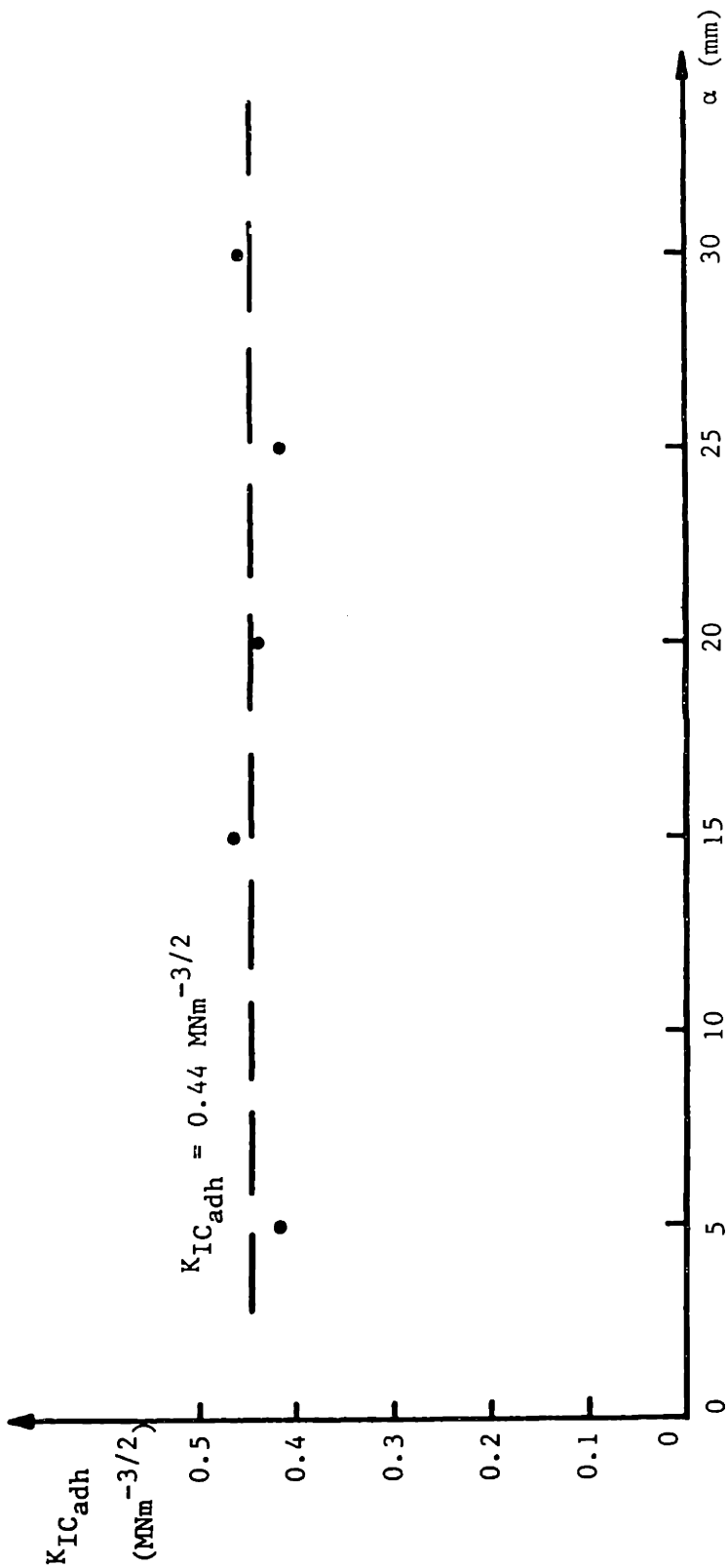

Fig. 4.24 Variation of the adhesive fracture toughness with the initial crack length.

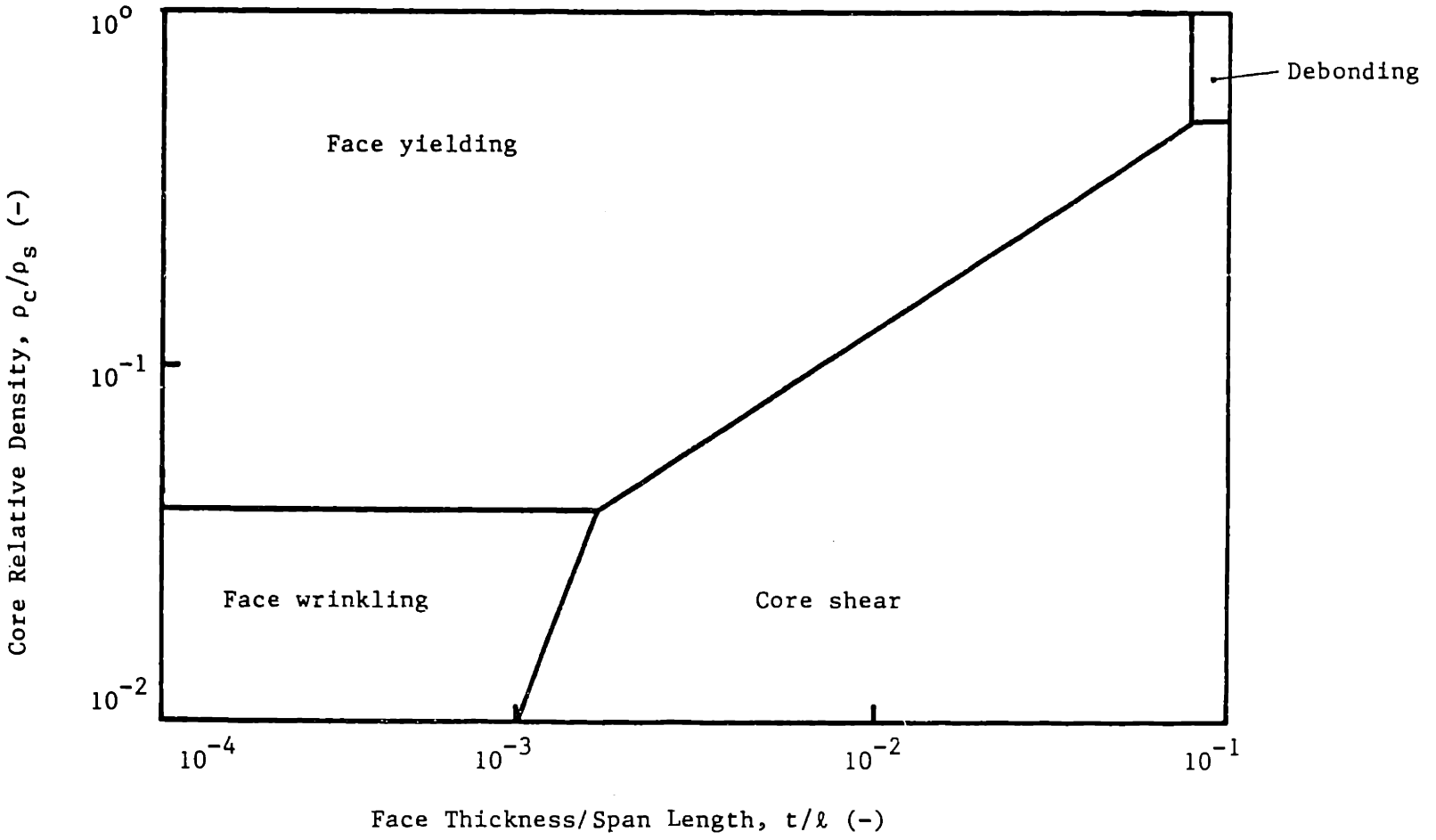

Fig. 4.25 Rectangular sandwich beam failure mode map (adhesive shear strentgth approach; simply supported beam under mid-span loading).

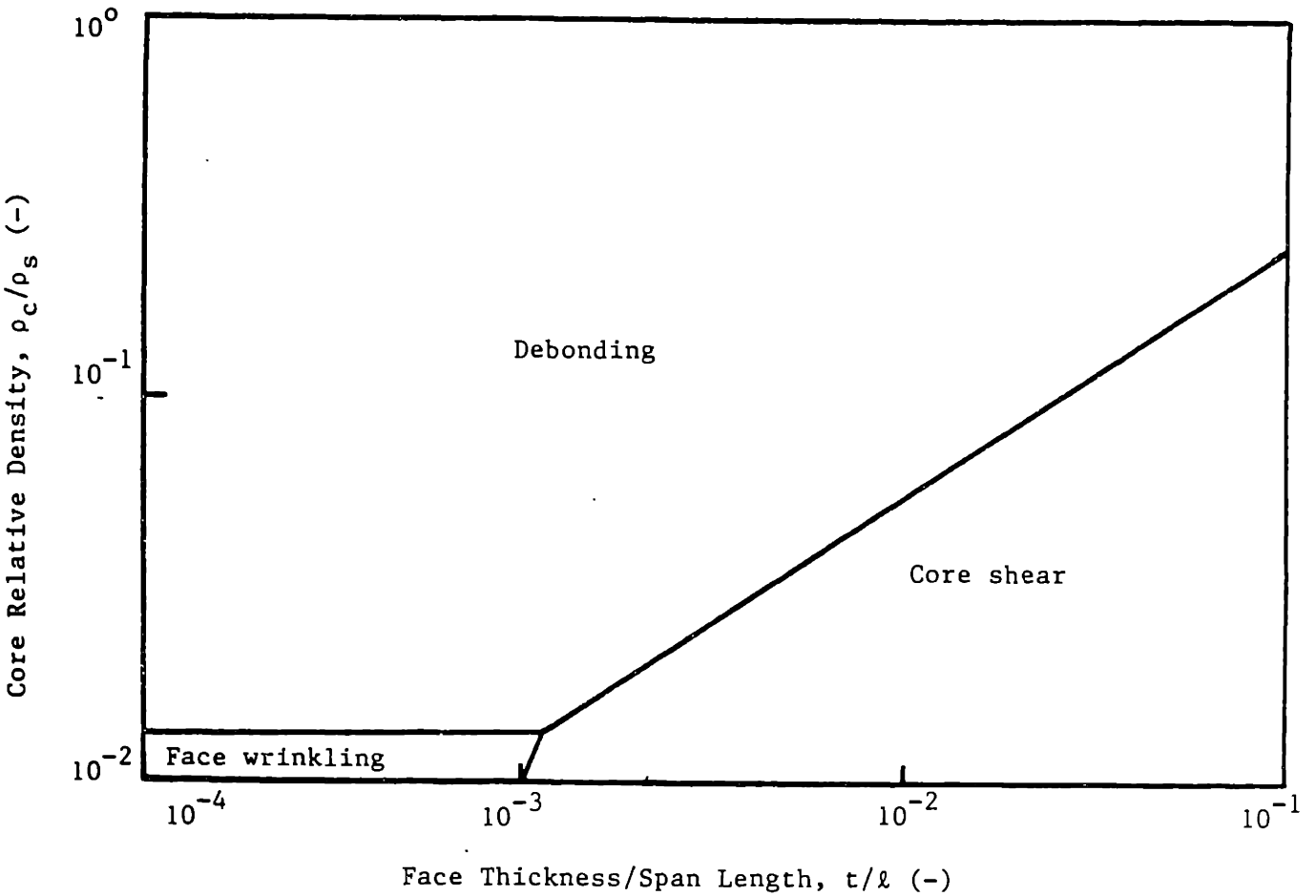

Fig. 4.26 Rectangular sandwich beam failure mode map (adhesive fracture approach - initial flaw size α = 0.0001m; simply supported beam under mid-span loading).

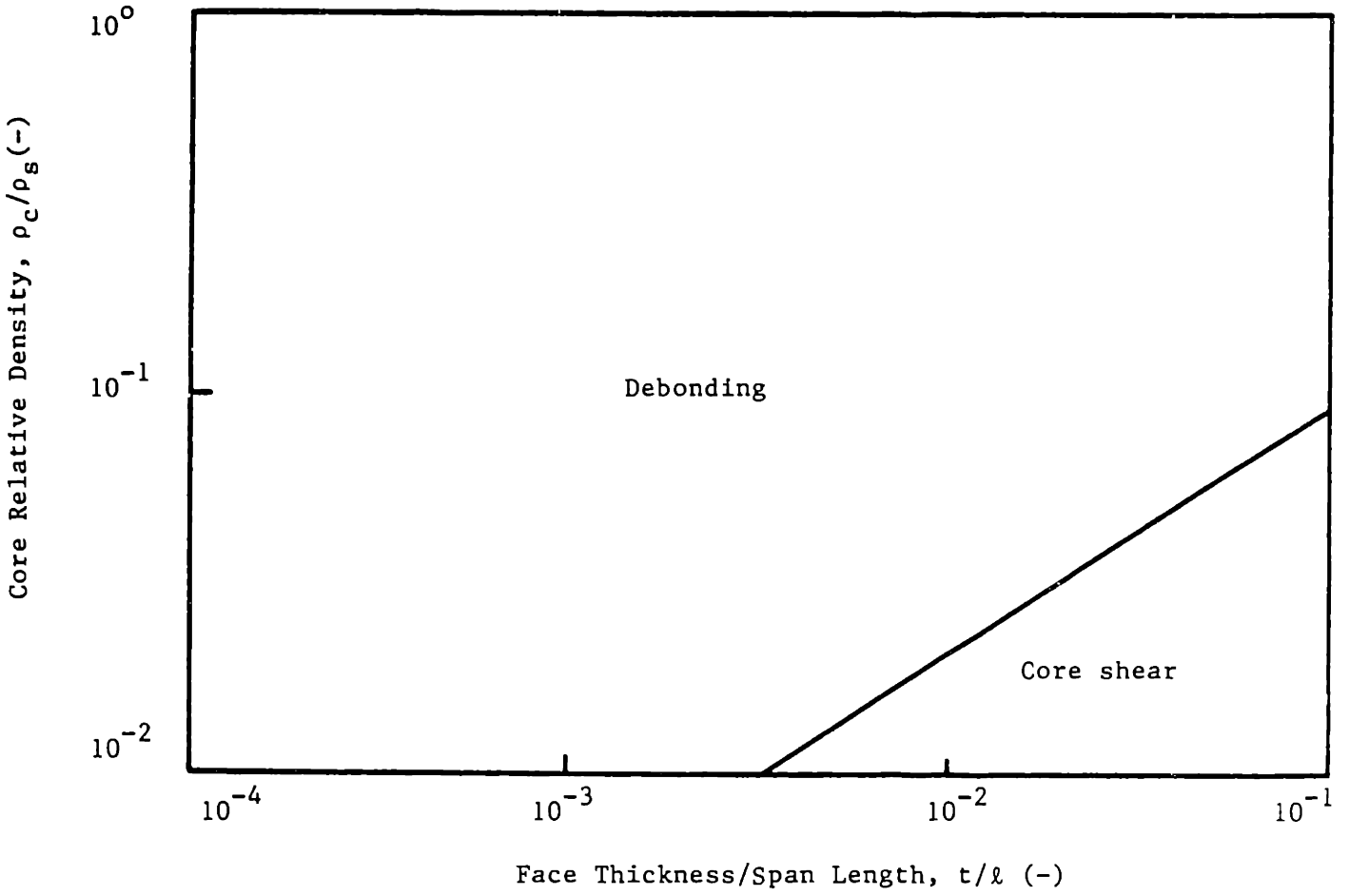

Fig. 4.27 Rectangular sandwich beam failure mode map (adhesive fracture approach-initial flaw size α=0.002mm; simply supported beam under mid-span loading).

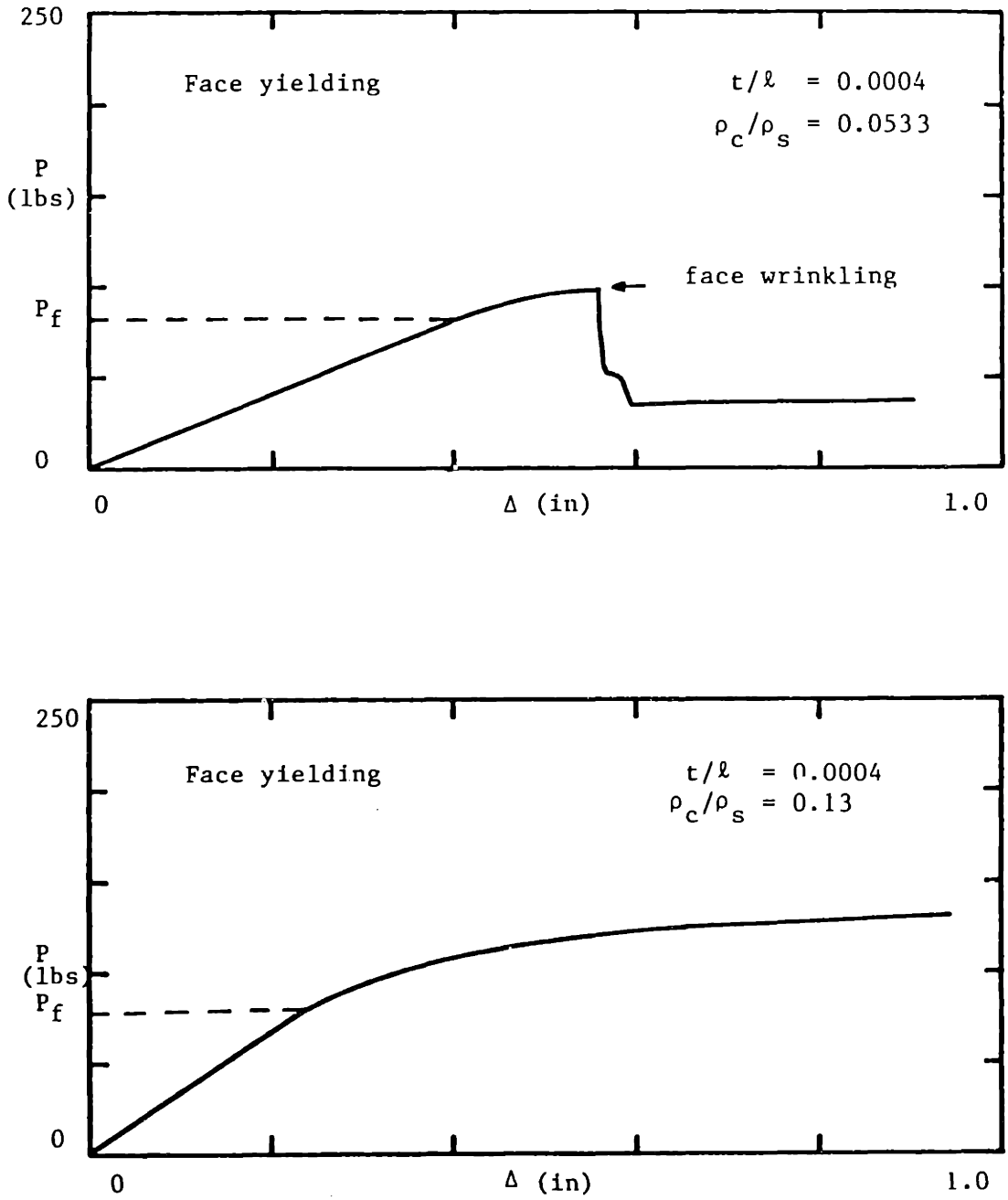

Fig. 4.28 Load-deflection curves for rectangular sandwich beams in 3-point bending; P_f = failure load.

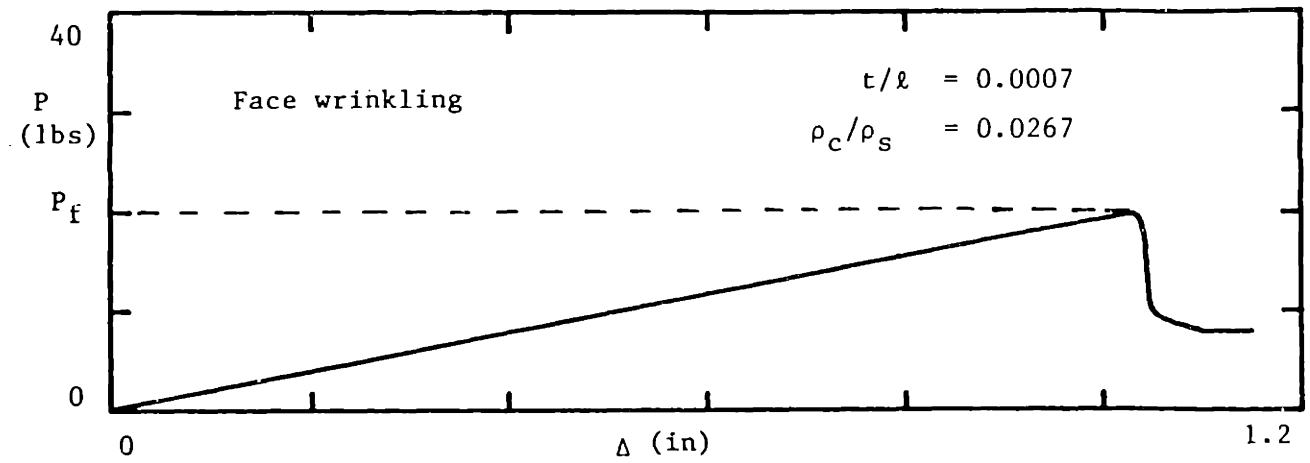

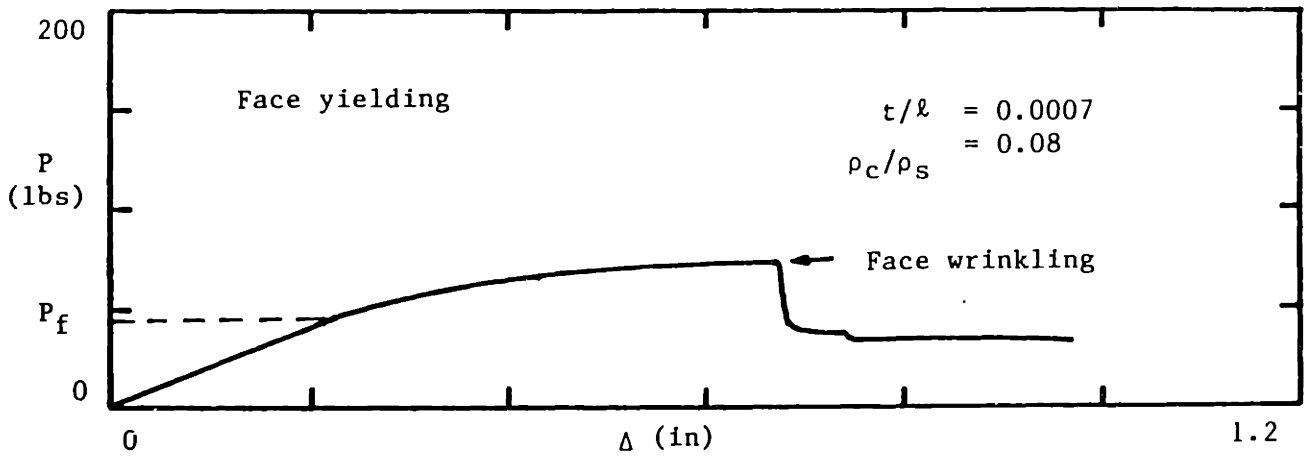

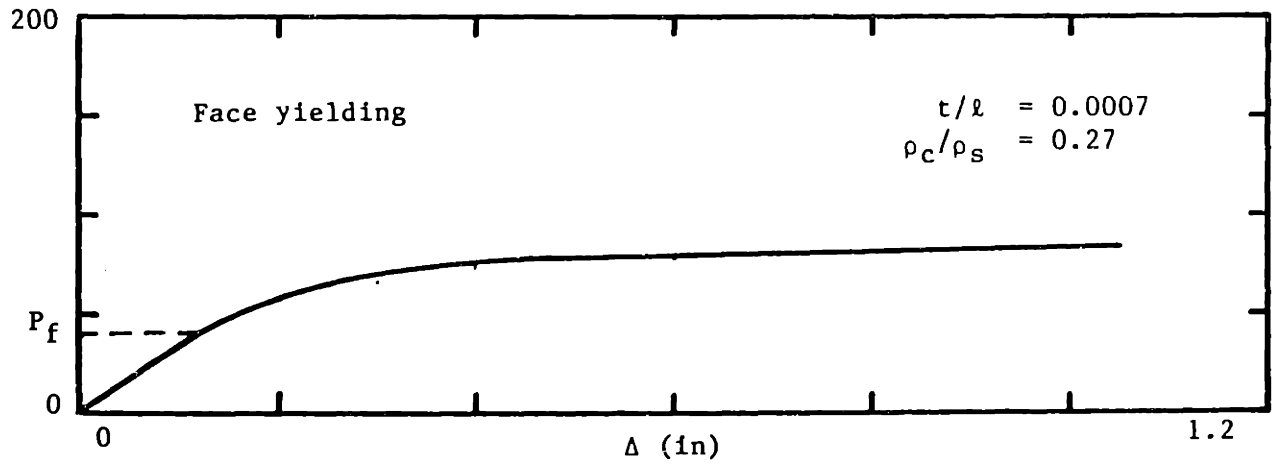

Fig. 4.28 continued.

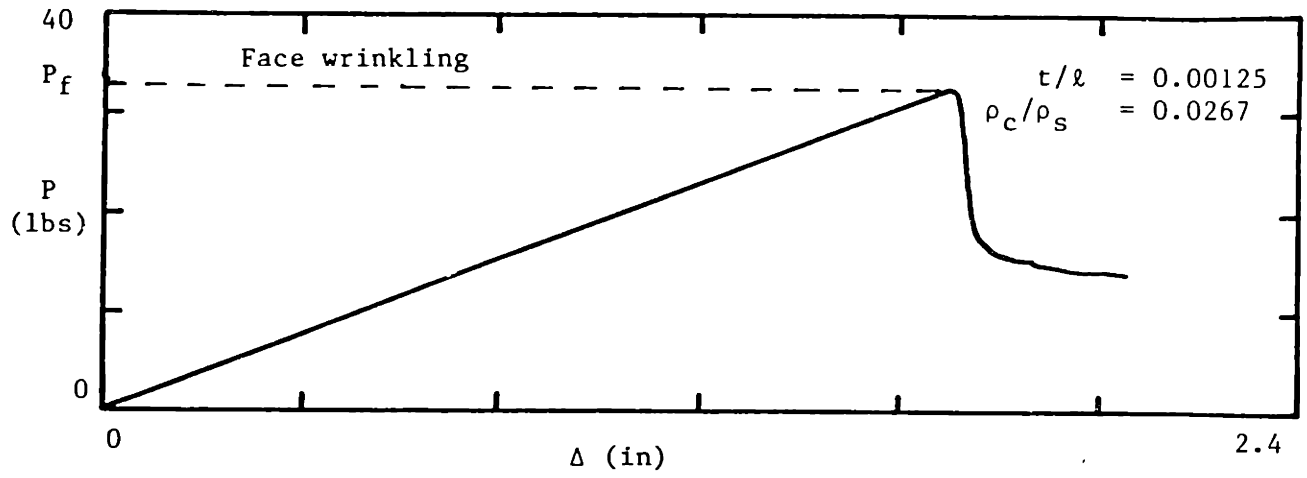

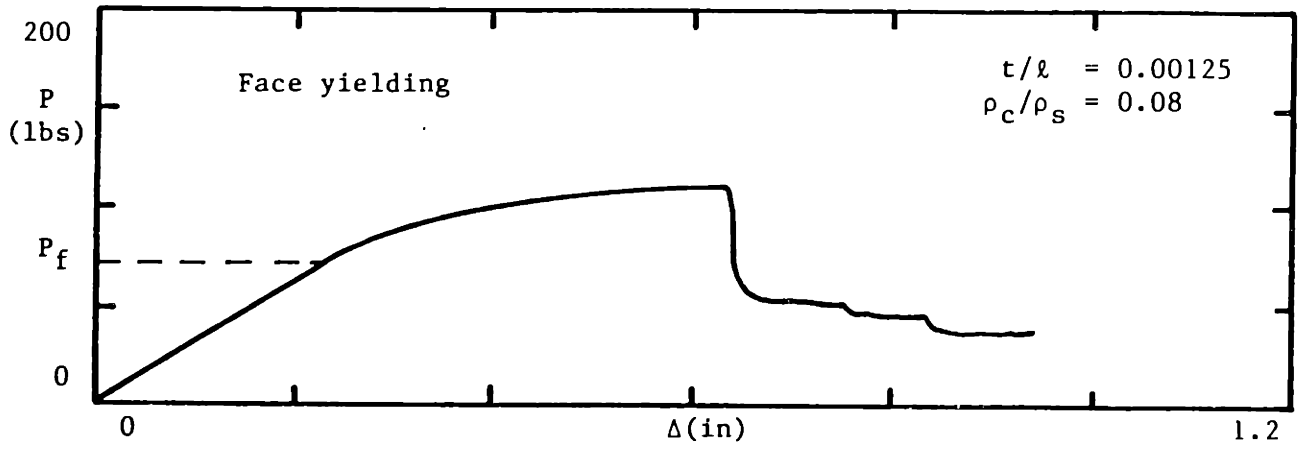

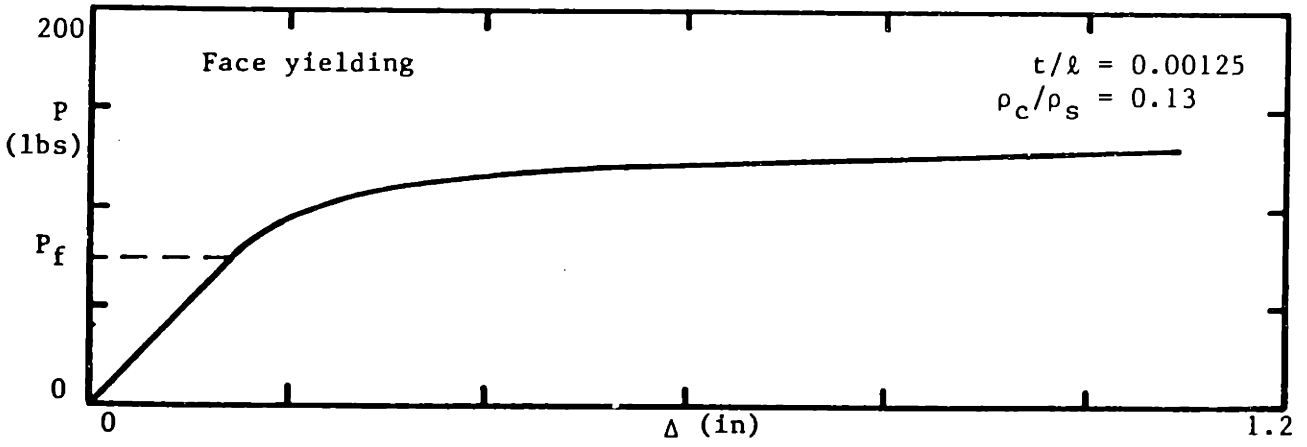

Fig. 4.28 continued.

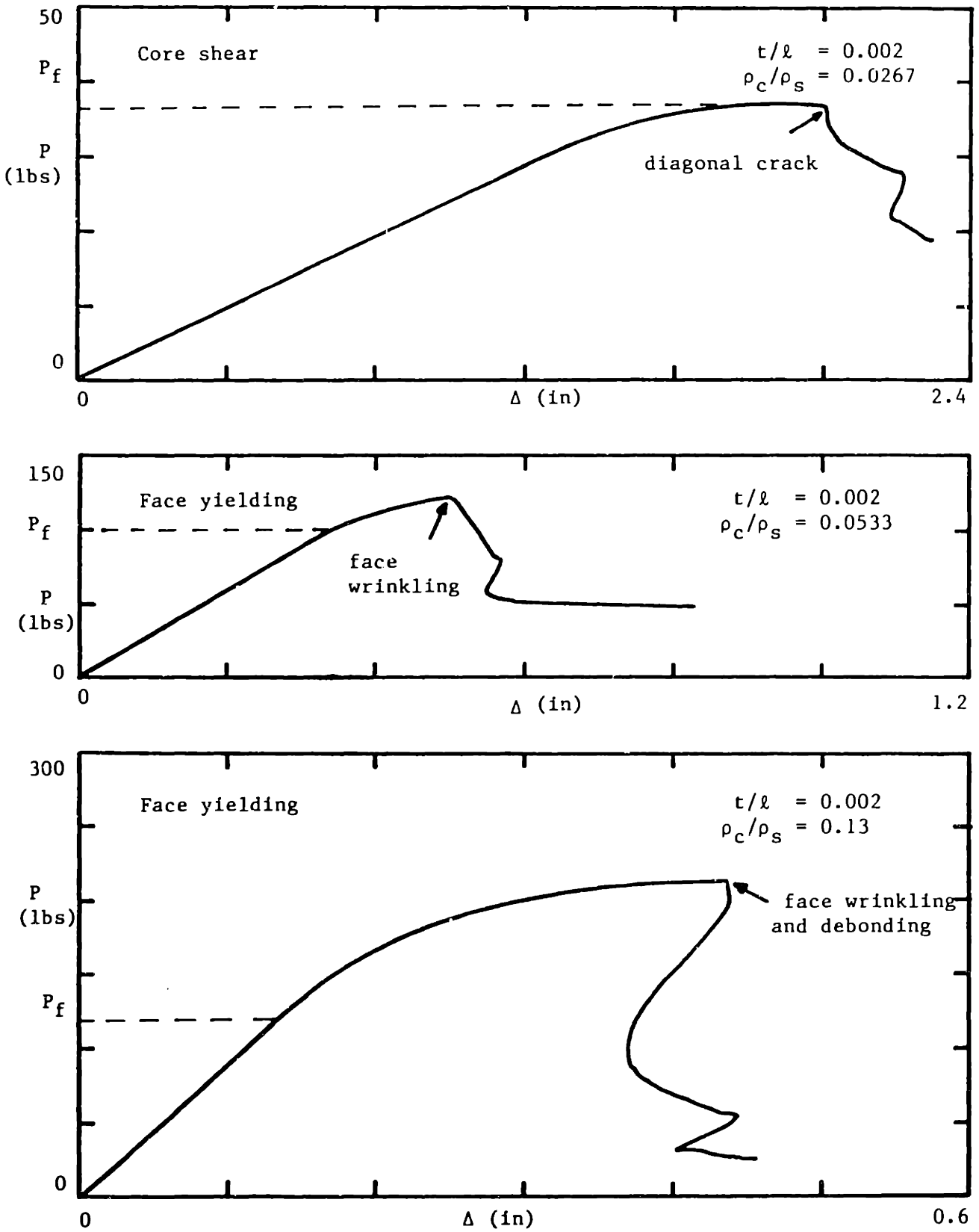

Fig. 4.28 continued.

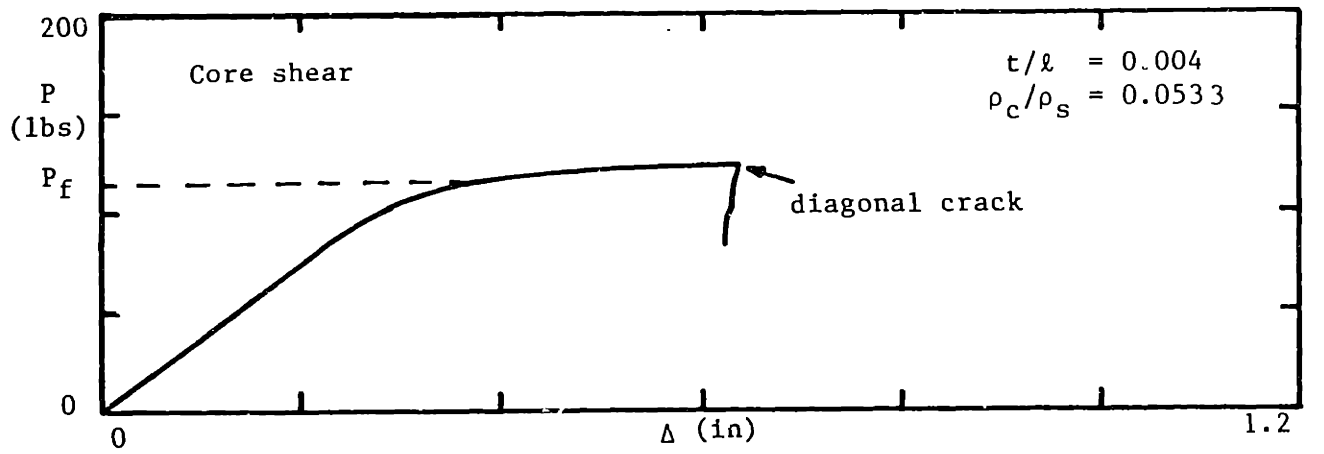

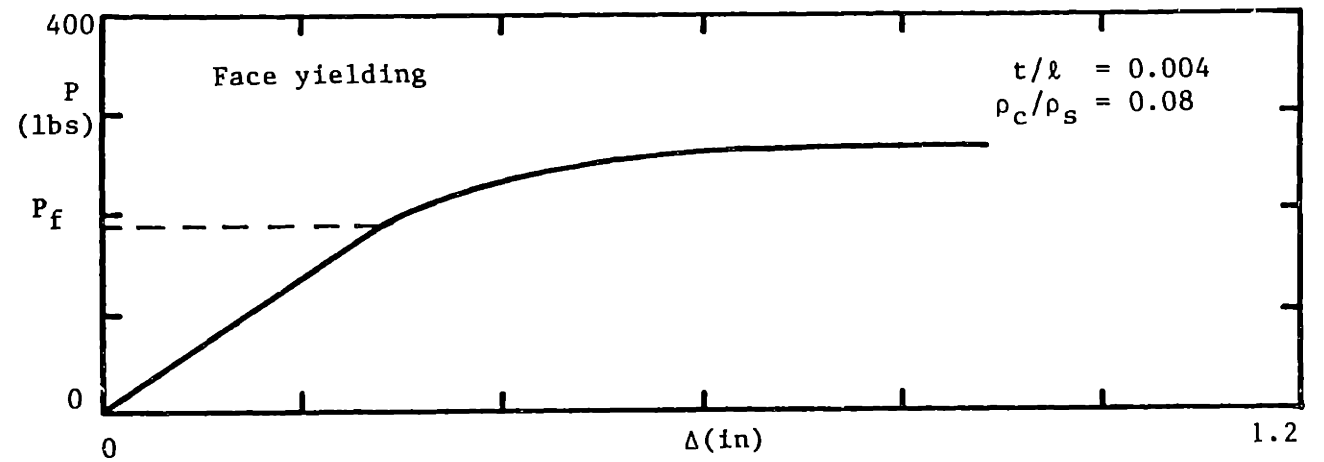

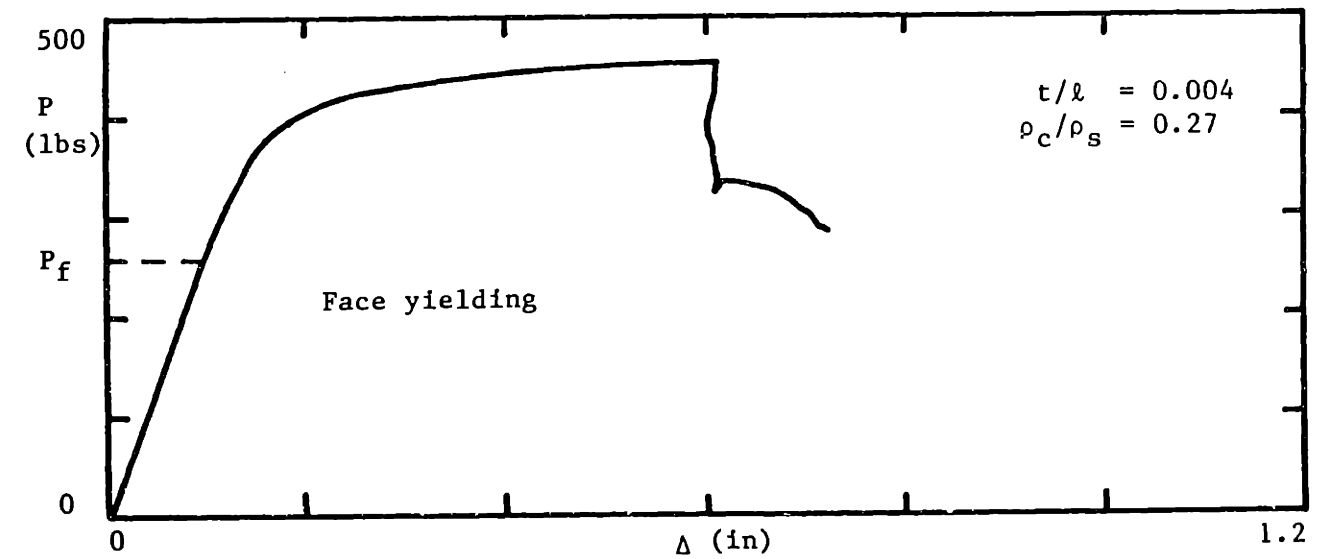

Fig. 4.28 continued.

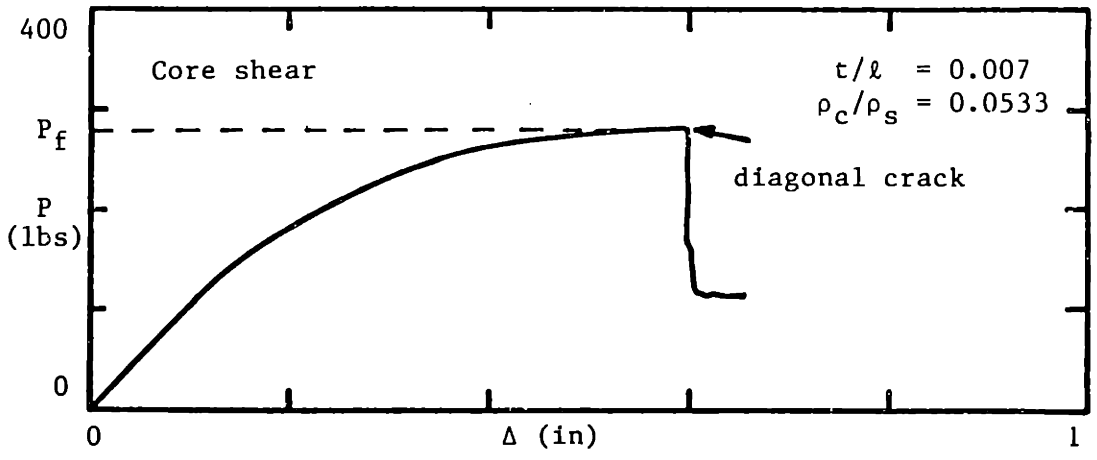

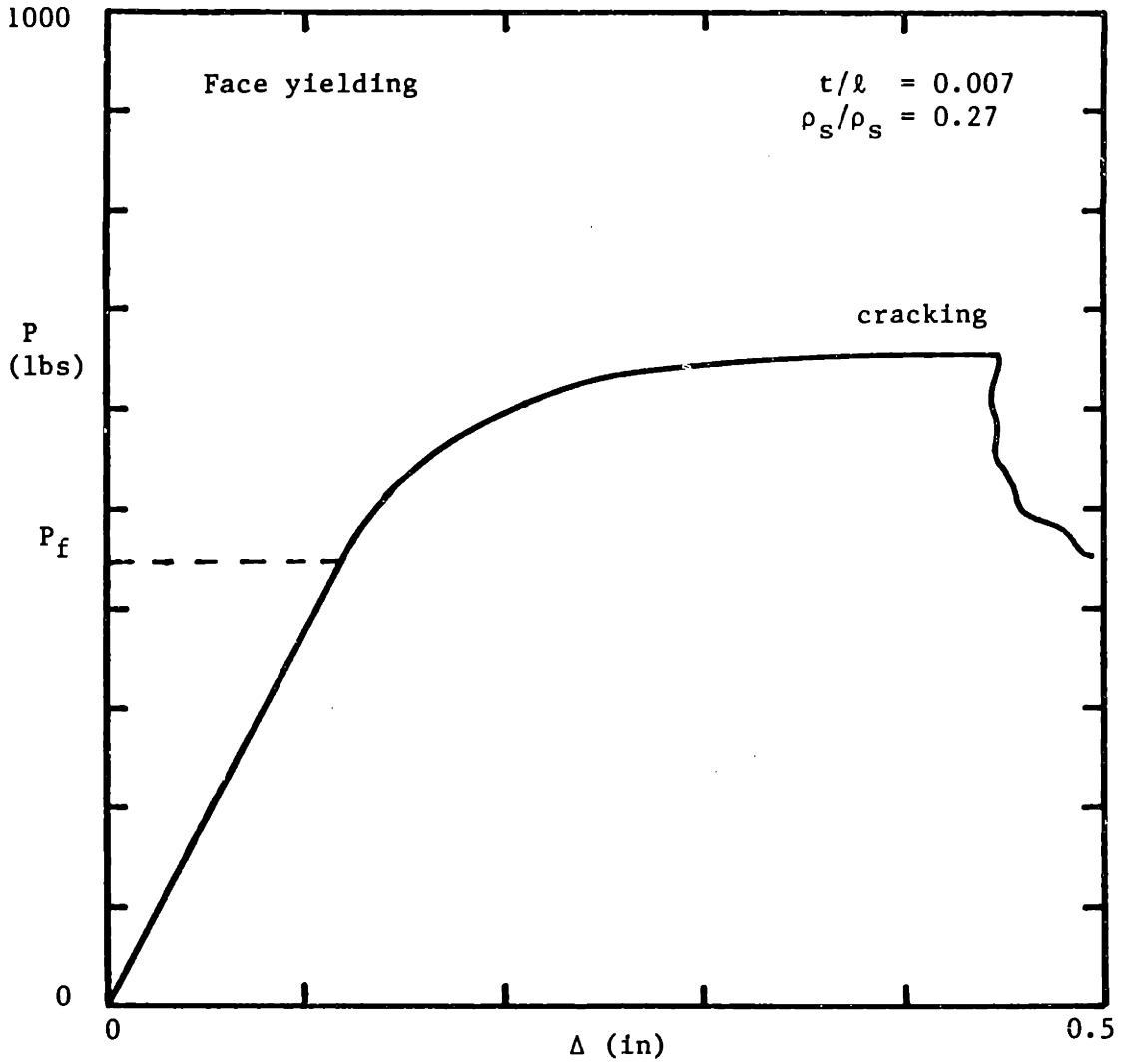

Fig. 4.28 continued.

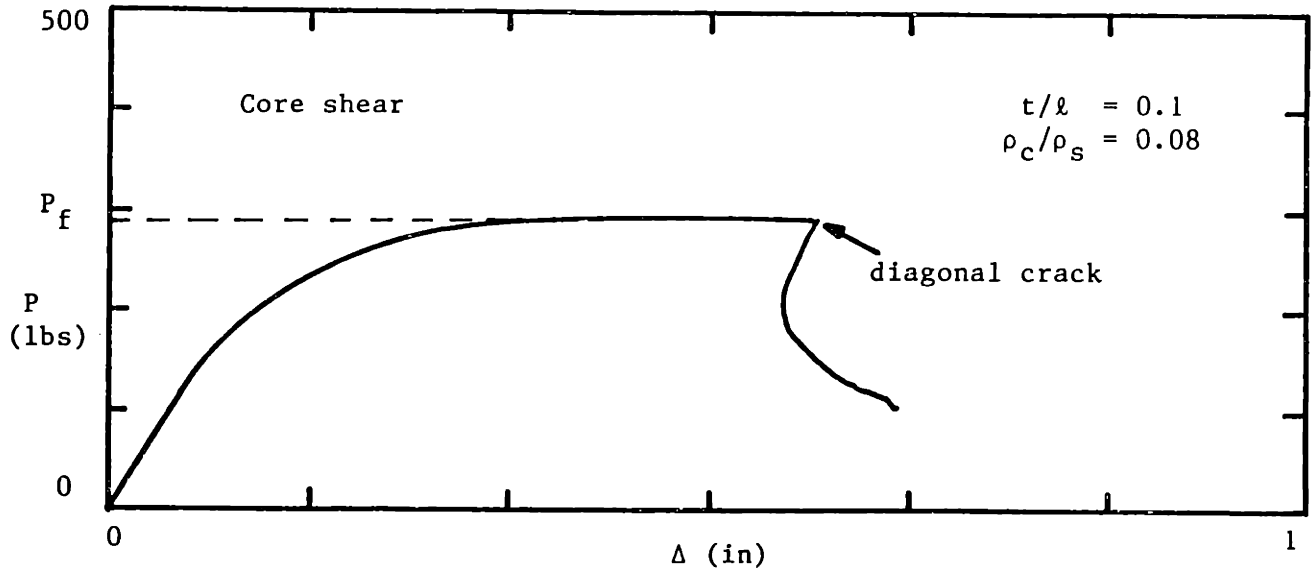

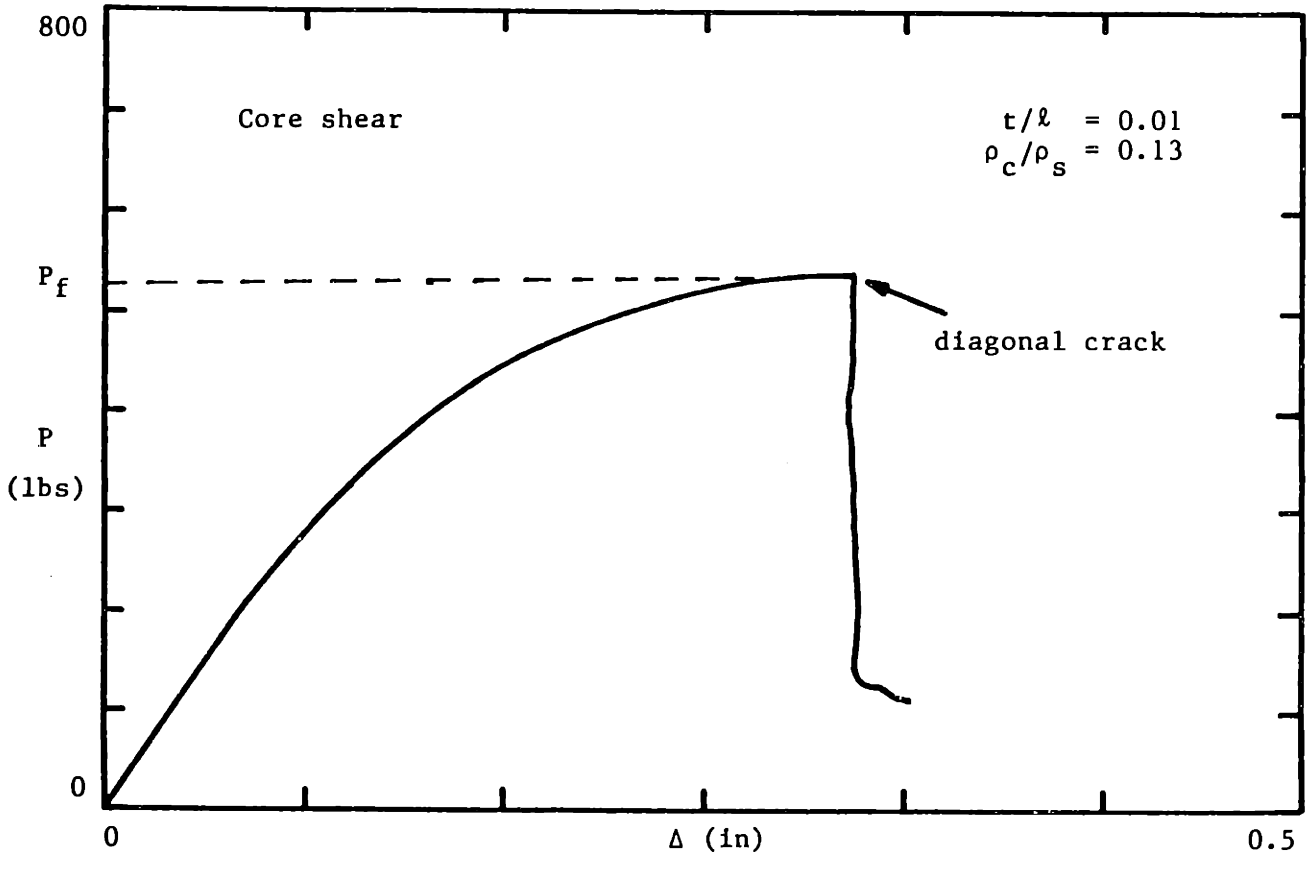

Fig. 4.28 continued.

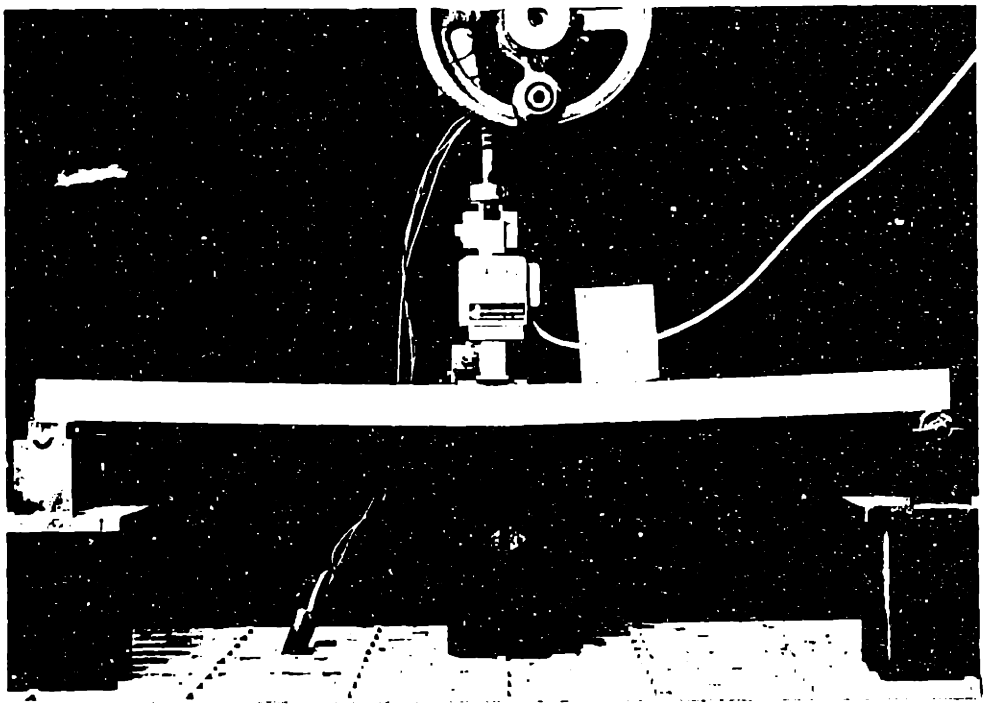

Face yielding - formation of Lüders bands

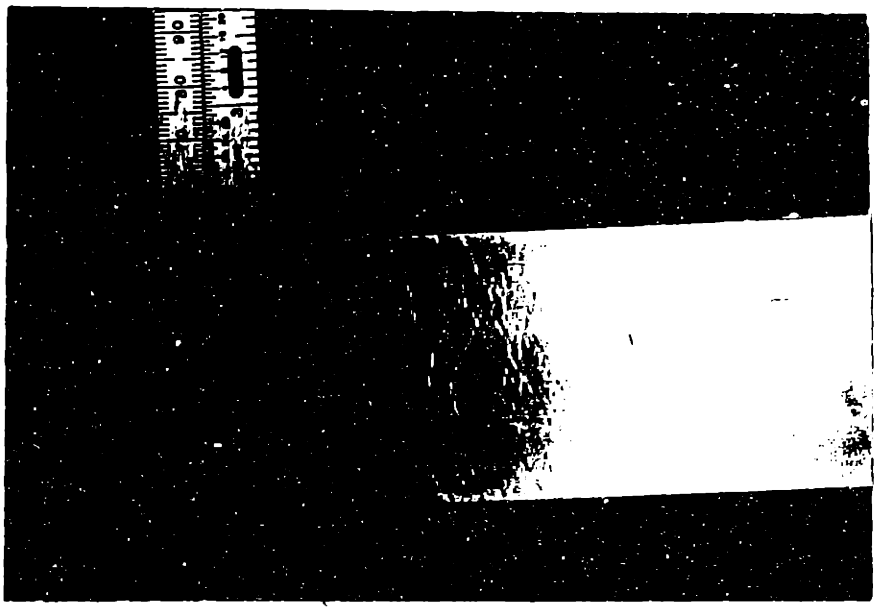

Fig. 4.29 Photographs of typical sandwich beams failure modes.

Face yielding and face rupture followed by core cracking

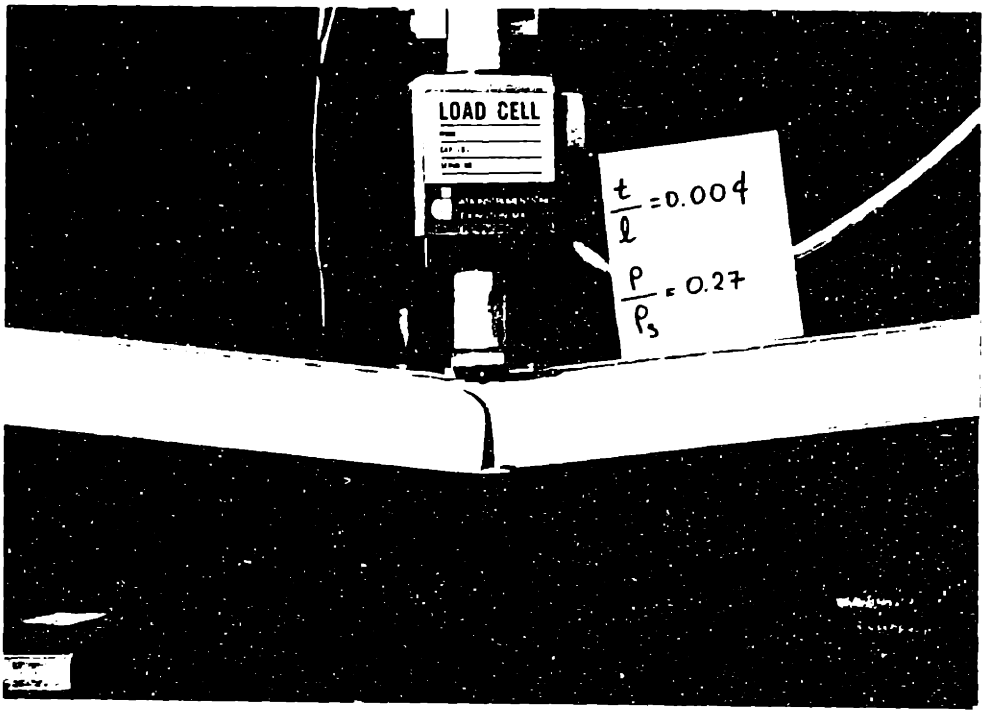

Fig. 4.29 continued.

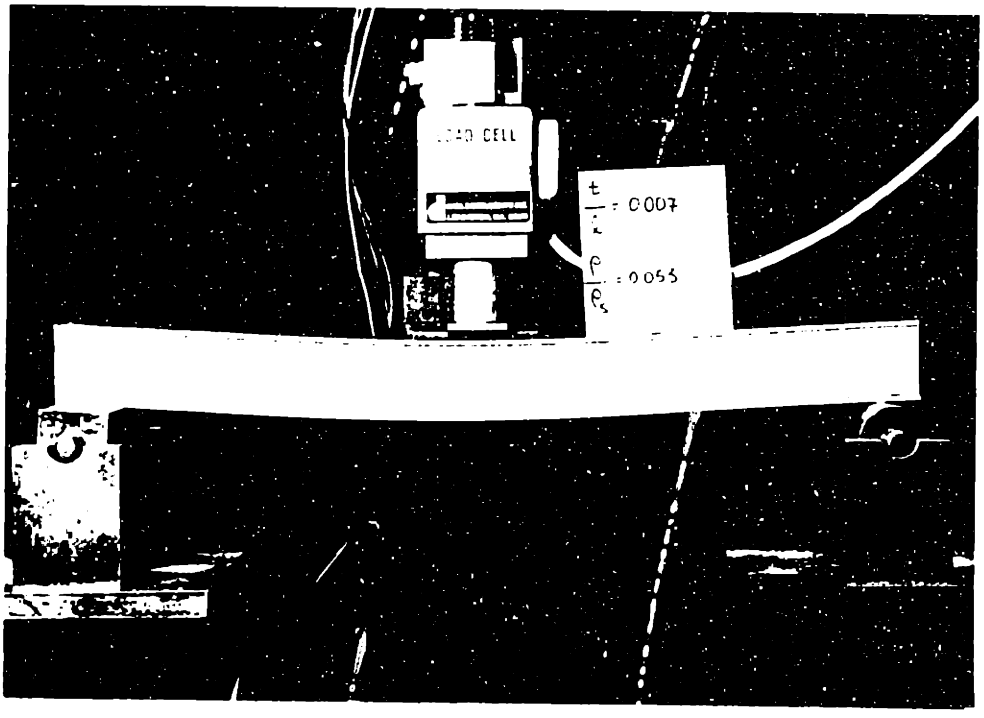

Core shear failure: first deviation from linearity in the P-Δ curve and formation of diagonal crack.

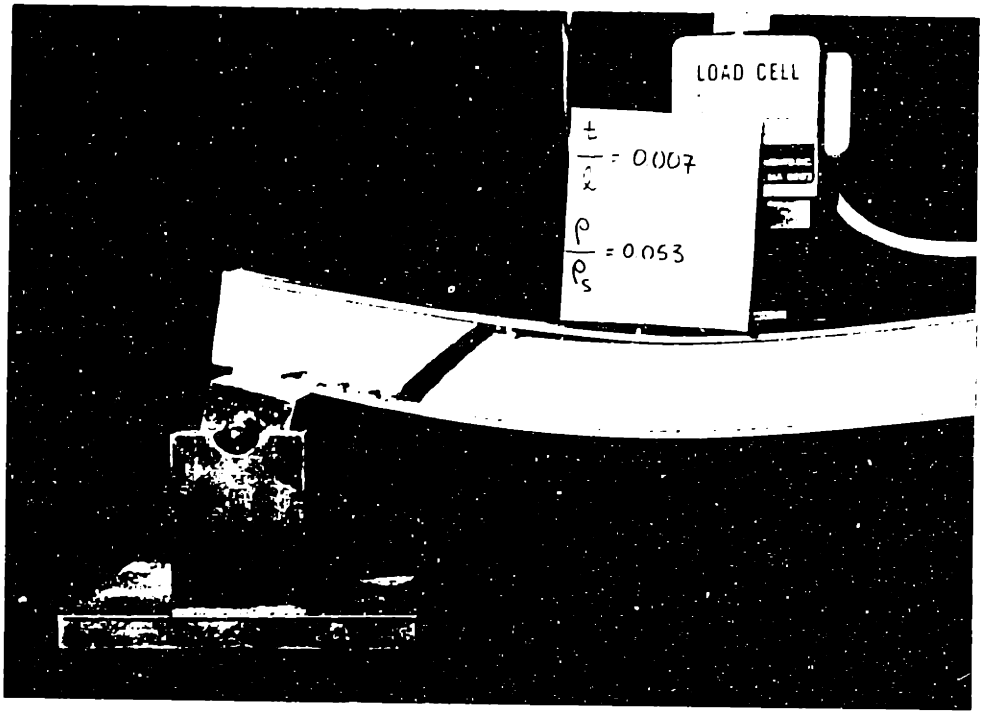

Fig. 4.29 continued.

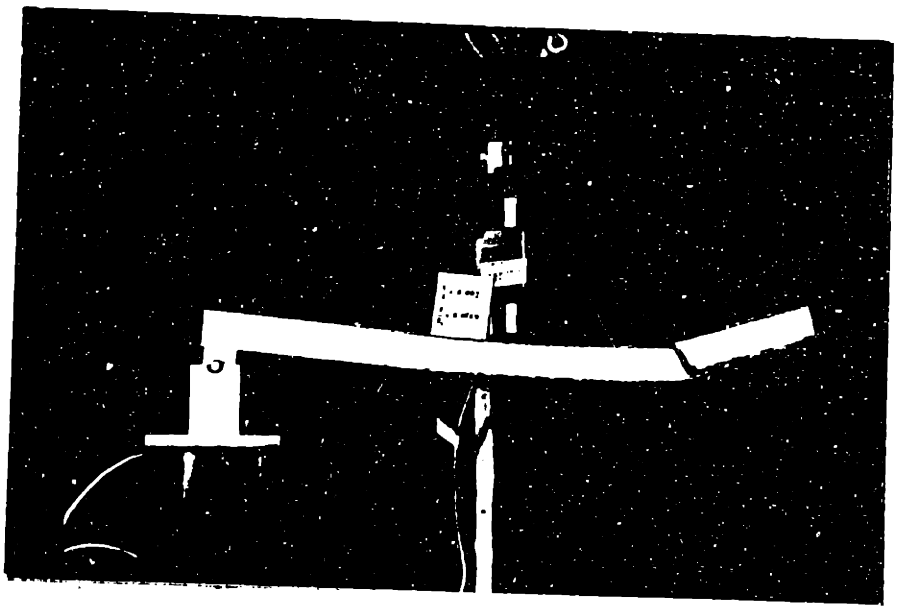

Core shear failure

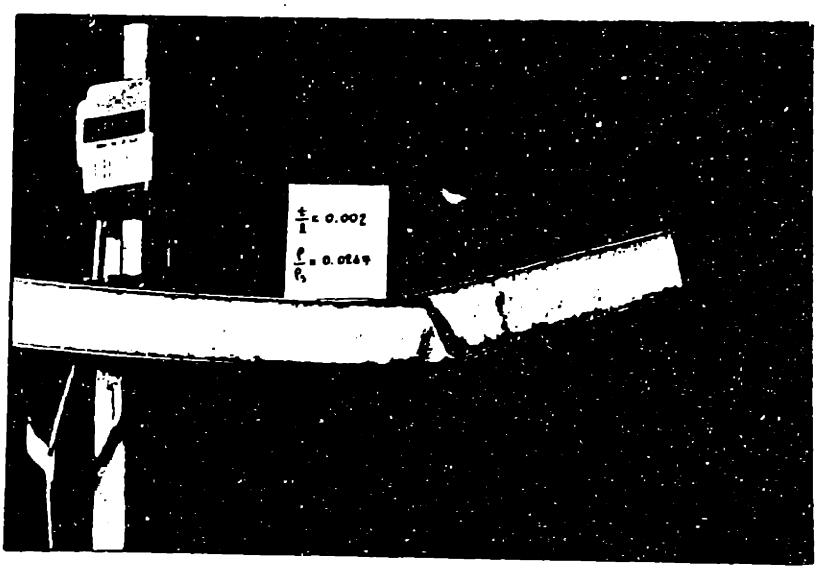

Fig. 4.29 continued.

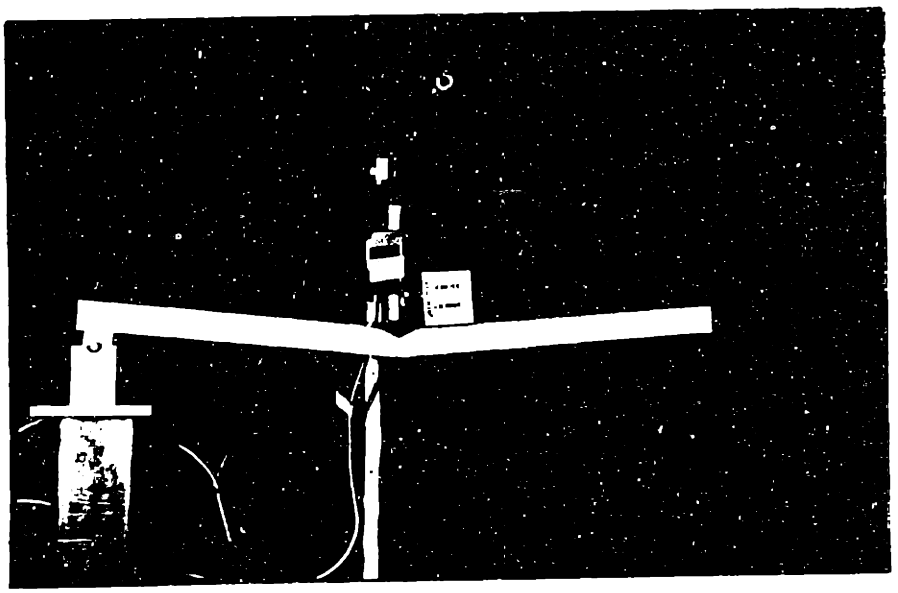

Face wrinkling failure

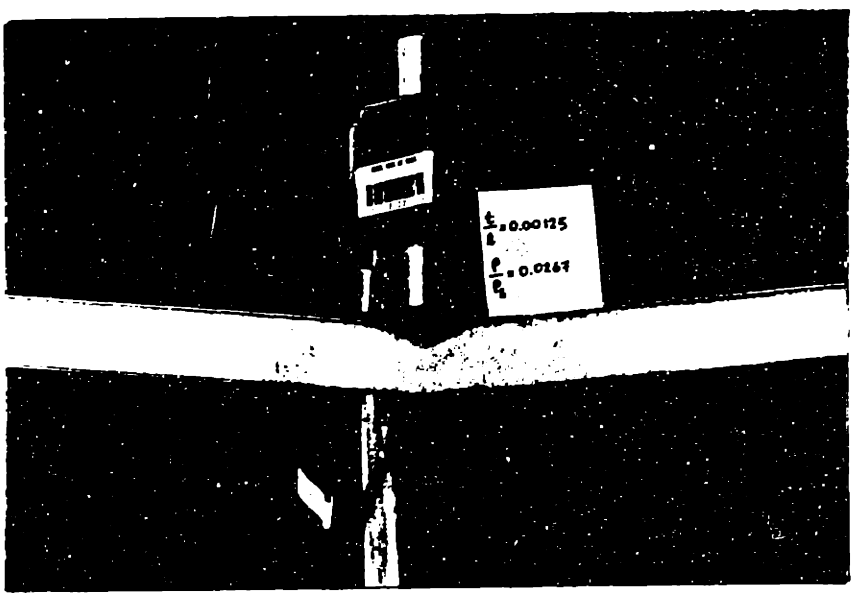

Fig. 4.29 continued.

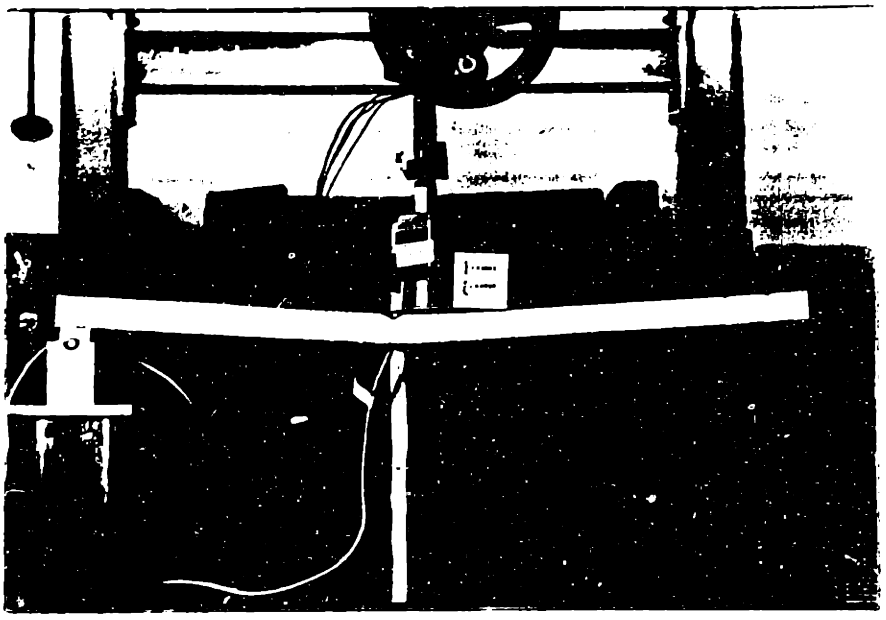

Face wrinkling failure

Fig. 4.29 continued.

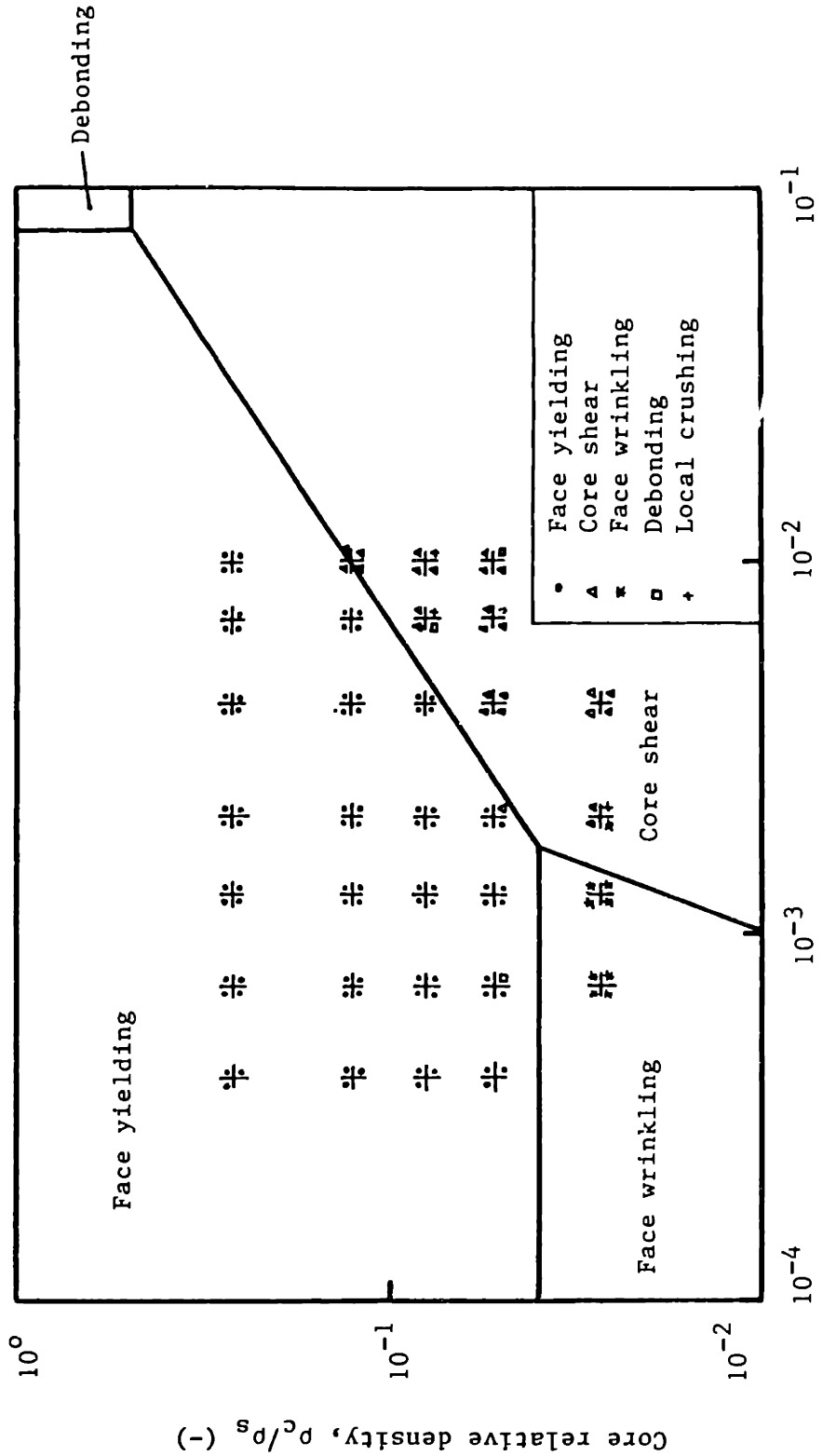

Fig. 4.30 Failure mode map and test data for rectangular sandwich beams (3-point bending).

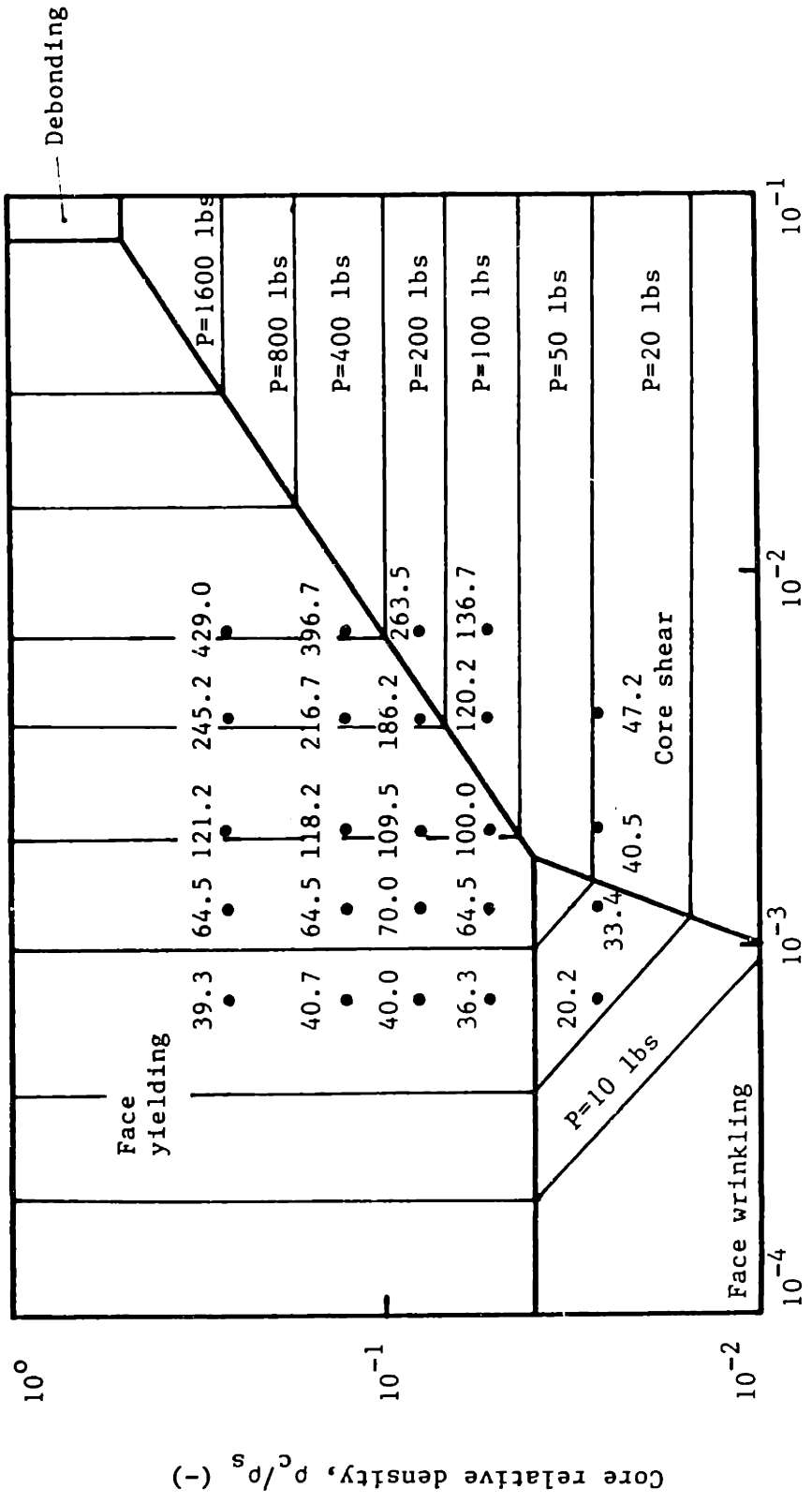

Fig. 4.31 Load contours and test data for rectangular sandwich beams in 3-point bending (b=c=1", d=c)

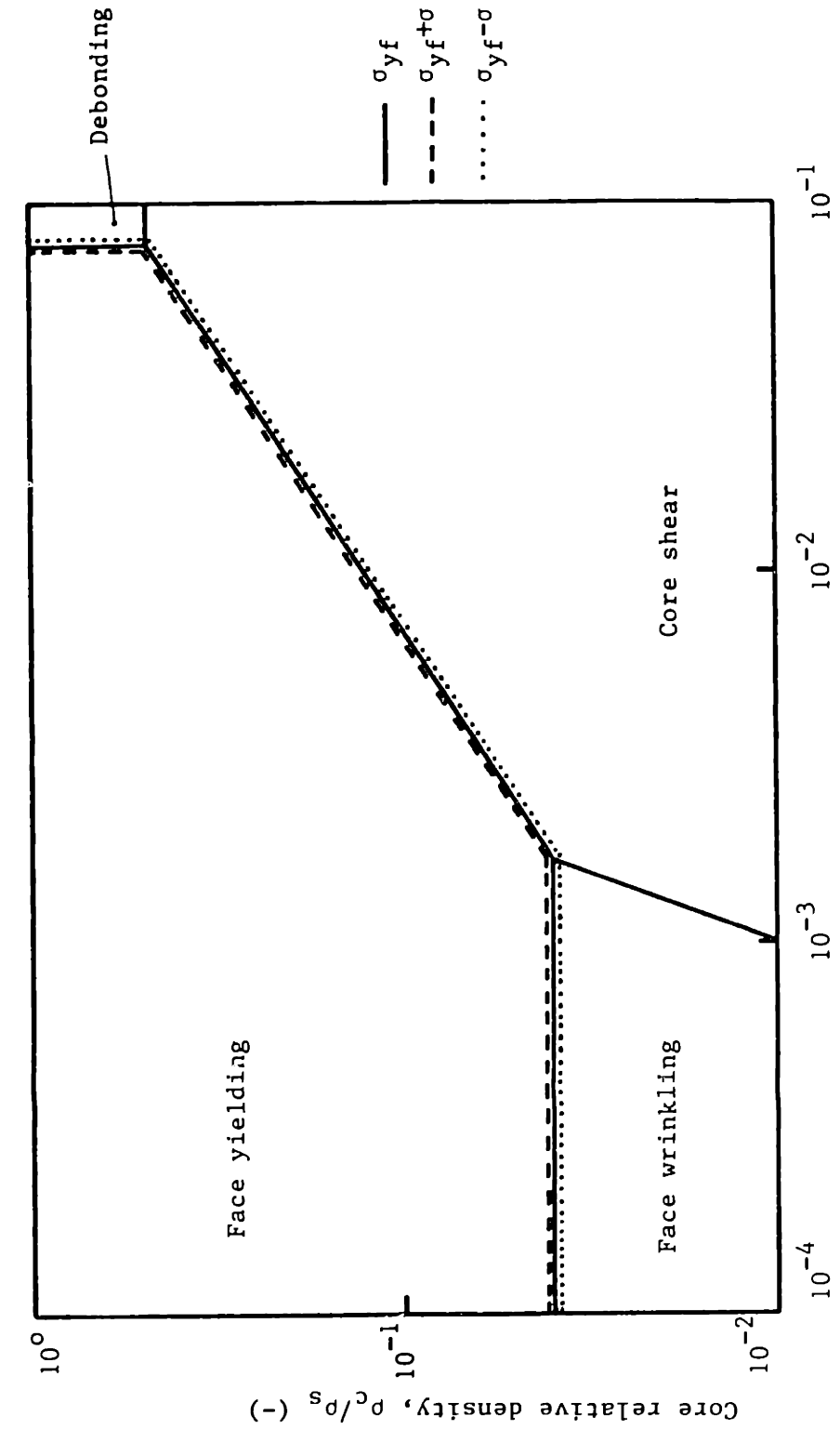

Fig. 5.1 The effect of the variation in the face yield strength, on the failure mode map.

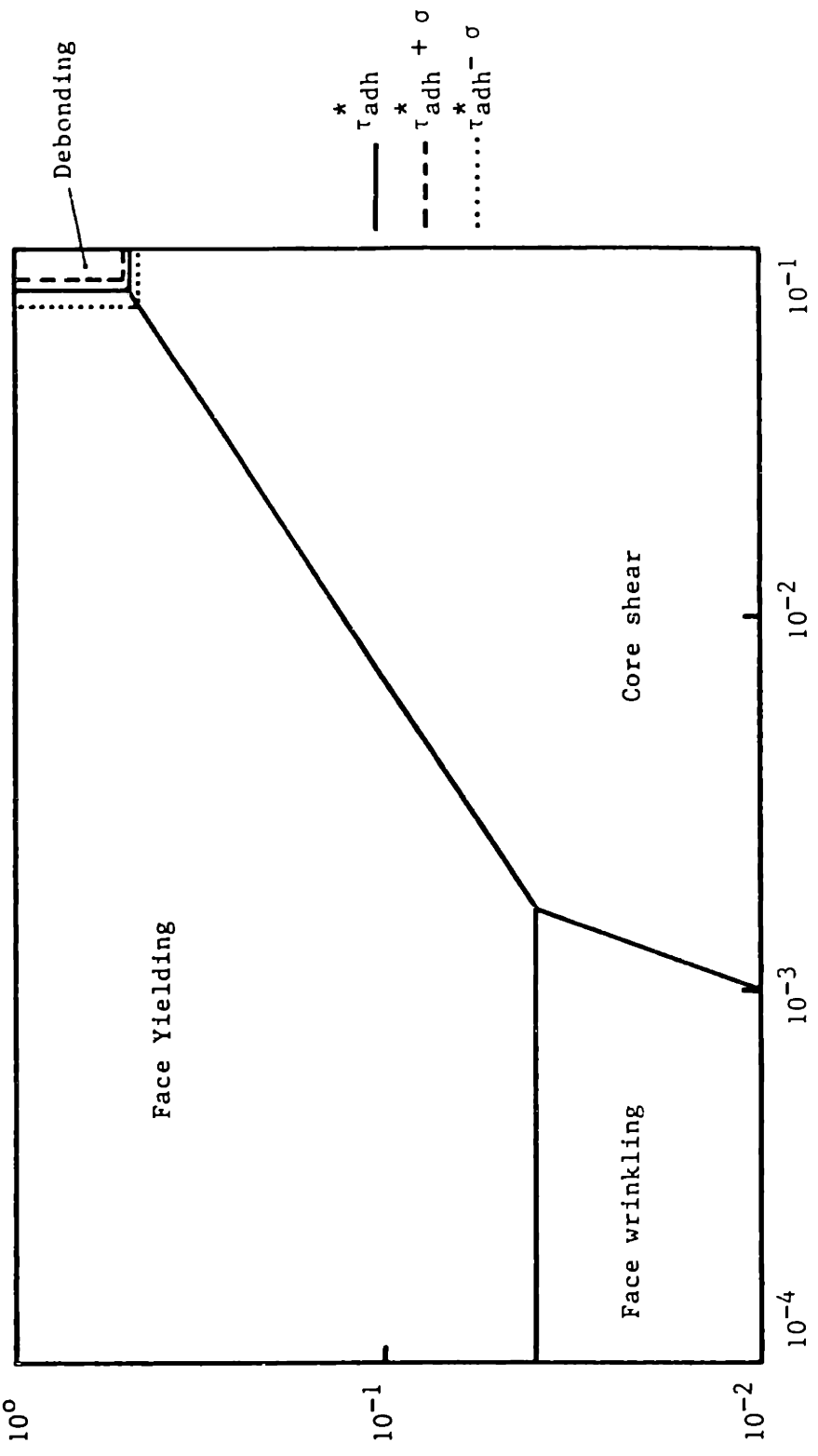

Fig. 5.2 The effect of the variation in the adhesive shear strength, on the failure mode map.

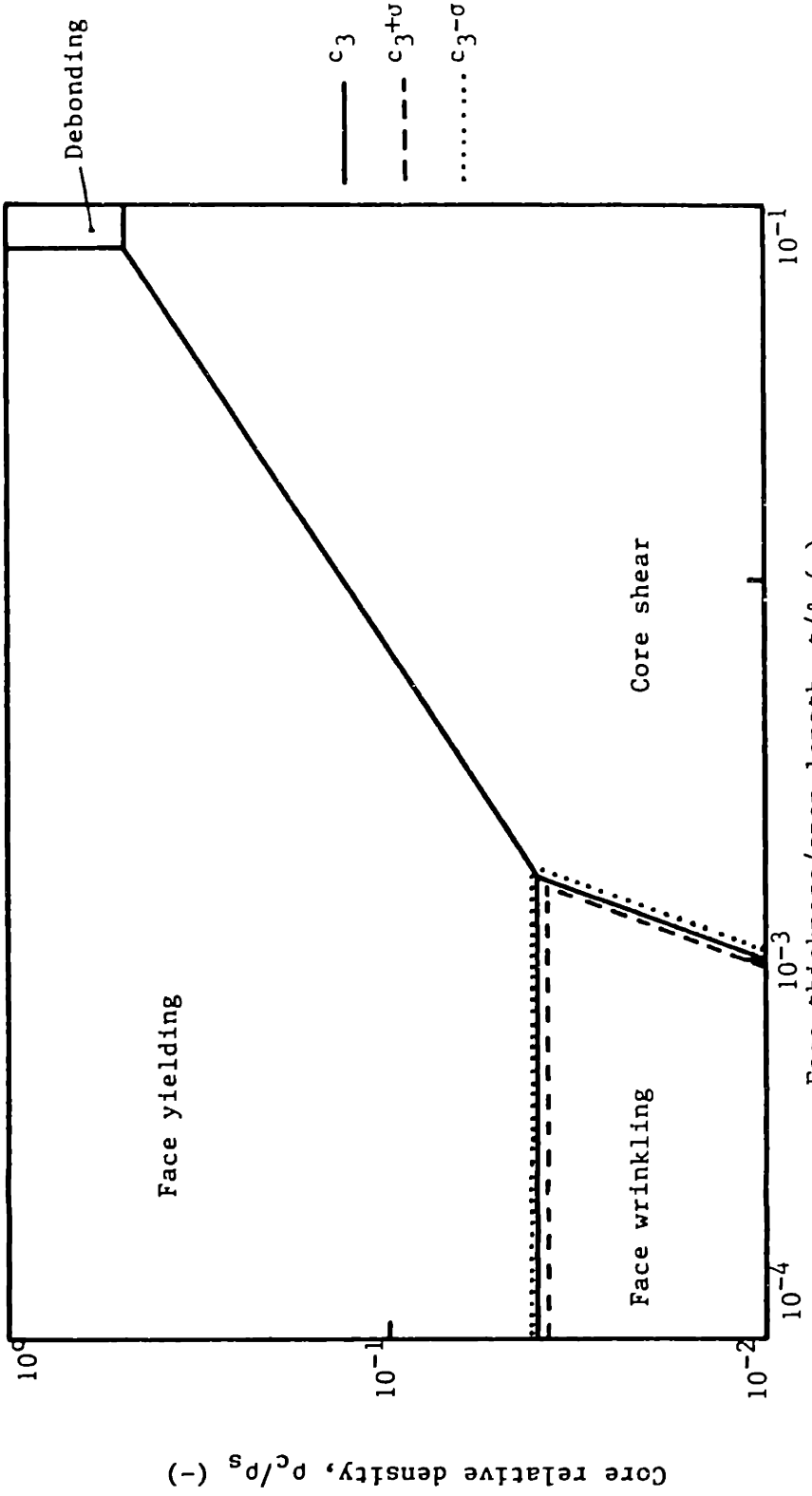

Fig. 5.3 The effect of the variation in the parameter c_3, on the failure mode map.

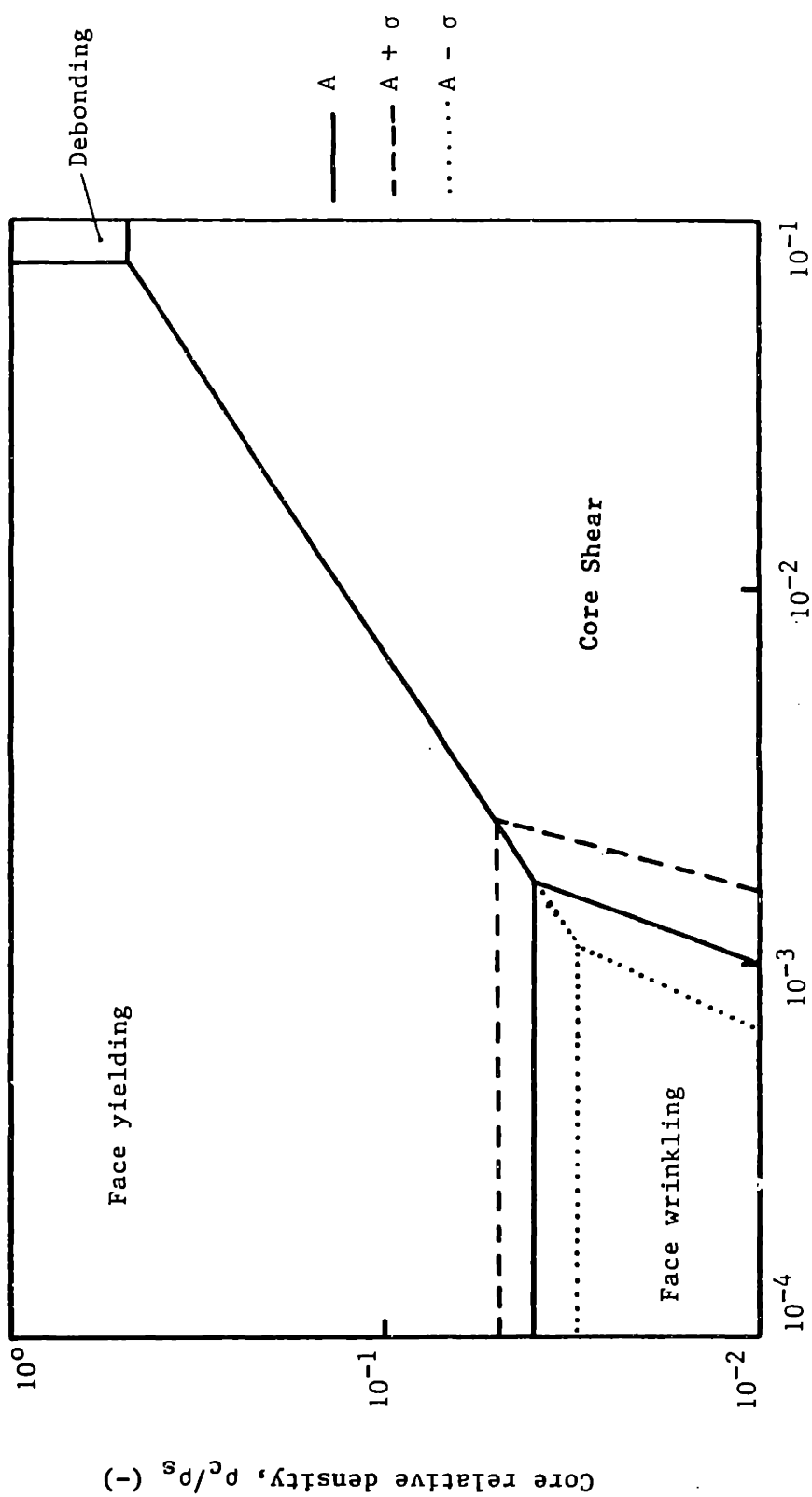

Fig. 5.4 The effect of the variation in the parameter A, on the failure mode map.

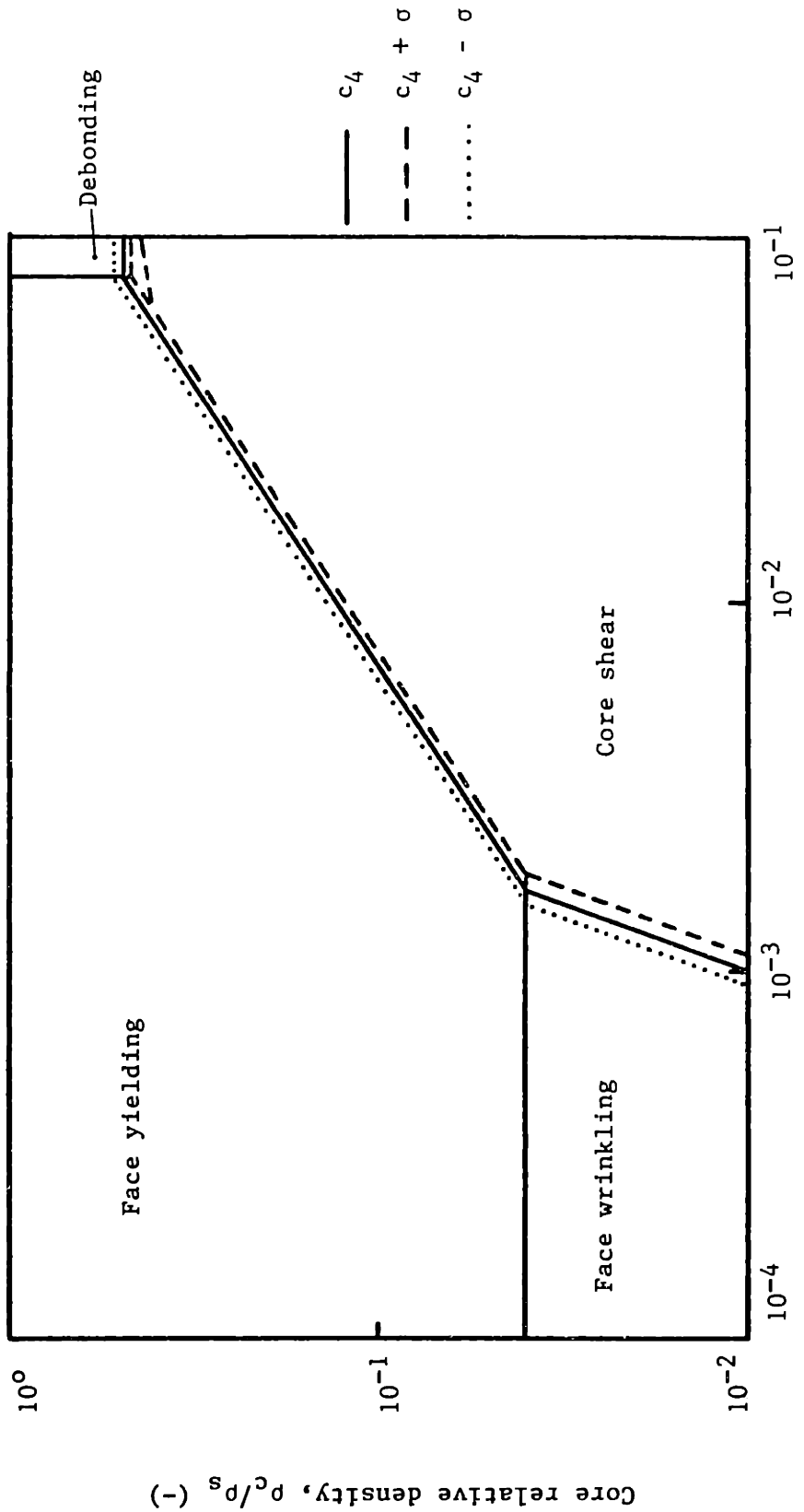

Fig. 5.5 The effect of the variation in the parameter c_4, on the failure mode map.

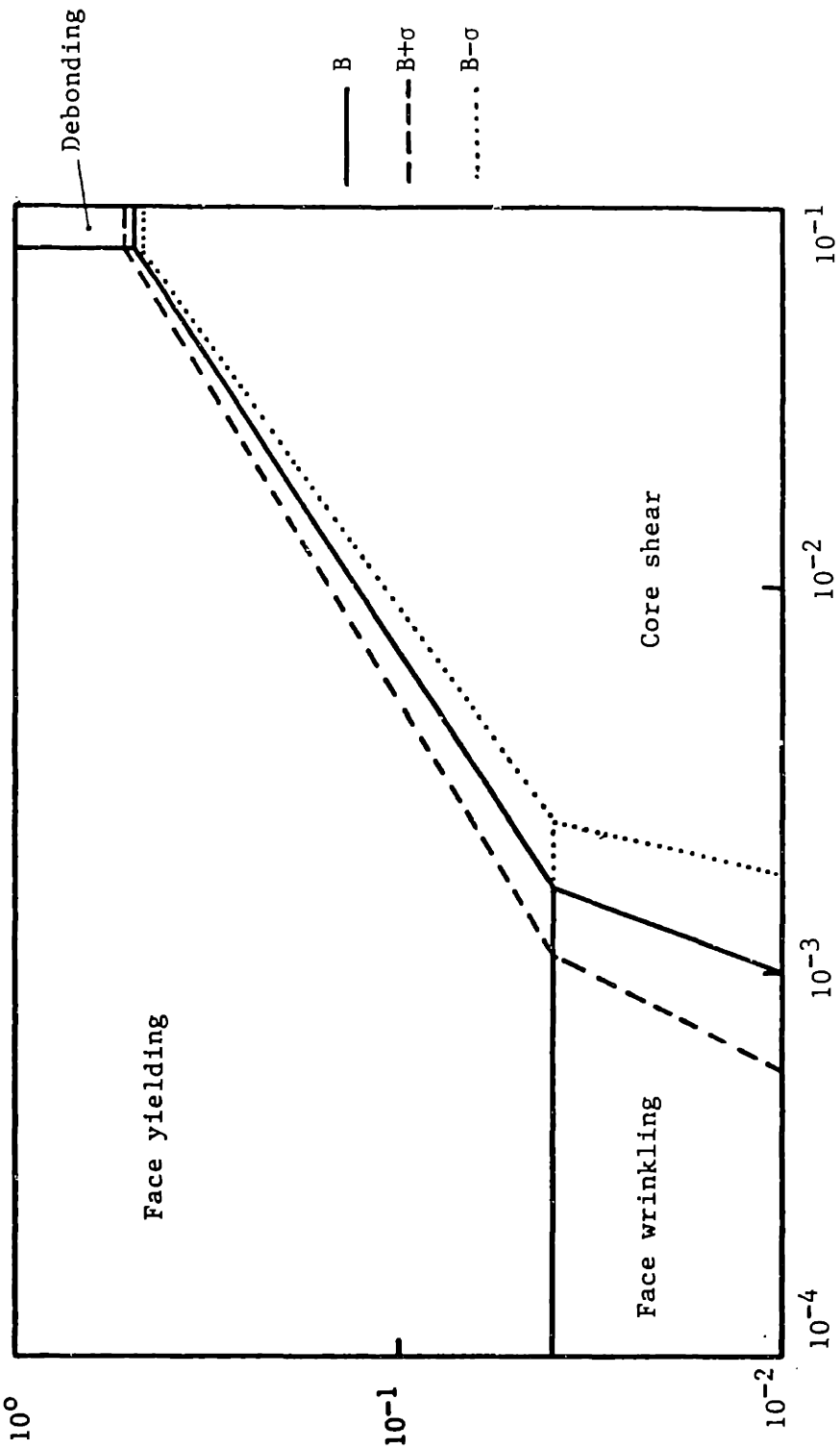

Fig. 5.6 The effect of the variation in the parameter B, on the failure mode map.

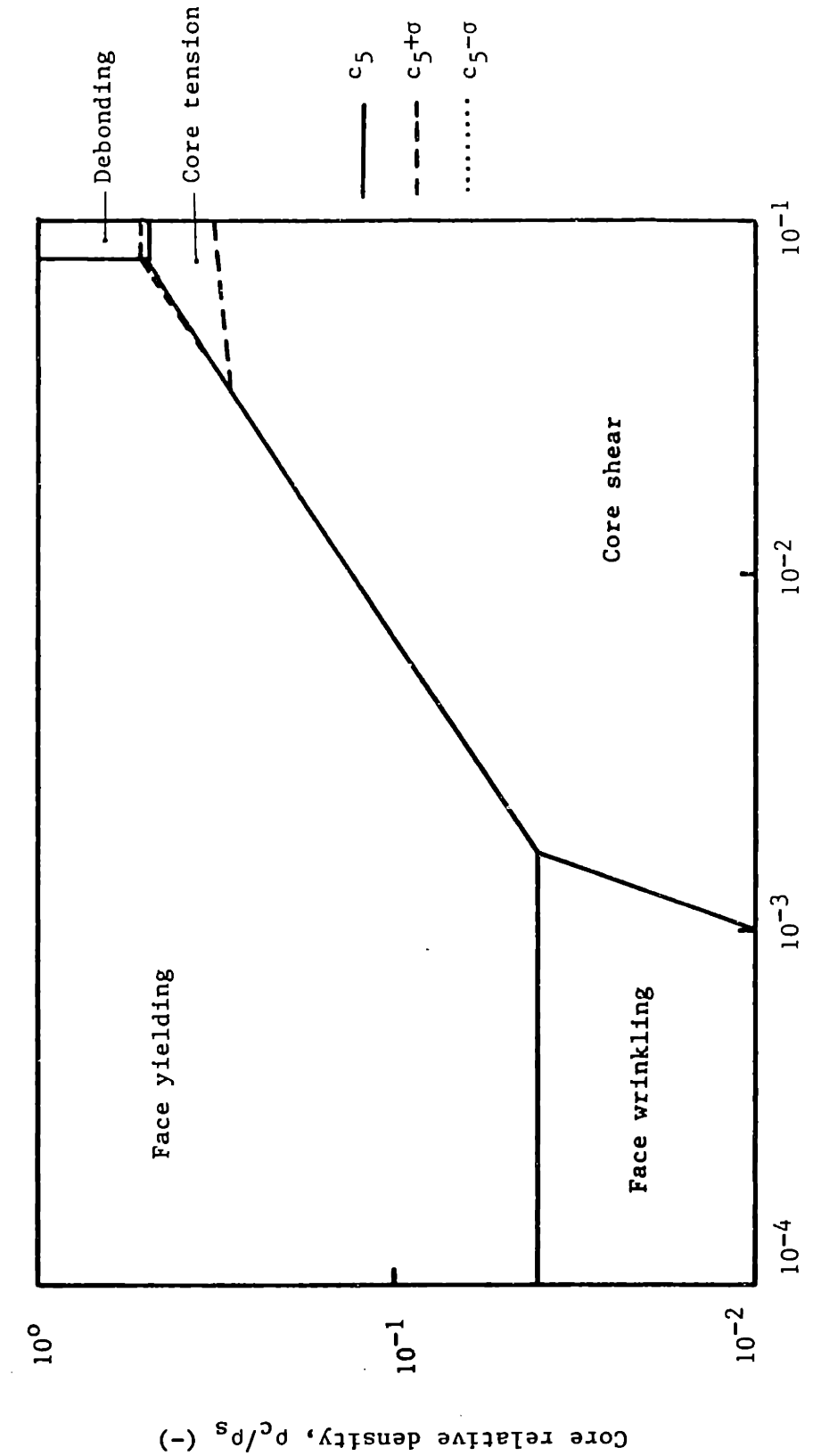

Fig. 5.7 The effect of the variation in the parameter c_5, on the failure mode map.

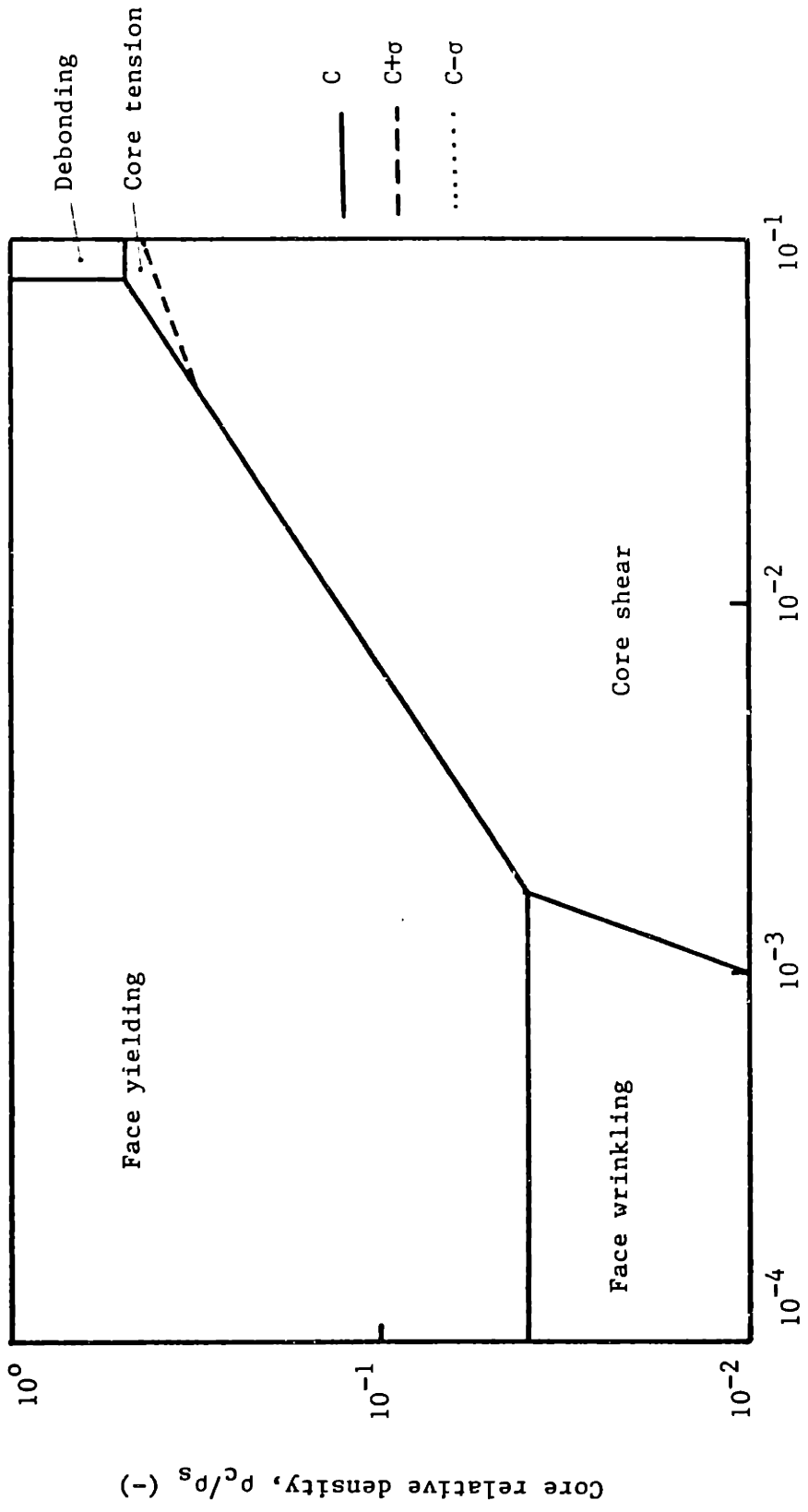

Fig. 5.8 The effect of the variation in the parameter C, on the failure mode map.

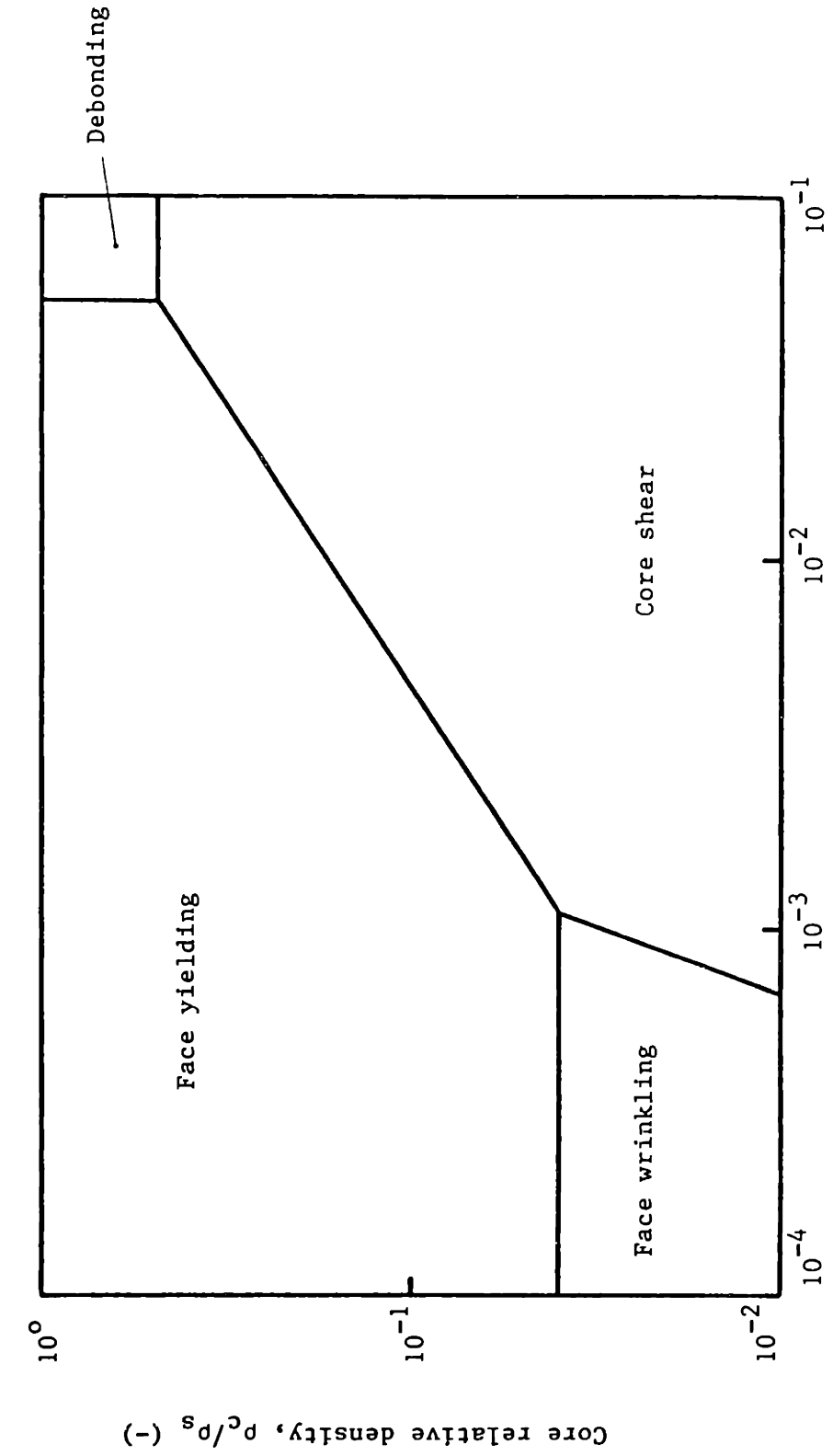

Fig. 5.9 Failure mode map for rectangular simply supported sandwich beam in 4-pt bending.

APPENDIX

COMPUTER PROGRAM FOR THE CONSTRUCTION OF FAILURE MODE MAPS FOR RECTANGULAR SANDWICH BEAMS

The program presented here was written in FORTRAN 77 and gives the failure mode map for sandwich beams with known loading and support conditions, material properties and beam geometry. The development of this code was consistent with the analysis and terminology presented throughout this work and the reader should have no difficulties in following the logic of the code. Minor adjustments are probably required, depending on the graphics device used each time.

```
C*****************************************
C                                        *
C  SANDWICH BEAMS FAILURE MECHANISMS     *
C                                        *
C*****************************************

      integer prevp,st,dt,m(360,240),eq
      real min,mi
C  set parameters st and dt for plotting
      st=360
      dt=240
C  material parameters
      es=1600.0
      ef=70000.0
      ys=127.0
      yf=103.45
      yb=13.5
      ds=1.2
      df=2.7
      c1=4.0
      c2=2.0
      c3=1.13
      c4=0.31
      c5=0.31
      a=1.71
      b=1.52
      c=1.39
C  range of relative density and t/l
      d1=-2.0
      d2=0.0
      tl1=-4.0
      tl2=-1.0
C  print data
      print*,'PROPERTIES OF THE SOLID CORE MATERIAL'
      print*,'Elastic Modulus                ES= ',es,' Mpa'
      print*,'Yield Strength                 YS= ',ys,' Mpa'
      print*,'Density                        DS= ',ds,' Kg/m^3'
      print*,'PROPERTIES OF THE SKIN AND ADHESIVE'
      print*,'Elastic Modulus of the skin    EF= ',ef,' Mpa'
      print*,'Yield Strength of the skin     YF= ',yf,' Mpa'
      print*,'Density of the skin            DF= ',df,' Kg/m^3'
      print*,'Shear Strength of adhesive     YB= ',yb,' Mpa'
      print*,'CONSTANTS'
      print*,'Loading                        C1= ',c1,' C2= ',c2
      print*,'Compressive Modulus equation   C3= ',c3,' A= ',a
      print*,'Shear Strength equation        C4= ',c4,' B= ',b
      print*,'Tensile Strength equation      C5= ',c5,' C= ',c
      print*,'RANGE OF LOG(D/Ds) D1 TO D2 = ',d1,' TO ',d2,'Kg/m^3'
      print*,'RANGE OF LOG(t/l) TL1 TO TL2= ',tl1,' TO ',tl2
C  identification of equation giving the smallest load
      do 11 i=1,st
      do 11 j=1,dt
      tn=10**(tl1+i*(tl2-tl1)/st)
      dn=10**(d1+j*(d2-d1)/dt)

      eq=1
      min=c1*yf*tn
      mi=0.57*c1*(c3**0.67)*(dn**(0.67*a))*(ef**0.33)*(es**0.67)*tn
      if(mi.lt.min) then
            min=mi
```

```
            eq=2
      endif
      mi=c2*yb
      if(mi.lt.min) then
            min=mi
            eq=3
      endif
      temp1=(c3*(dn**a)*es)/(2.0*c1*tn*ef)
      temp2=sqrt(temp1**2+(1.0/c2)**2)
      mi=(c4*(dn**b)*ys)/temp2
      if(mi.lt.min) then
            min=mi
            eq=4
      endif
      mi=(c5*(dn**c)*ys)/(temp1+temp2)
      if(mi.lt.min) then
            min=mi
            eq=5
      endif
C  eq :the number of the equation giving the lowest load
      m(i,j)=eq
11    continue

C  plotting!

      call move(150.0,57.0)
      call draw(150.0,720.0)
      call draw(940.0,720.0)
      call draw(940.0,57.0)
      call draw(150.0,57.0)

      do 22 j=dt,1,-1
      prevp=m(1,j)
      do 22 i=2,st
      if(m(i,j).ne.prevp) then
        prevp=m(i,j)
        call move(150.0+(i-1)*790.0/st,720.0-(dt-j)*663.0/dt)
        call draw(150.0+(i-1)*790.0/st,720.0-(dt+1-j)*663.0/dt)
      endif
 2    continue
      do 44 i=1,st
      prevp=m(i,dt)
      do 44 j=dt-1,1,-1
      if(m(i,j).ne.prevp) then
        prevp=m(i,j)
        call move(150.0+(i-1)*790.0/st,720.0-(dt-j)*663.0/dt)
        call draw(150.0+(i)*790.0/st,720.0-(dt-j)*663.0/dt)
      endif
 4    continue
      call endplt

      end
```